



Universität Hamburg
DER FORSCHUNG | DER LEHRE | DER BILDUNG

Characterization of SusD-homologs from the phylum Bacteroidota and their ability to bind distinct polymers

Dissertation

with the aim of achieving the degree of *Doctor rerum naturalium* (Dr. rer. nat.)
at the Faculty of Mathematics, Informatics and Natural Sciences,
Department of Biology of University of Hamburg

Submitted by

Myllena Pereira Silverio

born May 24, 1994, in Rio de Janeiro, RJ, Brazil

Hamburg 2024

The following evaluators recommend the admission of the dissertation:

Prof. Dr. Wolfgang R. Streit

Prof. Dipl.-Ing. Dr. Agnes Weiß

Date of Defence (Disputation): 13.12.2024

Eidesstattliche Versicherung:

Hiermit versichere ich an Eides statt, die vorliegende Dissertationsschrift selbst verfasst und keine anderen als die angegebenen Hilfsmittel und Quellen benutzt zu haben.

Sofern im Zuge der Erstellung der vorliegenden Dissertationsschrift generative Künstliche Intelligenz (gKI) basierte elektronische Hilfsmittel verwendet wurden, versichere ich, dass meine eigene Leistung im Vordergrund stand und dass eine vollständige Dokumentation aller verwendeten Hilfsmittel gemäß der Guten wissenschaftlichen Praxis vorliegt. Ich trage die Verantwortung für eventuell durch die gKI generierte fehlerhafte oder verzerrte Inhalte, fehlerhafte Referenzen, Verstöße gegen das Datenschutz- und Urheberrecht oder Plagiate.

Affidavit:

I hereby declare and affirm that this doctoral dissertation is my own work and that I have not used any aids and sources other than those indicated.

If electronic resources based on generative artificial intelligence (gAI) were used in the course of writing this dissertation, I confirm that my own work was the main and value-adding contribution, and that complete documentation of all resources used is available in accordance with good scientific practice. I am responsible for any erroneous or distorted content, incorrect references, violations of data protection and copyright law or plagiarism that may have been generated by the gAI.

Hamburg, 02.07.2024

A handwritten signature in black ink, appearing to read 'Myllena Pereira Silverio'. The signature is fluid and cursive, with the first name 'Myllena' being the most prominent part.

Myllena Pereira Silverio

Abstract

The phylum Bacteroidota comprises ubiquitous microorganisms with a distinguished way to acquire glucan. The “starch utilization system” (*sus*) operon presents genes that encode three glycoside hydrolases (GH; SusA, SusB and SusG), one transmembrane protein (SusC), three binding modules (SusD, SusE and SusF) and the transcriptional regulator SusR. SusD is an essential binding module that facilitates the bacterial acquisition of nutrients. Although SusD-like proteins were previously evaluated with distinct natural polymers, they were never characterized with synthetic polymers before. Synthetic polymers, especially fossil-fuel based pollutants, are a major concern because they accumulate in the environment and enter the food chain in the form of micro- or nanoplastics. The objective of this work was to characterize three *susD*-homologs from elephant feces (*susD70111* and *susD38489*) (Ilmberger et al., 2014) or cow rumen (*susD1*) (Rosewarne et al., 2014) metagenomes regarding their adsorption to plastics. Each protein presented an N-terminal signal peptide Sec/SPII, which was removed. Using pull-down assays, fluorescence measurements and surface plasmon resonance (SPR), SusD1 Δ 1-22 and SusD38489 Δ 1-25 were identified as cellulose binding modules, while SusD70111 Δ 1-20 preferentially bound chitin. The pull-down assays were also performed with polyethylene terephthalate (PET), polyamide 6 (nylon 6; PA6) and low-density polyethylene (LDPE), with preliminary adsorption detected for each protein. SPR analysis was performed for bis(2-Hydroxyethyl) terephthalate (BHET; a PET degradation product), in which the proteins are strongly bound. In every assay performed, SusD1 Δ 1-22 presented the best performance. Therefore, it was fused to two previously characterized enzymes with catalytic activity towards PET. However, an optimization of enzymatic activity was not observed. The proteins labelled with the fluorescence tag superfolder GFP (*sfGFP*) were also used for the construction of plastic reporter assays. Due to the high background of *sfGFP* with plastics, the data was not conclusive. The chitin binding module SusD70111 was fragmented and the truncated version named SusD70111_{F3} showed putative adsorption to PET and BHET. Structural and phylogenetic analysis of the binding modules revealed that SusD1 and SusD38489 share sequence and structure similarity, but SusD70111 is evolutionary distant and clusters with SusD-like proteins from a distinct niche (hot springs). Docking studies also pointed to the putative amino acids involved in protein-substrate adsorption. Here, SusD was characterized

with synthetic polymers for the first time. This work will aid in the construction of further translational protein fusions and improvements on the reporter analysis of micro- and nanoplastics.

Zusammenfassung

Das Phylum der Bacteroidota umfasst eine ubiquitär vorkommende Gruppe Mikroorganismen, die sich durch eine hohe Diversität an Glucanasen und Glycosylhydrolasen auszeichnen. Das Operon des „Stärkeverwertungssystems“ (*sus*) umfasst Gene, die für drei Glykosidhydrolasen (GH; SusA, SusB und SusG), ein Transmembranprotein (SusC), drei Bindungsmodule (SusD, SusE und SusF) und den Transkriptionsregulator SusR kodieren. SusD ist ein Stärke-Binde Protein an der Zelloberfläche. Obwohl SusD-ähnliche Proteine bereits mit verschiedenen natürlichen Polymeren untersucht wurden, wurden sie noch nie mit Hinblick auf ihre Bindung mit synthetischen Polymeren charakterisiert. Synthetische Polymere, insbesondere auf fossilen Brennstoffen basierende Kunststoffe (Plastik), stellen ein großes Problem dar, da sie sich in der Umwelt anreichern und in Form von Mikro- oder Nanoplastik in die Nahrungskette gelangen. Ziel dieser Arbeit war es, drei *susD*-Homologe aus Elefantenkot (*susD70111* und *susD38489*) (Ilmberger et al., 2014) oder aus Rinderpansen (*susD1*) (Rosewarne et al., 2014) Metagenomen hinsichtlich ihrer Adsorption an Kunststoffe zu charakterisieren. Jedes Protein wies ein N-terminales Signalpeptid Sec/SPII auf, das entfernt wurde. Mithilfe von Pull-down-Assays, Fluoreszenzmessungen und Oberflächenplasmonenresonanz (SPR) wurden *SusD1* Δ 1-22 und *SusD38489* Δ 1-25 als Cellulose-Bindungsmodule identifiziert, während *SusD70111* Δ 1-20 bevorzugt Chitin bindet. Die Pull-down-Tests wurden auch mit Polyethylenterephthalat (PET), Polyamid 6 (Nylon 6; PA6) und Polyethylen niedriger Dichte (LDPE) durchgeführt, wobei für jedes Protein eine erste Adsorption festgestellt wurde. Die SPR-Analyse wurde für Bis(2-Hydroxyethyl)terephthalat (BHET; ein PET-Abbauprodukt) durchgeführt, an das die Proteine stark gebunden sind. In jedem durchgeführten Test zeigte *SusD1* Δ 1-22 die beste Bindung. Daher wurde es mit zwei zuvor charakterisierten Enzymen mit katalytischer Aktivität gegenüber PET fusioniert. Eine Optimierung der enzymatischen Aktivität wurde jedoch nicht beobachtet. Die mit dem Fluoreszenz-Tag superfolder GFP (*sfGFP*) markierten Proteine wurden auch für die Konstruktion von Kunststoff-Reporter-Assays verwendet. Aufgrund des hohen Hintergrunds von *sfGFP* mit Kunststoffen waren die Daten nicht schlüssig. Das Chitinbindungsmodul *SusD70111* wurde fragmentiert und die verkürzte Version mit der Bezeichnung *SusD70111F3* zeigte eine putative Adsorption an PET und BHET. Eine strukturelle und phylogenetische Analyse der Bindungsmodule ergab,

dass SusD1 und SusD38489 Sequenz- und Strukturähnlichkeiten aufweisen, SusD70111 jedoch evolutionär weit entfernt ist und sich mit SusD-ähnlichen Proteinen aus einer anderen Nische (heiße Quellen) gruppiert. Docking-Studien wiesen auch auf die mutmaßlichen Aminosäuren hin, die an der Protein-Substrat-Adsorption beteiligt sein könnten. In der vorliegenden Dissertation wurde SusD zum ersten Mal mit Hinblick auf die Bindung von synthetischen Polymeren charakterisiert. Die in dieser Arbeit gewonnenen Erkenntnisse werden zukünftig bei der Konstruktion weiterer Reporterfusionen und Bindeproteinen für Mikro- und Nanokunststoffen eine wichtige Grundlage bieten.

List of articles

- **Silverio, M.P.**; Neumann, T.; Schaubruch, K.; Heermann, R.; Pérez-García, P.; Chow, J.; Streit, W.R. (2024). Metagenome-derived SusD-homologs affiliated with Bacteroidota bind to synthetic polymers. *Applied and Environmental Microbiology* 90(7):e0093324. DOI: [10.1128/aem.00933-24](https://doi.org/10.1128/aem.00933-24).

Furthermore, the results obtained have also been presented by me at the 10th Congress of European Microbiologists (FEMS 2023) in Hamburg and at the Microplastics Meeting 2024 promoted by Agilent Technologies and i3 Membrane GmbH at the Helmholtz-Zentrum Hereon in Geesthacht.

Table of Contents

Abstract	I
Zusammenfassung	III
List of Figures	IX
List of Tables	XVI
List of Abbreviations	XVII
I. Introduction	1
1.1 Gut microbiota of humans and animals	2
1.2 The importance of the operon <i>sus</i> to the phylum Bacteroidota	3
1.3 Affinity of SusD to various substrates	7
1.4 Fossil-fuel based polymers as ubiquitous pollutants	11
1.5 Enzymatic optimization with binding modules	12
1.6 Aim of the study	14
II. Materials and Methods	16
2.1 Origin of the samples	17
2.2 Bacterial strains and cultivation	17
2.3 Working with DNA	22
2.3.1 Cloning	22
2.3.2 Polymerase Chain Reaction (PCR).....	24
2.3.2.1 Touchdown PCR	24
2.3.2.2 Colony PCR.....	25
2.3.3 Electrophoresis.....	26
2.4 Working with protein	27
2.4.1 Protein expression.....	27
2.4.2 French press	28
2.4.3 Protein purification.....	28
2.4.4 SDS PAGE	29
2.4.5 Native and affinity PAGE	30
2.4.6 Western Blot.....	33
2.5 Protein activity screening	35
2.5.1 Pull-down assay of insoluble substrates	35
2.5.2 Fluorescence assay.....	36
2.5.3 Surface plasmon resonance (SPR) spectroscopy.....	38
2.5.4 β -galactosidase (<i>lacZ</i>) reporter	40
2.5.5 Enzymatic screening on agar plates containing synthetic substrates	40
2.5.6 Ultra-high-performance liquid chromatography (UHPLC) analysis	41

2.6 Bioinformatics	42
2.6.1 Phylogenetic analysis	42
2.6.2 Structural analysis	43
2.6.2.1 AlphaFold v.2.3.2.....	43
2.6.2.2 Structural studies using Chimera.....	43
2.6.2.3 Prediction of tetratricopeptide repeat using TPRpred.....	44
III. Results	45
3.1 Main characteristics of SusD	46
3.2 Phylogenetic analysis	48
3.3 Protein purification and concentration	50
3.4 Pull-down assay	51
3.5 Affinity PAGE	52
3.6 Screening of the fluorescence signal	54
3.6.1 Natural polymers	54
3.6.2 Synthetic polymers	57
3.7 Characterization of SusD70111_{F3}	59
3.8 Binding kinetics with SPR analysis	60
3.9 Enzymatic activity of <i>lcc-wt</i> and <i>pet30ΔporC</i> fused with <i>susD1</i>	64
3.10 <i>lacZ</i> reporter	67
3.11 Structural comparison and docking	70
3.11.1 Docking with natural polymers	70
3.11.1.1 Cellulose.....	70
3.11.1.2 Chitin.....	73
3.11.2 Docking with synthetic polymers	75
3.11.2.1 PET	75
3.11.2.2 BHET.....	79
3.11.3 Structural alignment and prediction of tetratricopeptide repeat.....	80
IV. Discussion & Outlook	82
4.1 SusD as part of the Bacteroidotal operon <i>sus</i> and their substrate in nature	83
4.2 SusD adsorption to synthetic polymers	86
4.2.1 Structural characteristics	86
4.2.2 Translational fusion of SusD1 and known PETases.....	89
4.2.3 PET modifications.....	90
4.3 Other promising plastic binding modules	92
4.3.1 SusE-G.....	92
4.3.2 PilF	93

4.3.3 Hydrophobins	95
V. Supplementary Material	99
5.1 Primers and Touchdown PCR cycles	100
5.2 Structural analysis	108
5.3 Figures	110
5.4 DNA and amino acid sequences	114
5.4.1 DNA.....	114
5.4.2 Amino acid.....	116
VI. Acknowledgement	117
VII. References	119

List of Figures

Figure 1: Schematic representation and operon map from *susA* to *susG* and the transcriptional regulator *susR*. **A)** Protein distribution in a microorganism from the phylum Bacteroidota. The top layer represents the outer membrane, with the binding proteins SusD-F, as well as the α -amylase SusG, responsible for breaking the substrates into oligosaccharides of easy transport (Bakolitsa et al., 2010; Foley et al., 2016). SusD is associated with the TonB-dependent β -barrel protein SusC, which facilitates the transport of oligosaccharides to the periplasm (Bakolitsa et al., 2010; Bjursell et al., 2006; Bolam & Koropatkin, 2012; Cho & Salyers, 2001; Foley et al., 2016). SusA is a neo-pullulanase and SusB a α -glucosidase enzyme, being both located in the periplasm (Foley et al., 2016). SusR regulator, activated by maltose, is placed on the inner membrane (Bakolitsa et al., 2010; Bjursell et al., 2006; Foley et al., 2016). **B)** Organization of the operon *sus*, encoding the genes *susRABCDEFG*. *SusR* is represented in red, the promoter represented in green and the genes responsible for encoding *susA* to *susG* in distinct shades of blue. Created in BioRender.com.

..... 4

Figure 2: Structure of the complexes RagA/RagB and SusC/SusD. **A)** RagA/RagB complex in an open state (PDB accession number 6SML) (Madej et al., 2020). **B)** After the ligand is bound, RagA/RagB adopts a closed state (6SM3) (Madej et al., 2020). RagA is represented in red and RagB in green and they belonged to the microorganism *Porphyromonas gingivalis*. **C)** SusC/SusD complex open (6ZLT) (Gray et al., 2021). **D)** SusC/SusD closed (6ZLU) (Gray et al., 2021). SusC is represented in pink and SusD in orange. The structures are from *Bacteroides thetaiotaomicron*. In general, the nutrient acquisition mechanism of both protein complexes resembles a “pedal bin” model. 6

Figure 3: Polymers produced from fossil-fuel sources. From top to bottom and in the order of highest to lowest scale production: chemical structure of polyethylene (PE), polypropylene (PP), polyvinyl chloride (PVC), polyurethane (PU), polyamide (nylon; PA), polyethylene terephthalate (PET), polystyrene (PS) and neoprene (from the family of synthetic rubbers; SR). Designed with ChemDraw Professional© v.22.0.0.22..... 12

Figure 4: Structure of the final chimeras produced by translational fusion, with protein sizes (kDa) indicated. **A)** Fusion of *susD1Δ1-22* with the enzymes *lcc-wt* (Sulaiman et al., 2012) and *pet30ΔporC* (Zhang et al., 2021). A (GS)₁₇ linker (51 bp) was used. The His₆-tag was positioned to the C-terminus of the enzyme. This cloning was performed by Tabea Neumann as part of her Master thesis. **B)** Fusion of *susD1Δ1-22* and *susD38489Δ1-25* with *lacZ*. A GGGGS linker (15 bp) was used, and the His₆-tag was positioned to the C-terminus of *lacZ*. *SusD70111Δ1-20* was not fused to *lacZ* due to low protein yield. **C)** Fusion of *susD1Δ1-22* and *susD70111Δ1-20* with *sfGFP*. A GGGGS linker (15 bp) was used, and the His₆-tag was positioned to the C-terminus of *sfGFP*. *SusD38489Δ1-25* was fused to *sfGFP* as part of another study and, therefore, it will not be displayed here. 23

Figure 5: Schematic representation of the affinity gel. From the bottom to the top: 12% separating gel was prepared as described on Table 11, and 2 mL was dispensed between the glasses. Next, the polymer gel was prepared, replacing the H₂O_{dd} by the substrate. 2 mL of this suspension was added to the top of the separating gel (after the polymerization). The

stacking gel was prepared according to Table 11 and dispensed on the top of the polymer gel, after the complete polymerization. The final result was a gel with 3 layers. Created in BioRender.com.....	32
Figure 6: Schematic representation of the fluorescence assay, divided in three steps. Created in BioRender.com.	37
Figure 7: UHPLC control curves. A) Calibration curve of terephthalic acid (TPA). B) Acetonitrile gradient. The assays for SusD1 Δ 1-22 were conducted by Tabea Neumann during her Master thesis.....	42
Figure 8: Upstream-downstream map of <i>susD38489</i>, <i>susD70111</i> and <i>susD1</i>. As expected, the neighbour analysis revealed the presence of <i>susC</i> (in black) positioned upstream <i>susD</i> . Downstream of <i>susD</i> , it was possible to identify genes encoding hypothetical proteins (grey) and glycoside hydrolases (GH) of distinct families (red, purple and salmon). Adjacent to <i>susD70111</i> , genes encoding GH were not found. This data was retrieved from the metagenome analysis of elephant feces (Ilmberger et al., 2014) and cow rumen (Rosewarne et al., 2014). <i>SusD70111</i> and <i>susD38489</i> presented contigs with sizes 11 and 16 kb, respectively. <i>SusD1</i> contig size was not identified.....	47
Figure 9: Side view of the predicted structure of SusD70111, SusD1 and SusD38489 WT (green) and their respective mutants lacking the N-terminal signal peptide Sec/SPII (salmon). The signal peptide (red arrow) of SusD70111 has 57 bp (19 aa), while SusD1 and SusD38489 have 60 bp (20 aa) and 71 bp (24 aa) respectively.	48
Figure 10: Phylogenetic tree of SusD1, SusD38489 and SusD70111. A bootstrap tree of proteins from the family of binding modules SusD and RagB was constructed. The tree was rooted at the RagB proteins from the oral pathogen <i>Porphyromonas gingivalis</i> , which was considered the external group (Acuna-Amador et al., 2018; Hall et al., 2005; Hanley et al., 1999; Nagano et al., 2007; Nelson et al., 2003; Watanabe et al., 2011). SusD-homologs from gut (Gharechahi et al., 2022; Rosewarne et al., 2014) and feces (green), wastewater and food fermentation metagenomes (blue) (Crognale et al., 2021) were found by BLASTp, using the NCBI “Non-redundant protein sequences” Database. RagB proteins are identified in pink. The SusD-homologs from hot springs (Wang et al., 2019) (purple) were included, because they represent a distinct niche. The branch lengths and NCBI accession numbers can be found in the tree.....	49
Figure 11: Polyacrylamide gels from each protein purification. A) SusD1 Δ 1-22 (63.2 kDa); B) SusD38489 Δ 1-25 (65.6 kDa); C) SusD70111 Δ 1-20 (64.3 kDa); D) Proteins after buffer exchange to potassium phosphate buffer 0.1 M pH 7. From left to right: SusD1 Δ 1-22, SusD38489 Δ 1-25 and SusD70111 Δ 1-20. The ladder used was PageRuler® unstained protein ladder #26614 (Thermo Fisher Scientific, Massachusetts, USA). L: protein ladder; -: cell culture before protein expression; +: cell culture after protein expression; DEBRIS: cell debris; FT: flow through; W1: 1 st wash; W2: 2 nd wash; E1: 1 st elution; E2: 2 nd elution; E3: 3 rd elution; E4: 4 th elution; E5: 5 th elution; E6: 6 th elution; E7: 7 th elution; E8: 8 th elution; E9: 9 th elution; E10: 10 th elution; E11: 11 th elution.	50
Figure 12: Nitrocellulose membrane of the Western Blot performed for the fractions collected from each pull-down assay. The ladders PageRuler™ prestained protein ladder (#26616) or PageRuler™ Plus prestained protein ladder (#26619) from Thermo Fisher	

Scientific (Massachusetts, USA) were applied onto the gels. **A)** SusD70111Δ1-20 (64.3 kDa) and SusD1Δ1-22 (63.2 kDa), could be detected from microcrystalline cellulose (MC) and PET powder after the elution with Triton 2% (v/v). However, no protein could be detected from PET after 30 days of incubation under UV-C light (PET*). **B)** SusD1Δ1-22 was also tested with the synthetic polymers LDPE and PA6. The putative adsorption of this protein towards LDPE appeared to be the weakest, when compared to the other substrates. L: ladder; FT: flow through; W1: washing fraction 1; W2: washing fraction 2; E1: elution fraction 1; E2: elution fraction 2; E3: elution fraction 3. The assays for SusD1 were conducted by Tabea Neumann during her Master thesis. SusD38489Δ1-25 was evaluated as part of another work and it will not be displayed here.51

Figure 13: Native gel and affinity PAGE performed for the proteins SusD1Δ1-22 (63.2 kDa) and SusD38489Δ1-25 (65.6 kDa). The ladder PageRuler™ Plus prestained protein ladder (#26619, Thermo Fisher Scientific, Massachusetts, USA) was used as a “ruler”, ensuring that each protein would run similarly. Although native gels are not ideal for determining protein size in kDa, they are well-suited for identifying dimers, as demonstrated by the detection of SusD1 dimers in the negative control (NC; gel without substrate). CMC and PET: affinity PAGE, with a layer containing the substrates carboxymethylcellulose and PET, respectively.53

Figure 14: *E. coli* BL21(DE3) carrying genes that encode the translational protein fusions with sfGFP. A neon green color is visible under UV-C light and in the presence of 100 mg/mL of ampicillin and 1 mM of IPTG. SusD38489Δ1-25 was performed as part of another work, and it will not be presented here.54

Figure 15: Protein adsorption captured by fluorescence measurements. A) Fractions of the flow through (FT), first and second washes (W1 and W2, respectively). 200 μL of each was transferred to a 96-well microtiter plate, with transparent flat bottom and black walls. After gently shaking the plates for 3 sec, the fluorescence measurements were collected from the bottom at excitation of 485 nm and emission of 510 nm. The bars represent the mean value of the measurements collected in triplicates. Error bars represent the standard deviation. Red star represents a measurement indicated as “overflow”, meaning that most of the protein was already lost in that step. The incubations were carried out with 20 μM of protein. sfGFP or the buffer used for each incubation (potassium phosphate buffer, 0.1 M pH 6) plus the substrate were the negative controls. **B)** Following the procedure mentioned above, microcrystalline cellulose (MC) was resuspended in 200 μL of fresh buffer and transferred to the plates.55

Figure 16: Fluorescence measurements after protein incubation with chitin. Each protein at a final concentration of 20 μM incubated with 0.01 g of chitin. After removing the flow through and washing the substrate twice with potassium phosphate buffer 0.1 M pH 6, chitin powder was resuspended in fresh buffer and transferred to a 96-well microtiter plate, with transparent flat bottom and black walls. The plate was mixed for 3 sec and sfGFP measurements were collected from the bottom, at excitation of 485 nm and emission of 510 nm. The bars represent the mean value calculated from triplicates, while the error bars represent the standard deviation. The negative controls were sfGFP or buffer plus chitin.56

Figure 17: Fluorescence measurements after protein incubations with synthetic polymers. A) The synthetic polymers PA6, PET and LDPE were incubated with 20 μM of each

protein. The negative control consisted of potassium phosphate buffer 0.1 M pH 6 with each substrate. Besides, sfGFP was also used as a negative control. PET foil had a very high background in the negative controls and the measurements were not significant. sfGFP bound PA6 and LDPE, but SusD1 Δ 1-22 and SusD70111 Δ 1-25 bound PA6 and LDPE slightly better, respectively. **B)** An attempt to remove the background caused by sfGFP was testing distinct pHs, ranging from 4 to 7. PA6 was the substrate selected for this trial, once it presented the general lowest background for sfGFP. At pH 7, sfGFP presented the strongest background. At pHs 5 and 4, all the proteins denatured. Therefore, the selected pH for the tests were pH 6. The bars represent mean values obtained from tests performed in triplicates, while the error bars represent standard deviation. In each test, the substrate measured was the foil resuspended in 200 μ L of fresh buffer and transferred to the 96-well microtiter plates with transparent flat bottom and black walls. The measurements were performed after gently shaking the plates for 3 sec, from the bottom of the microtiter plate at excitation of 485 nm and emission of 510 nm.58

Figure 18: Main features of the truncated protein SusD70111_{F3}. **A)** Pull-down assay performed with the crude cell extract of SusD70111_{F3} showed putative binding towards PET, since the protein band could be detected after the elution with Triton X-100 2% (v/v). There was no visible protein band on the washing fractions. L: PageRuler™ prestained protein ladder (#26616, Thermo Fisher Scientific, Massachusetts, USA); FT: flow through; W1 and W2: washes 1 and 2, respectively; E1 and E2: elution 1 and 2, respectively. **B)** Predicted structure of SusD70111 (64.5 kDa; dark blue) and SusD70111_{F3} (25.4 kDa; dark magenta). The protein structure was mainly composed of α -helices, which is in accordance with previously-described SusD-homologs (Koropatkin et al., 2009). Six β -strands were present within the structure of SusD70111, in which four of them form β -hairpins. **C)** Predicted structure of SusD70111_{F3} in evidence. Four out of six β -strands were present in SusD70111_{F3}, because they were positioned near the C-terminus of SusD70111.59

Figure 19: Chemical structure of microcrystalline cellulose (MC), carboxymethylcellulose (CMC) and chitin, the natural polymers evaluated in this work. Designed with ChemDraw Professional© v.22.0.0.22.60

Figure 20: Chemical structure of PET and its constituents bis(2-Hydroxyethyl) terephthalate (BHET), mono-2-hydroxyethyl-terephthalate (MHET), terephthalic acid (TPA) and ethylene glycol (EG). Figure adapted from (A. Li et al., 2023). Designed with ChemDraw Professional© v.22.0.0.22.61

Figure 21: Sensorgrams obtained from the Surface Plasmon Resonance (SPR) spectroscopy. SusD70111 Δ 1-20 could not be evaluated with this approach, since the protein did not bind to the analytical chip. **A)** SusD1 Δ 1-22 and carboxymethylcellulose (CMC). Association rate: $5.2 \times 10^3/M*s$ (k_a); dissociation rate: $7.0 \times 10^{-5}/s$ (k_d); overall affinity: $K_D=14$ nM. **B)** SusD1 Δ 1-22 and bis(2-Hydroxyethyl) terephthalate (BHET). Association rate: $k_a=5.0 \times 10^5/M*s$; dissociation rate: $k_d=1.2 \times 10^{-4}/s$; overall affinity: $K_D=0.3$ nM. **C)** SusD38489 Δ 1-25 and CMC. Association rate: $k_a=5.0 \times 10^3/M*s$; dissociation rate: $k_d=6.3 \times 10^{-4}/s$; overall affinity: $K_D=124$ nM. **D)** SusD38489 Δ 1-25 and BHET. Association rate: $k_a=1.2 \times 10^5/M*s$; dissociation rate: $k_d=1.0 \times 10^{-3}/s$; overall affinity: $K_D=10$ nM. **E)** Truncated protein SusD70111_{F3} and CMC. Association rate: $k_a=6.6 \times 10^3/M*s$; dissociation rate: $k_d=2.0 \times 10^{-4}/s$; overall affinity: $K_D=0.3$

- nM. **F)** SusD70111_{F3} and BHET. Association rate: $k_a=9.4 \times 10^4/M*s$; dissociation rate: $k_d=1.5 \times 10^{-4}/s$ and overall affinity: $K_D=1.6$ nM. Each curve was subtracted by the reference curve, used as a negative control.....64
- Figure 22: Enzymatic screening using agar plates with the substrates of interest. A)** Activity plates of SusD1Δ1-22 fused with LCC-WT (Sulaiman et al., 2012) on bis(2-Hydroxyethyl) terephthalate (BHET; top) and polycaprolactone (PCL; bottom). **B)** SusD1Δ1-22 fused with PET30ΔPorC (Zhang et al., 2021) on a BHET agar plate. The experiments were performed with 10 μL of crude cell extract. Red arrows indicate the translational fusions.65
- Figure 23: Chromatograms of PET30ΔPorC (top) (Zhang et al., 2021) and SusD1Δ1-22::PET30ΔPorC (bottom) after 72 and 120 h of incubation with amorphous PET foil.** The 72-h incubation presented a peak with an area of 1.3692 (TPA concentration of 1.7543 μM), whereas the 120-h incubation had an increased area of 1.6601 (TPA concentration of 2.127 μM).....66
- Figure 24: Chromatograms of LCC-WT (top) (Sulaiman et al., 2012) and SusD1Δ1-22::LCC-WT (bottom) after 72h and 120 h of incubation with amorphous PET foil.** LCC-WT TPA concentration after 72 h: 17.734 μM and after 120 h: 55.391 μM. However, the TPA concentration of SusD1Δ1-22::LCC-WT decreased to 4.499 μM after 72 h and 4.559 μM after 120 h.67
- Figure 25: Colony PCR of the translational protein fusions of *susD1Δ1-22* and *susD38489Δ1-25* with *lacZ*.** The *susD*-homologs had their N-terminal signal peptide removed and were fused to the C-terminal with the enzyme. The red arrows represent the clones with expected size that were randomly selected and further analyzed by Sanger sequencing. *SusD1Δ1-22* final construct had 2106 bp and *susD38489Δ1-25* had 2139 bp. A His₆-tag was positioned on the C-terminal of each construct. The ladder applied to the gel was GeneRuler™ 1 Kb DNA ladder (Thermo Fisher Scientific, Massachusetts, USA).68
- Figure 26: Structure of SusD1 and SusD38489 docking with microcrystalline cellulose (MC). A)** Side view of SusD1 with 180° rotation. **B)** Bottom view of SusD38489 structure with the predicted binding sites. Both proteins presented three putative binding sites, formed by pockets on the proteins' surface. The surfaces were color-coded by hydrophobicity, where blue represents the most hydrophilic and yellow represents the most hydrophobic residues.....72
- Figure 27: Side view of SusD70111 docking with chitin.** The amino acids found in the putative binding site are shown in detail. Three putative binding sites were found, which appear to be in pockets. The surface was color-coded by hydrophobicity: blue represents the most hydrophilic and yellow the most hydrophobic residues.73
- Figure 28: Structural alignment of SusD1 and SusD38489 with SusD1[†] and SusD2 (Mackenzie et al., 2012) and SusD70111 with CusDI and CusDII (Larsbrink et al., 2016).** The NCBI or PDB accession numbers are provided. †: Not the same SusD1 as the one characterized in this work. Red square and pink triangle represent the amino acids found in the carboxymethylcellulose docking of SusD38489 and SusD1, respectively. Purple star and yellow heart are the residues found in the microcrystalline cellulose docking of SusD1 and SusD38489, respectively. Blue smiley represents the amino acids identified at the putative binding site of SusD70111 with chitin.74

- Figure 29: Docking of SusD with PET trimer. A) and B)** SusD1 and SusD38489 with exposed amino acids around the putative binding site. In SusD38489, the underlined one-letter coded residues N147, W83, I86 and H88 were also identified in SusD1. The residues represented in italic show that the amino acids in the same structural position were replaced. Besides, V and Q at distinct positions were also identified on both proteins. **C) and D)** SusD1 and SusD38489, respectively, with surface color-coded by hydrophobicity. Yellow represents the most hydrophobic while blue represents the most hydrophilic residues.76
- Figure 30: SusD70111 docking with PET trimer.** Two putative binding sites were identified and the amino acids present in each region were exposed. The docking sites were structurally distinct to SusD1 and SusD38489 and the residues possible involved in protein binding were also not the same.77
- Figure 31: Structure of the truncated protein SusD70111_{F3}.** The docking was performed with PET trimer and the residues located around the putative binding site were exposed. ...78
- Figure 32: Structural alignment of SusD1, SusD38489 and SusD70111.** The black bar indicates the region where the tetratricopeptide was predicted in SusD70111. However, SusD1 and SusD38489 did not present a tetratricopeptide region, suggesting that both proteins are non-conserved. These two proteins share structural and sequence similarity, with the residues S79, Y80, W83, I86, H88, Y146 and N147 being found in the putative binding sites (indicated with a star).....81
- Figure 33: Proposed changes to PET chain after exposure to UV-C light.** Figure adapted from (Falkenstein et al., 2020). Designed with ChemDraw Professional© v.22.0.0.22.91
- Figure 34: Structural analysis of SusD1, SusD70111 and PilF, a protein responsible for the type IV pilus biogenesis in *Pseudomonas aeruginosa*.** PilF was previously identified as a structural homolog of SusD (Koropatkin et al., 2008). **A)** SusD1 (in pink) presented similarity with the chain B of PilF (light green). **B)** SusD70111 (red) was like chain A of PilF (forest green).....94

- Figure S1: DNA ladders used for the 0.8% agarose electrophoresis. A)** GeneRuler™ 1 Kb DNA Ladder. **B)** GeneRuler™ 100 bp DNA Ladder. Both ladders were manufactured by Thermo Fisher Scientific (Massachusetts, USA)..... 108
- Figure S2: Protein ladders used for SDS PAGE and Western Blot. A)** PageRuler™ unstained protein ladder (#26614) used for SDS PAGE. **B)** and **C):** PageRuler™ prestained protein ladder (#26616) and PageRuler™ prestained plus protein ladder (#26619), respectively. Both prestained ladders were used for Western Blot, affinity and native PAGE. All the protein ladders were manufactured by Thermo Fisher Scientific (Massachusetts, USA)..... 108
- Figure S3: Translational fusion of *susD1Δ1-22* and *susD38489Δ1-25* with *lacZ*.** To check for the correct expression of *lacZ* by its capability of degrading X-GAL, agar plates containing LB, 100 mg/mL of ampicillin, 1 mM of isopropyl-β-D-thiogalactopyranoside (IPTG) and 20 mg/mL of X-GAL were prepared. The proteins were cloned and transformed in the expression vector *E. coli* BL21(DE3), and incubated overnight at 37 °C. X-GAL is the natural substrate of *lacZ* and, when utilized, produces a visible blue color on the bacterial colonies..... 109
- Figure S4: Structure of SusD70111_{F3} docking with chitin.** Two putative binding sites were identified. The amino acids were exposed and identified by one letter code. The same sites were also predicted for CMC binding..... 109
- Figure S5: Docking studies of SusD1Δ1-22 or SusD70111Δ1-20 fused with sfGFP. A)** SusD1Δ1-22::sfGFP::His₆-tag docking with PET trimer. One putative binding site was detected, being the same as the WT protein. **B)** SusD70111Δ1-20::sfGFP::His₆-tag docking with PET trimer. Two putative binding sites were detected, the same ones as the WT proteins. In both scenarios, the fusion with sfGFP appeared to not interfere with protein adsorption..... 110
- Figure S6: Docking of SusD1 (A) and SusD38489 (B) with bis(2-Hydroxyethyl) terephthalate (BHET).** In both cases, two putative binding sites were detected. The amino acids are presented with one-letter code. Red indicates when the residue was also found in the predicted binding site of PET trimer, while underline points to the occurrence of the same residue in both SusD1 and SusD38489..... 111

List of Tables

Table 1:	<i>SusD</i> -homologs and their respective substrates.	8
Table 2:	Constructs used in this work.	19
Table 3:	Bacterial competent cells used in this work.	22
Table 4:	PCR pipetting calculation.	24
Table 5:	Touchdown PCR conditions.	25
Table 6:	3-step PCR conditions.	26
Table 7:	Universal primer pair for the colony PCR.	26
Table 8:	Recipe of the autoinduction medium (Studier, 2005).	27
Table 9:	Recipe used for the preparation of SDS PAGE gels.	30
Table 10:	Recipe of the other reagents required to run the SDS PAGE.	30
Table 11:	Recipe used for the preparation of native and affinity polyacrylamide gels.	31
Table 12:	Recipe of 5x protein loading dye and 10x native running buffer pH 8.3.	31
Table 13:	Amount of each reagent required for the preparation of solutions used for Western Blot.	34
Table 14:	Average values obtained during protein purification and considered for the pull-down assay.	35
Table 15:	Characteristics of the protein pockets identified with GeoMine (Diedrich, 2021). ...	79
Table 16:	Binding modules that could be further tested regarding their adsorption to PET or other synthetic polymers.	97
Table S1:	Primers and Touchdown PCR cycling conditions for the signal peptide removal and <i>susD70111_{F3}</i> to produce <i>susD70111_{F3}</i>	98
Table S2:	C-terminal <i>susD</i> fusion to superfolder GFP (<i>sfGFP</i>).	100
Table S3:	<i>SusD1Δ1-22</i> fusion to <i>pet30ΔporC</i> [72] and <i>lcc-wt</i> [73]	102
Table S4:	<i>SusD1Δ1-22</i> and <i>susD38489Δ1-25</i> fusion to <i>lacZ</i> . The negative control (<i>lacZ</i> in pET21a(+)) was also prepared following the conditions described.	104
Table S5:	Amino acids identified in the putative binding sites of <i>SusD1</i> , <i>SusD38489</i> , <i>SusD70111</i> and <i>SusD70111_{F3}</i> . Docking was performed with microcrystalline cellulose (MC), carboxymethylcellulose (CMC), chitin, PET trimer and bis(2-Hydroxyethyl) terephthalate (BHET).	106

List of Abbreviations

Å:	Ångström;	°C:	Degree Celsius;
Å²:	Ångström squared;	C₆H₉Na₃O₉:	Sodium citrate dihydrate;
Å³:	Ångström cubed;	C₆H₈O₇:	Citric acid;
A:	Ampere;	CBMs:	Carbohydrate binding modules;
Aa:	Amino acids;	ChBD:	Chitin binding domain;
APS:	Ammonium persulfate solution;	CMC:	Carboxymethyl-cellulose;
<i>B. thetaiotaomicron</i>:	<i>Bacteroides thetaiotaomicron</i> ;	DMF:	Dimethylformamide;
<i>B. ovatus</i>:	<i>Bacteroides ovatus</i> ;	DMSO:	Dimethyl sulfoxide;
<i>B. fluxus</i>:	<i>Bacteroides fluxus</i> ;	DNA:	Deoxyribonucleic acid;
<i>B. fragilis</i>:	<i>Bacteroides fragilis</i> ;	E1-11	Elution 1 to 11;
BCIP:	5-Bromo-4-chloro-3-indolyl phosphate;	<i>E. coli</i>:	<i>Escherichia coli</i> ;
BHET:	Bis(2-hydroxyethyl) terephthalate;	EDTA:	Ethylenediaminetetraacetic acid;
BLASTp:	Basic local alignment search tool (proteins);	EG:	Ethylene glycol;
Bp:	Base pairs;	F1-F5:	Fractions 1-5;
BSA:	Bovine serum albumin;	F2, F3, F3a and F5:	Fragments 2, 3, 3a and 5

FAST-PETase:	Functional, active, stable and tolerant PETase;	k_d:	Dissociation rate;
FCWusD:	SusD-homolog from the fungal cell wall utilization locus;	K_D:	Overall affinity;
FT:	Flow through;	kDa:	Kilodalton;
G:	Grams;	KH₂PO₄:	Potassium phosphate;
GH:	Glycoside hydrolase;	L:	Litre;
H₂O_{dd}:	Bidistilled water;	<i>L. cyclotis</i>:	<i>Loxodonta cyclotis</i> ;
H:	Hours;	LacZ:	β-galactosidase;
HCl:	Hydrochloric acid;	LB:	Lysogeny Broth medium;
HEPES:	4-(2-hydroxyethyl)-1-piperazineethanesulfonic acid	LCC-WT:	Leaf-compost cutinase wild type;
HF:	High fidelity;	LDPE:	Low-density polyethylene;
His₆:	Hexahistidine-tag;	M*s:	Meter per second;
IPTG:	Isopropyl-β-D-thiogalactopyranoside ;	m:	Mili;
IsPETase:	<i>Ideonella sakaiensis</i> PETase;	M:	Molar;
ITC:	Isothermal titration calorimetry;	MC:	Microcrystalline cellulose;
K₂HPO₄:	Dipotassium phosphate;	Min:	Minutes;
k_a:	Association rate;	MLG:	Mixed linkage glucan;
Kb:	Kilobase;	MgSO₄-SL:	Magnesium sulphate solution;
KCl:	Potassium chloride;	MgCl₂:	Magnesium Chloride;

MHET:	Mono-2-hydroxyethyl-terephthalate;	PA(6):	Polyamide (6; nylon 6);
MU-GAL:	MU- β -D-galactopyranoside;	PAGE:	Polyacrylamide gel electrophoresis;
N:	Binding stoichiometry;	PBS:	Phosphate buffered saline;
n:	Nano (10^{-9});	PCL:	Polycaprolactone;
NA:	Not applied;	PCR:	Polymerase chain reaction;
NaCl:	Sodium chloride;	PE:	Polyethylene;
Na₂HPO₄:	Disodium phosphate;	PET:	Polyethylene terephthalate;
Na₂SO₄:	Sodium sulphate;	<i>P. aeruginosa</i>:	<i>Pseudomonas aeruginosa</i>
NanU:	Extracellular neuramine uptake protein;	<i>P. gingivalis</i>:	<i>Porphyromonas gingivalis</i> ;
NBT:	Nitro blue tetrazolium chloride;	Pmol:	Picomol (10^{-12} moles);
NC:	Negative control;	PP:	Polypropylene;
NCBI:	National Center for Biotechnology Information;	PS:	Polystyrene;
ND:	Not defined;	Psi:	Pound force per square;
NH₄Cl:	Ammonium chloride;	PVC:	Polyvinyl Chloride;
NiNTA:	Nickel affinity chromatography;	PU:	Polyurethane;
Nm:	Nanometer;	PUL:	Polysaccharide utilization loci;
OD₆₀₀:	Optical density;	RagB:	Receptor antigen B;

List of Abbreviations

RFU:	Relative fluorescence units;	UV:	Ultraviolet;
Rpm:	Revolutions per minute;	V:	Volts;
RU:	Response Unities;	V/v:	Volume per volume;
SDS:	Sodium dodecyl sulphate;	W1-2	Wash one and two;
Sec:	Seconds;	WT:	Wild type;
Sec/SPII:	Secretion signal peptide;	W/v:	Weight per volume;
SfGFP:	Superfolder GFP;	X-GAL:	5-bromo-4-chloro-3-indolyl- β -D-galactopyranoside;
SGBPs:	Surface glycan binding proteins;	x g:	Relative centrifugal force unit;
SPR:	Surface plasmon resonance;	μ:	Micro (10^{-6});
SR:	Synthetic rubber;	ΔG:	Free-Gibbs energy;
Sus(A-G; R):	Starch utilization system (Proteins SusA-F; transcriptional regulator SusR);		
TAE:	Tris base, acetic acid and EDTA;		
T_{ann}:	Annealing temperature;		
TBS(T):	Tris-buffered saline (Tween 20);		
TEMED:	Tetramethylethylenediamine;		
TFA:	Trifluoroacetic acid;		
T_m:	Melting temperature;		
TPA:	Terephthalic acid;		
UHPLC:	Ultra-high-performance liquid chromatography;		

I. Introduction

1.1 Gut microbiota of humans and animals

Gut microbiota is the name given to a complex of microorganisms that inhabit the gastrointestinal tract (Magne et al., 2020; Zhang et al., 2023). Some of these microorganisms have a symbiotic relationship with their host, by preventing pathogen colonization and degrading nutrients that the host is not able to digest (Magne et al., 2020; Zhang et al., 2023). In humans, a healthy microbiota is largely occupied by microorganisms from the phyla Bacteroidota and Bacillota, followed by Pseudomonadota, Actinomycetota and Verrucomicrobiota (Magne et al., 2020; Qin et al., 2010). However, the diversity ratio might be affected by distinct factors such as nutrition, age and sex (Campaniello et al., 2022). Herbivores (including hindgut (Ilmberger et al., 2014; Kandel et al., 2020; Li et al., 2022) and foregut (Wu et al., 2022; Zeineldin et al., 2018) fermenters) can also be affected by the same factors.

Previous studies have characterized the microbiota of Asian elephants (*Elephas maximus*), originally distributed throughout South and Southeast Asia (Ilmberger et al., 2014; Kandel et al., 2020; Li et al., 2022; Zhang et al., 2023). These animals are generalist herbivores with elongated hindgut, and the food fermentation occurs in the colon or caecum (Ilmberger et al., 2014). Elephants have a rapid digestion of the food, which is advantageous due to their body size and allows them to eat more (Ilmberger et al., 2014). Similarly, there is a predominance of the phyla Bacteroidota and Bacillota, followed by Pseudomonadota (Kandel et al., 2020; Li et al., 2022). As observed by Li et al., wild elephants displayed higher abundance of Pseudomonadota than semi-captive elephants (Li et al., 2022). The microbiome of the African savanna elephant (*Loxodonta africana*) and the African forest elephant (*Loxodonta cyclotis*) presented the same three phyla mentioned above, but with distinct ratios (Budd et al., 2020).

Foregut fermenters (or ruminants) represent another group of herbivores, able to effectively digest lignocellulose by prolonged chewing (Dai et al., 2012; Ilmberger et al., 2014). Representatives of this group include bovine, sheep, goat and deer. The rumen microbiota is responsible for the prevention of diseases (Hu et al., 2022; Zeineldin et al., 2018) and the maintenance of homeostasis has shown importance on husbandry, with proposed enhanced milk quality (Xue et al., 2020). The phyla Bacillota and Bacteroidota are also largely identified on the rumen microbiota, both with different specialized mechanisms of nutrient acquisition (Zeineldin et al., 2018). In this work, we focus on the acquisition of nutrients by the phylum Bacteroidota.

1.2 The importance of the operon *sus* to the phylum Bacteroidota

A remarkable characteristic of the phylum Bacteroidota is the presence of the Polysaccharide Utilization Locus (PUL), responsible for the degradation of carbohydrates that are indigestible for the host (Bjursell et al., 2006; Foley et al., 2016). The operon *sus* (Starch Utilization System) is an important part of PUL, presenting genes that encode three glycoside hydrolases (GH; *susA*, *susB* and *susG*), one Ton-B dependent porin (*susC*), three binding proteins (*susD*, *susE* and *susF*; frequently referred to as “Surface Glycan Binding Proteins” (SGBPs) (Correia et al., 2021; Tamura et al., 2021; Tamura et al., 2019)), as well as a transcriptional regulator induced by maltose (*susR*) (Bakolitsa et al., 2010; Foley et al., 2016; Shipman et al., 2000) (Figure 1). *Bacteroides thetaiotaomicron* is the model of many PUL studies, and it was previously shown that these microorganisms redirect their “carbohydrate foraging machinery” according to the nutrients available from the host’s diet (Bolam & Koropatkin, 2012; Sonnenburg et al., 2005).

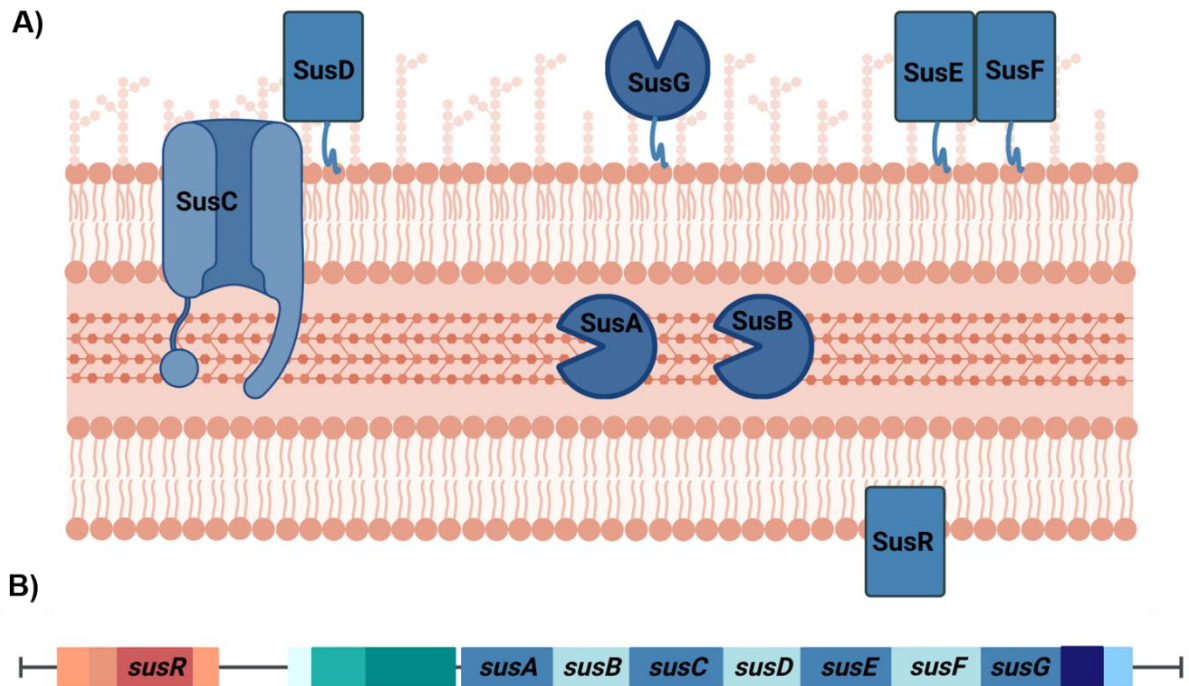


Figure 1: Schematic representation and operon map from *susA* to *susG* and the transcriptional regulator *susR*. **A)** Protein distribution in a microorganism from the phylum Bacteroidota. The top layer represents the outer membrane, with the binding proteins SusD-F, as well as the α -amylase SusG, responsible for breaking the substrates into oligosaccharides of easy transport (Bakolitsa et al., 2010; Foley et al., 2016). SusD is associated with the TonB-dependent β -barrel protein SusC, which facilitates the transport of oligosaccharides to the periplasm (Bakolitsa et al., 2010; Bjursell et al., 2006; Bolam & Koropatkin, 2012; Cho & Salyers, 2001; Foley et al., 2016). SusA is a neo-pullulanase and SusB a α -glucosidase enzyme, being both located in the periplasm (Foley et al., 2016). SusR regulator, activated by maltose, is placed on the inner membrane (Bakolitsa et al., 2010; Bjursell et al., 2006; Foley et al., 2016). **B)** Organization of the operon *sus*, encoding the genes *susRABCDEF*G. *SusR* is represented in red, the promoter represented in green and the genes responsible for encoding *susA* to *susG* in distinct shades of blue. Created in BioRender.com.

SusD-homologs have been found in most of the sequenced gut Bacteroidota (Cameron et al., 2014). The gene pair *susC/susD* comprises approximately 18% of *B. thetaiotaomicron* genome (Bjursell et al., 2006; Goulas et al., 2016; Martens et al., 2009). SusC (approximately 115 kDa) is an active transporter that works in complex with the binding module SusD, which makes the nutrient acquisition efficient even at low concentrations (Bolam & van den Berg, 2018). While SusC is a β -barrel transmembrane protein (Bjursell et al., 2006; Bolam & van den Berg, 2018), SusD

structure mostly comprises α -helices (Bolam & Koropatkin, 2012; Foley et al., 2016). For this reason, SusD-homologs are very distinct from CBMs, in which a typical structure presents a β -sandwich of 100 up to 150 residues (Bolam & Koropatkin, 2012). Likewise, SusD-homologs does not have detectable homology to known CBMs (Koropatkin et al., 2008).

Interestingly, Zhu *et al.* reported that *Cytophaga hutchinsonii* strain CH428 presented only two copies of *susC* and *susD* genes. Through site-directed mutagenesis, the authors demonstrated that neither of these genes was essential for cellulose uptake and degradation (Zhu et al., 2015). Therefore, this finding led to the suggestion that *C. hutchinsonii* might employ alternative mechanisms for cellulose utilization that do not involve the PUL system (Zhu et al., 2015).

The complex SusC/SusD works with a “pedal bin” mechanism (Glenwright et al., 2017; Gray et al., 2021). When the ligand is bound to SusD, the complex adopts a closed state and the transport mediated by TonB is activated (Glenwright et al., 2017; Gray et al., 2021). The structure and function of this complex is probably conserved, as the proteins from the receptor antigen A and B (RagA/RagB) family behave similarly. RagA and B are largely described in the oral pathogen *Porphyromonas gingivalis* (phylum Bacteroidota). Previously, *P. gingivalis* RagA/RagB had predicted similarity to *B. thetaiotaomicron* SusC/SusD (Goulas et al., 2016; Hall et al., 2005; Hanley et al., 1999). A quick search for RagA/RagB in the [PDB Database](#) (accessed on 07/02/2024; (Berman et al., 2000; Burley et al., 2021)) revealed the complex structure is an open (6SML) or closed (6SM3) state (Madej et al., 2020) (Figure 2A and B). The search for SusC/SusD complex also retrieved distinct conformations of the complex (PDB accession numbers 6ZLT and 6ZLU) (Gray et al., 2021) (Figure 2C and D).

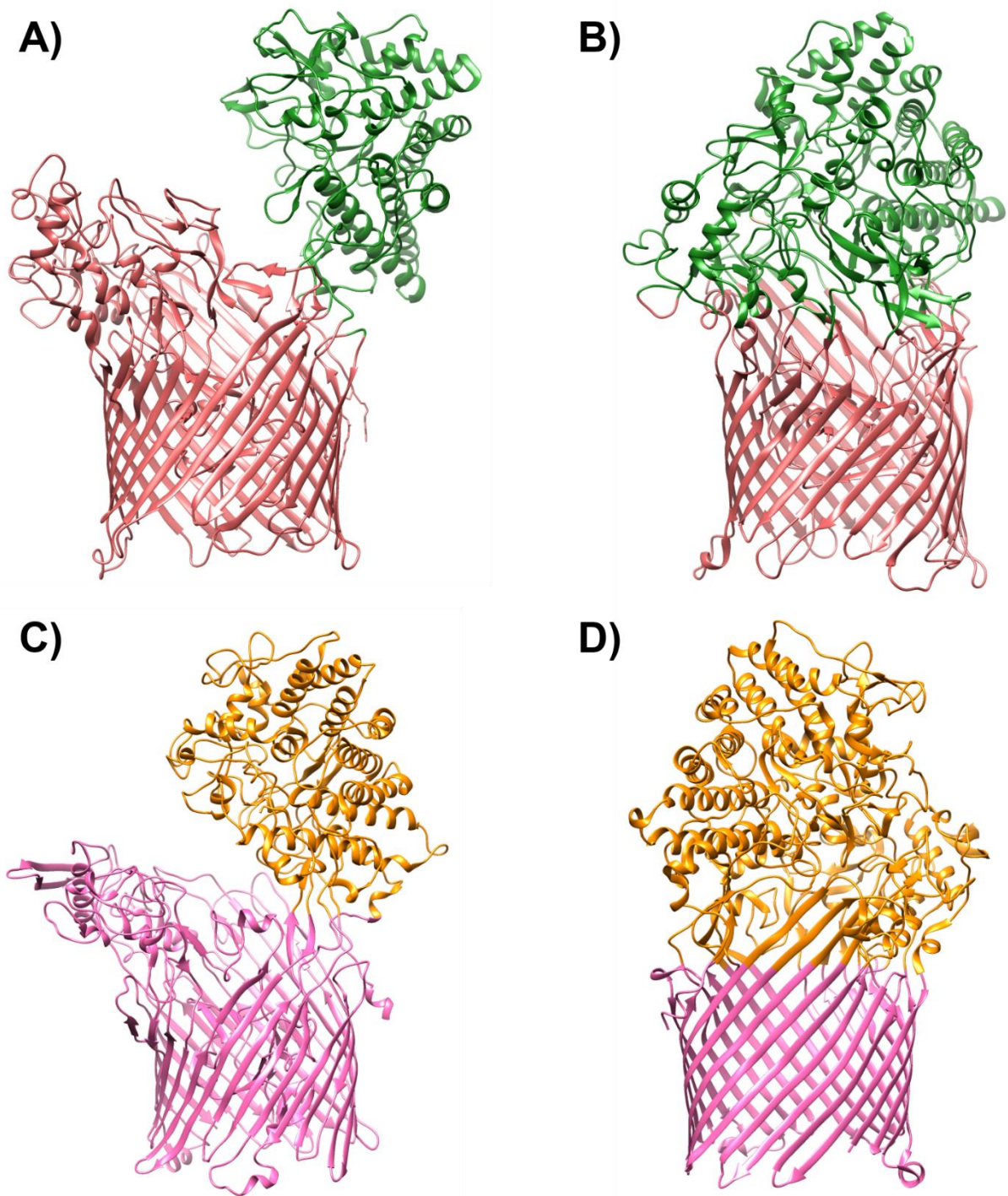


Figure 2: Structure of the complexes RagA/RagB and SusC/SusD. **A)** RagA/RagB complex in an open state (PDB accession number 6SML) (Madej et al., 2020). **B)** After the ligand is bound, RagA/RagB adopts a closed state (6SM3) (Madej et al., 2020). RagA is represented in red and RagB in green and they belonged to the microorganism *Porphyromonas gingivalis*. **C)** SusC/SusD complex open (6ZLT) (Gray et al., 2021). **D)** SusC/SusD closed (6ZLU) (Gray et al., 2021). SusC is represented in pink and SusD in orange. The structures are from *Bacteroides thetaiotaomicron*. In general, the nutrient acquisition mechanism of both protein complexes resembles a “pedal bin” model.

1.3 Affinity of SusD to various substrates

The archetypal operon *sus* was first characterized by Salyers group (Anderson & Salyers, 1989; Cho & Salyers, 2001). This operon was part of a PUL of *B. thetaiotaomicron* and encoded proteins that were essential for the bacterial growth on amylose, amylopectin, pullulan, and maltooligosaccharides not shorter than three glucose unities (Anderson & Salyers, 1989; Koropatkin et al., 2008). SusC and SusD form an outer membrane complex and, alongside the GH SusG, are considered the minimal proteins required for *B. thetaiotaomicron* growth on starch (Cho & Salyers, 2001; Foley et al., 2016). SusD is able to detect starch even at low concentrations (Cameron et al., 2014), while the presence of SusE and SusF increase the affinity to starch by approximately 20% each (Martens et al., 2009; Shipman et al., 2000). Furthermore, the inframe deletion of *susD* (Δ *susD*) could not grow on maltooligosaccharides larger than maltopentaose, and the growth in maltopentaose and maltotetraose was impaired (Koropatkin et al., 2008). Therefore, it was suggested that SusD was dispensable for the utilization of small oligosaccharides (maltotriose and maltose) (Foley et al., 2016; Koropatkin et al., 2008).

This work focuses on SusD, due to its importance on substrate adsorption. The name “Starch Utilization System” represented a suitable nomenclature, but it has become obsolete nowadays. Besides starch, *susD*-homologs have also been described to bind cellulose (Dai et al., 2012; Mackenzie et al., 2012), xylan (Dodd et al., 2011), the algae compounds laminarin and pustulan (Mystkowska et al., 2018) and many others. In previous work, SusD-homologs have also shown better affinity for long-chain saccharides (Correia et al., 2021; Tamura et al., 2019). Table 1 summarizes previously reported SusD-homologs’ adsorption to distinct substrates.

Table 1: *SusD*-homologs and their respective substrates.

Protein	Microorganism	Binding	Reference
FCWusD	<i>Chitinophaga pinensis</i>	Curdlan, yeast β -glucan, lichenan, and barley β -glucan (β 1,3-glucans)	(Lu et al., 2023)
SGBP _{MLG-A}	<i>Bacteroides ovatus</i>	Barley, lichenan and microalgae enriched β -glucan fraction (Mixed Linkage β 1,3-1,4-Glucans); Tamarind xyloglucan, konjac glucomannan, hydroxyethylcellulose (β 1,4-linked backbone with glucosyl residues); Microcrystalline cellulose (β 1,4-D-glucose)	(Correia et al., 2021; Tamura et al., 2019)
SGBP A	<i>Bacteroides fluxus</i> and <i>Bacteroides thetaiotaomicron</i>	Laminarioligosaccharide (β 1,3-glucan)	(Tamura et al., 2021)
SusD-213	<i>Zobellia galactanivorans</i>	Xyloglucan (highly branched plant cell wall polysaccharides)	(Salmean et al., 2018)
SusD	<i>Gramella sp.</i>	Laminarin (β 1,3-D-glucose with β 1,6-linked side chains) and pustulan (β 1,6-glucan)	(Mystkowska et al., 2018)
SusD	<i>B. thetaiotaomicron</i>	Fungal cell wall glycan (β 1,6-glycan)	(Temple et al., 2017)

I. Introduction

SusD 3296	<i>B. thetaiotaomicron</i>	β -cyclodextrin (cyclic α 1,4-linked glucose subunits)	(Chaudet & Rose, 2016)
SusD 4558 and 4561	<i>Flavobacterium johnsoniae</i>	Chitin (β 1,4-linked N-acetyl-D-glucosamine)	(Larsbrink et al., 2016)
SusD	Uncultured <i>Bacteroides</i>	Xylooligosaccharides (2-7 xylose molecules linked by β 1,4 glycosidic bonds)	(Tauzin et al., 2016)
NanU	<i>Bacteroides fragilis</i>	Sialic acid (α -keto-acid sugars)	(Phansopa et al., 2014)
SusD1 [†] and SusD2	Uncultured <i>Bacteroides</i>	Various forms of cellulose (β 1,4-D-glucose)	(Mackenzie et al., 2012)
SusD 1043	<i>B. thetaiotaomicron</i>	Mucin (O-linked glycan)	(Koropatkin et al., 2009)
SusD	<i>B. thetaiotaomicron</i>	Starch with ≥ 6 glucose unities (α 1,4-linked sugars) α - and γ -cyclodextrin (cyclic α 1,4-linked glucose subunits)	(Koropatkin et al., 2008)

†: A different SusD1 protein from the one analyzed in the present work. FCWusD: SusD-homolog from the fungal cell wall utilization locus (FCWUL); SGBP A: surface glycan binding protein A; MLG: mixed linkage glucan; NanU: extracellular neuramine uptake protein.

The SGBP named BoSGBP_{MLG-A} is a *susD*-homolog from *B. ovatus* that binds mixed linkage glucan (MLG) by mediated shape complementation of the binding site with a twisted conformation of the oligosaccharide backbone (Tamura et al., 2019). Mutations on the binding site, as well as a knocked-out mutant, resulted on impaired MLG utilization (Correia et al., 2021; Tamura et al., 2019). MLG is a linear polysaccharide of D-glucopyranose with blocks of β 1,4-linked residues flanked by single β 1,3-linkages (Correia et al., 2021). They are usually present in cereal crops such as oats and barley (Correia et al., 2021; Dejean et al., 2020; Tamura et al., 2021). Other types of β -linkage glucan include β 1,4-, β 1,3-, and β 1,6-glucans. β 1,4-linked glucans compound the backbone of the most abundant polysaccharides on earth: cellulose (with β 1,4-D-glucose; found in plant cell walls (Dai et al., 2012)) and chitin (β 1,4-linked N-acetyl-D-glucosamine; Fungi and in the exoskeleton of arthropods (Larsbrink et al., 2016)). When compared to β 1,3 glucan, β 1,4-linked glucan chains are rigid and hydrophobic (Correia et al., 2021). β 1,3-glucans are flexible and hydrophilic chains, commonly found in Fungi and plants, while β 1,6-glucans are mainly from edible fungus (Dejean et al., 2020; Tamura et al., 2021).

In this work, the characterization of three *susD*-homologs adsorption to natural and synthetic polymers was addressed. It was the first time that *susD*-homologs were screened with synthetic polymers from non-sustainable origin. The following topics address the relevance of finding suitable binding modules to deal with the plastic pollution problem.

1.4 Fossil-fuel based polymers as ubiquitous pollutants

The importance of screening for binding modules with high affinity and easy detection of synthetic polymers relies on the fact that around 360 to 400 million metric tons of plastics are produced worldwide every year, while the recycling rates are still not effective (Chow et al., 2022). Due to the low-cost production, many plastics are conceived as single-use material and, consequently, inappropriately disposed of in landfills or in the environment (Chow et al., 2022; Geyer et al., 2017; Roy et al., 2011). Furthermore, small-size particles (micro- and nanoplastics) can be found in almost every ecological niche (Blasing & Amelung, 2018; Brandon et al., 2019; Chow et al., 2022; Geyer et al., 2017; Jambeck et al., 2015). Micro (1 μ m-5 mm diameter) and nanoplastics (1 nm-1 μ m) might even accumulate in the food chain and impact human and animal homeostasis (Chow et al., 2022). For example, vinyl chloride is carcinogenic to humans and animals (Gricajeva, 2021; Rudel et al., 2007). Recently, microplastics were found for the first time in human placenta (Ragusa et al., 2021) and in human blood (Leslie et al., 2022).

Fossil-fuel-based polymers account for most of the synthetic polymers produced (>95%) for over 80 years (Chow et al., 2022). Because of the thermostability, the biodegradation of these materials is a very slow process, which sometimes takes hundreds of years in nature (Roy et al., 2011). The main types (from largest to lowest scale production) includes polyethylene (PE), polypropylene (PP), polyvinyl chloride (PVC), polyurethane (PU), polyamide (PA), polyethylene terephthalate (PET), polystyrene (PS) and synthetic rubber (SR; Figure 3) (Chow et al., 2022; Kumari et al., 2019). From being the source to produce packaging (plastic bags, films and bottles),

medical implants and laboratory supplies, to the application in the construction, clothing and automotive industries, plastics are ubiquitous in our lives.

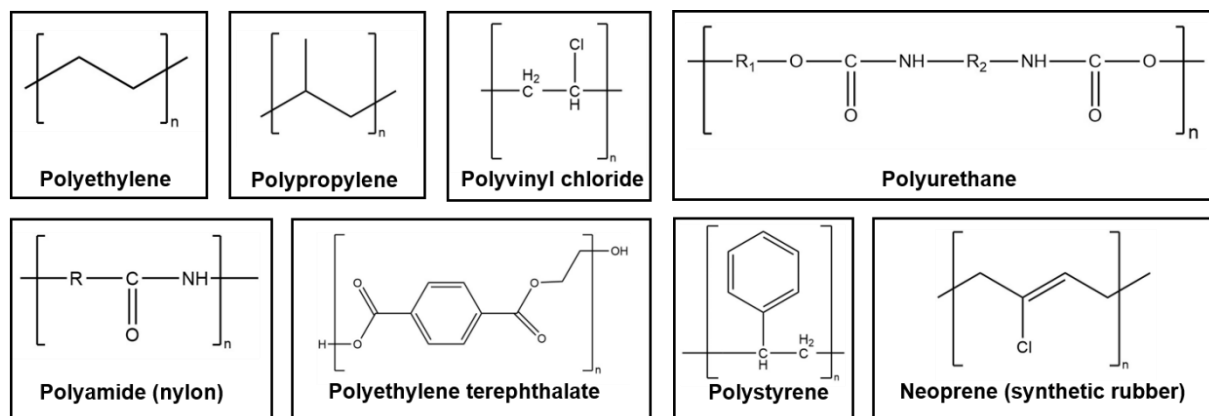


Figure 3: Polymers produced from fossil-fuel sources. From top to bottom and in the order of highest to lowest scale production: chemical structure of polyethylene (PE), polypropylene (PP), polyvinyl chloride (PVC), polyurethane (PU), polyamide (nylon; PA), polyethylene terephthalate (PET), polystyrene (PS) and neoprene (from the family of synthetic rubbers; SR). Designed with ChemDraw Professional© v.22.0.0.22.

1.5 Enzymatic optimization with binding modules

On the industrial scale, there are distinct ways to tune enzymes that also present activity towards fossil-fuel based polymers, especially PET (known as PETases and usually related to the α/β -hydrolase family (Danso et al., 2018)). One of them consists of the construction of mutants, which in some cases present enhanced activity towards PET when compared to the wild type (WT) (Lu et al., 2022). The manipulation of the catalytic domains can generate a more promiscuous enzyme (Roda, 2021). For example, Qu *et al.* demonstrated that the addition of salt bridges in the flexible region of IsPETase improved the thermal stability by 7.4 to 8.7 °C, with 4.3 times more degradation product release than the WT (Qu et al., 2023). Computer-assisted strategies are also being successfully employed. Cui *et al.* generated an enzyme with

ten mutation sites of IsPETase and increased melting temperature of 31 °C, named DuraPETase (Cui, 2021). Using a machine learning algorithm, Lu *et al.* constructed a PET hydrolase mutant named FAST-PETase with increased temperature and pH ranges, in addition to the ability of degrading post-consumer PET (Lu *et al.*, 2022). Finally, a variant named TurboPETase was recently described by Cui *et al.* (Cui *et al.*, 2024). TurboPETase present enhanced performance, when compared to well-known PETases. The assays revealed that solid PET is nearly entirely depolymerized within 8 h (Cui *et al.*, 2024).

Another approach consists of the addition of a non-catalytic binding domain, because the WT enzymes degrading natural substrates (such as cellulases and chitinases) usually present a catalytic and a non-catalytic binding domain (Graham, 2022; Ji *et al.*, 2021). The hydrophobic structure of PET might be challenging for enzymatic adsorption, and the suitable non-catalytic binding module would tune enzymatic activity by anchoring the enzyme to the substrate (Weber *et al.*, 2019). Previous works on the literature describe distinct families of carbohydrate binding modules (CBMs) fused to natural substrate degraders and their activity towards PET (Graham, 2022; Weber *et al.*, 2019). Besides, a chitin binding domain (ChBD) (Xue *et al.*, 2021) and anchor peptides (Ji *et al.*, 2021) were also previously reported to have improved adsorption towards PET. Similarly, when SusD presents additional adsorption towards plastics, the translational fusion with previously described PETases might be performed.

1.6 Aim of the study

The first part of this work focuses on the characterization of three *susD*-homologs: two of them from previously described elephant feces metagenome (named *susD70111* and *susD38489*) (Ilmberger et al., 2014) and one from cow rumen metagenome (*susD1*) (Rosewarne et al., 2014). The N-terminal signal peptide was removed, originating the mutants *susD70111* Δ 1-20, *susD38489* Δ 1-25, *susD1* Δ 1-22. Bioinformatics analysis of protein structure and docking were also performed.

In this initial part, we wanted to establish a fast and reliable protocol for the screening of binding proteins with natural and synthetic polymers, with particular focus on PET. Translational protein fusions of *susD* with the fluorescent label superfolder GFP (*sfGFP*) or the β -galactosidase *lacZ* were constructed and reporter assays were performed. Besides, quantitative assays using Surface Plasmon Resonance (SPR) were also performed.

The second part of this work comprised the fragmentation of *SusD70111* (64.5 kDa) respecting its conserved domains. Six truncated proteins were produced, with sizes ranging from 12.7 to 37.9 kDa.

The final part consisted of the fusion of *susD1* Δ 1-22 (which presented promising binding performance) and a PETase lacking the C-terminal signal peptide *PorC* (secreted by T9SS from the phylum Bacteroidota), presenting low performance towards PET (*pet30* Δ *porC*) (Zhang et al., 2021). Remarkably, several PET hydrolase genes were previously found in bacteria affiliated with the phylum Bacteroidota (Danso et al., 2018). Therefore, we wanted to evaluate if the fusion with a Bacteroidotal binding

module would improve the enzymatic activity. *SusD1Δ1-22* was also fused with the benchmark *lcc-wt* (Sulaiman et al., 2012).

II. Materials and Methods

2.1 Origin of the samples

SusD70111 and *susD38489* were found in elephant faeces metagenomes. The female Asian elephant was a 6-years-old adult living in the Zoo Hagenbecks Tierpark (Hamburg, Germany). She was breast-feeding a three-weeks-old male elephant called Assam. The faecal samples were collected aseptically by the Zoo staff and further information is provided in the original publication (Ilmberger et al., 2014).

SusD1 was isolated from cow rumen metagenome, and it was found in the Hidden Markov Model by Voss group at the University of Stuttgart (Stuttgart, Germany). Briefly, rumen samples were collected from six *Bos indicus* by ruminal fistulation. Further information regarding the sample preparation and anaerobic growth is provided in the original publication, in which *SusD1* belongs to the fosmid clone *Sc00044* (Rosewarne et al., 2014).

2.2 Bacterial strains and cultivation

Table 2 lists relevant constructs prepared during this work. Each construct was cloned using the pET21a(+) vector (5.4 kbp; Novagen/Merck, Darmstadt, Germany). It has a T7-*lac*- promoter and is induced by lactose (*lacI*). This vector encodes a C-terminal His₆-tag and resistance to ampicillin. Besides, it is also suitable for heterologous protein expression. The constructs were transformed into *Escherichia coli* DH5 α and *E. coli* BL21(DE3) for recombinant protein expression (Table 3). *SusD70111* Δ 1-20 was also transformed into *E. coli* T7 Express, which is an enhanced BL21 derivative.

The buffers and media were autoclaved at 121 °C for 25 min. Empty glasses and microtubes were autoclaved under the same conditions, with a drying cycle afterwards.

Bacterial cultures were grown under aerobic conditions in lysogeny broth or agar (LB; 10 g/L of tryptone, 10 g/L of NaCl, 5 g/L of yeast extract and, when required, 12 g/L of agar). The cultures incubated overnight at 37 °C, with constant shaking. Besides, a stock of 100 µg/µL of ampicillin was prepared using water as the solvent and a final concentration of 100 mg/mL was added to each culture.

To visualize the expression of proteins fused to *sfGFP*, LB agar plates with the addition of 1 mM isopropyl-β-D-thiogalactopyranoside (IPTG) and 100 mg/mL of ampicillin were also prepared. In the case of successful protein expression, the colonies were neon green under UV-C light.

The gene *susD* was also fused with *lacZ*, with the intention of creating an enzymatic reporter. In this case, LB agar plates were prepared as described above and included 20 mg/mL of 5-bromo-4-chloro-3-indolyl-β-D-galactopyranoside (X-GAL). X-GAL stock solution had a final concentration of 20 µg/µL, diluted in dimethylformamide (DMF). The stock solution and plates were always stored in the dark. When LacZ degrades X-GAL, two products are released (galactose and 5-bromo-4-chloro-3-hydroxyindole). The last product quickly oxidizes, generating 5,5'-dibromo-4,4'-dichloro-indigo, which presents a dark blue color. Therefore, this color is visible in the bacterial colonies.

Table 2: Constructs used in this work.

Plasmid	Characteristics	Reference
pET21a(+>:: <i>susD70111</i>	<i>susD70111</i> from elephant feces metagenome (1767 bp, 588 aa). Cloned with the restriction enzymes <i>NdeI</i> and <i>Sall</i> .	(Ilmberger et al., 2014)
pET21a(+>:: <i>susD70111</i> Δ 1-20	<i>susD70111</i> without the N-terminal signal peptide Sec//SPII (57 bp, 19 aa). Cloned with the restriction enzymes <i>NdeI</i> and <i>Sall</i> .	This work
pET21a(+>:: <i>susD70111</i> _{F3}	Fragmentation of <i>susD70111</i> (687 bp, 229 aa). Cloned with the restriction enzymes <i>NdeI</i> and <i>Sall</i> .	This work
pET21a(+>:: <i>susD1</i>	<i>susD1</i> from cow rumen metagenome (1749 bp, 580 aa). Cloned with the restriction enzymes <i>NdeI</i> and <i>Sall</i> .	Voss group (University of Stuttgart, Stuttgart, Germany)
pET21a(+>:: <i>susD1</i> Δ 1-22	<i>susD1</i> without the N-terminal signal peptide Sec//SPII (66 bp, 22 aa). Cloned with the restriction enzymes <i>NdeI</i> and <i>Sall</i> .	Tabea Neumann's Master thesis
pET21a(+>:: <i>susD38489</i>	<i>susD38489</i> from elephant feces metagenome (1812 bp, 603 aa). Cloned with the restriction enzymes <i>NdeI</i> and <i>Sall</i> .	(Ilmberger et al., 2014)
pET21a(+>:: <i>susD38489</i> Δ 1-25	<i>susD38489</i> without the N-terminal signal peptide Sec//SPII (71 bp, 24 aa). Cloned with the restriction enzymes <i>NdeI</i> and <i>Sall</i> .	This work
pET21a(+>:: <i>pet30</i> Δ <i>porC</i>	<i>pet30</i> hydrolase lacking the C-terminal Por-domain (834 bp, 278 aa).	(Zhang et al., 2021)

II. Materials and Methods

pET21a(+):: <i>lcc-wt</i>	Leaf-compost cutinase (786 bp, 262 aa).	(Sulaiman et al., 2012)
pET21a(+):: <i>susD1Δ1-22::lcc-wt</i>	<i>susD1</i> lacked the N-terminal signal peptide (Sec/SPII) and fused to the N-terminal of <i>lcc-wt</i> . A (GS) ₁₇ linker was inserted between the proteins. <i>susD1</i> was flanked by <i>NdeI</i> and <i>Sall</i> , while <i>lcc-wt</i> was flanked by <i>NotI</i> and <i>XhoI</i> .	Tabea Neumann's Master thesis
pET21a(+):: <i>susD1Δ1-22::pet30ΔporC</i>	<i>susD1</i> lacked the N-terminal signal peptide (Sec/SPII) and fused to the N-terminal of <i>pet30ΔporC</i> . A (GS) ₁₇ linker was inserted between the proteins. <i>susD1</i> was flanked by <i>NdeI</i> and <i>Sall</i> , while <i>pet30ΔporC</i> was flanked by <i>NotI</i> and <i>XhoI</i> .	Tabea Neumann's Master thesis
pET21a(+):: <i>susD70111Δ1-20::sfGFP</i>	Fusion of superfolder GFP (<i>sfGFP</i>) (714 bp, 238 aa) with the C-terminal of <i>susD70111Δ1-20</i> . A GGGGS linker (15 bp) was inserted between the proteins. Ligation independent cloning.	This work
pET21a(+):: <i>susD1Δ1-22::sfGFP</i>	Fusion of <i>sfGFP</i> with the C-terminal of <i>susD1Δ1-22</i> . A GGGGS linker (15 bp) was inserted between the proteins. Ligation independent cloning.	This work
pET21a(+):: <i>susD70111_{F3}::sfGFP</i>	Fusion of <i>sfGFP</i> with the C-terminal of <i>susD70111_{F3}</i> (687 bp, 229 aa). A GGGGS linker (15 bp) was used to separate the proteins. Ligation independent cloning.	This work

II. Materials and Methods

pET21a(+>:: <i>susD70111</i> _{F3a} :: <i>sfGFP</i>	Fusion of <i>sfGFP</i> with the C-terminal of <i>susD70111</i> _{F3a} (339 bp, 99 aa). A GGGGS linker (15 bp) was used to separate the proteins. Ligation independent cloning.	This work	
pET21a(+>:: <i>sfGFP</i>	Sequence encoding the green fluorescence protein <i>sfGFP</i> , with excitation at 485 nm and emission of 510 nm.	Addgene USA)	(Massachusetts,
pET21a(+>:: <i>susD1Δ1-22</i> :: <i>lacZ</i>	Fusion of the C-terminal of <i>susD1Δ1-22</i> (1695 bp, 565 aa) with the β-galactosidase <i>lacZ</i> (366 bp, 122 aa). The proteins were separated by a GGGGS linker (15 bp). Ligation independent cloning.	This work	
pET21a(+>:: <i>susD38489Δ1-25</i> :: <i>lacZ</i>	Fusion of the C-terminal of <i>susD38489Δ1-25</i> (1729 bp, 587 aa) with the β-galactosidase <i>lacZ</i> . The proteins were separated by a GGGGS linker (15 bp). Ligation independent cloning.	This work	
pET21a(+>:: <i>lacZ</i>	β-galactosidase used as negative control on the reporter assays.	This work	
<i>pBBR1MCS</i>	This plasmid was used for the amplification of <i>lacZ</i> . Chloramphenicol resistance.	Addgene USA)	(Massachusetts,

*SusD70111*_{F3}: Truncated fragment 3 of *susD70111*; *lcc-wt*: leaf-compost cutinase wild type; *sfGFP*: superfolder GFP.

Table 3: Bacterial competent cells used in this work.

Strain	Phenotype	Reference
<i>Escherichia coli</i> DH5 α	F ⁻ <i>endA1 glnV44 thi-1</i> <i>recA1 relA1 gyrA96 deoR</i> <i>nupG purB20</i> ϕ 80d <i>lacZ</i> Δ M15 Δ (<i>lacZYA-</i> <i>argF</i>) U169, <i>hsdR17</i> (rK ⁻ mK ⁺), λ ⁻	(Hanahan, 1983) Invitrogen (Karlsruhe, Germany)
<i>E. coli</i> BL21(DE3)	F ⁻ <i>ompT gal dcm lon</i> <i>hsdS_B</i> (r _B ⁻ m _B ⁻) λ (DE3 [<i>lacI</i> <i>lacUV5-T7p07 ind1 sam7</i> <i>nin5</i>] [<i>malB</i> ⁺] _{K-12} (λ ^S))	(Studier & Moffatt, 1986) Merck (Darmstadt, Germany)
<i>E. coli</i> T7 Express (High Efficiency)	<i>fhuA2 lacZ::T7 gene1 [lon]</i> <i>ompT gal sulA11 R(mcr-73::miniTn10--Tet^S)2</i> <i>[dcm] R(zgb-210::Tn10--Tet^S)</i> <i>endA1 Δ(mcrC-mrr)114::IS10</i>	New England Biolabs (Massachusetts, USA)

2.3 Working with DNA

2.3.1 Cloning

The N-terminal signal peptide Sec/SPII was identified with [SignalP DTU v.6.0 server](#) by selecting the feature “Gram-negative bacteria” (accessed on 25/07/2021; (Teufel et al., 2022)). The deletion of the first 57, 60 and 71 bp from *susD70111*, *susD1* and *susD38489*, respectively, was performed.

Polymerase chain reaction (PCR) product purification was carried on with the “GeneJet gel extraction and DNA clean-up” micro kit, following the protocol “PCR clean-up, dimers removal” provided by the manufacturer (Thermo Fisher Scientific, Massachusetts, USA). When indicated on Table 2, the genes were inserted with the addition of two palindromic endonuclease restriction sites (*NdeI/SalI*; *NotI/XhoI*). Translational protein fusions with *sfGFP* and *lacZ* were carried out by ligation independent cloning. Supplementary Tables S1 to S4 provide the primer pairs and PCR cycles used. Figure 4 shows the approach used for the fusion of *susD* with *lcc-wt* and *pet30ΔporC* (A), *lacZ* (B) and *sfgfp* (C).

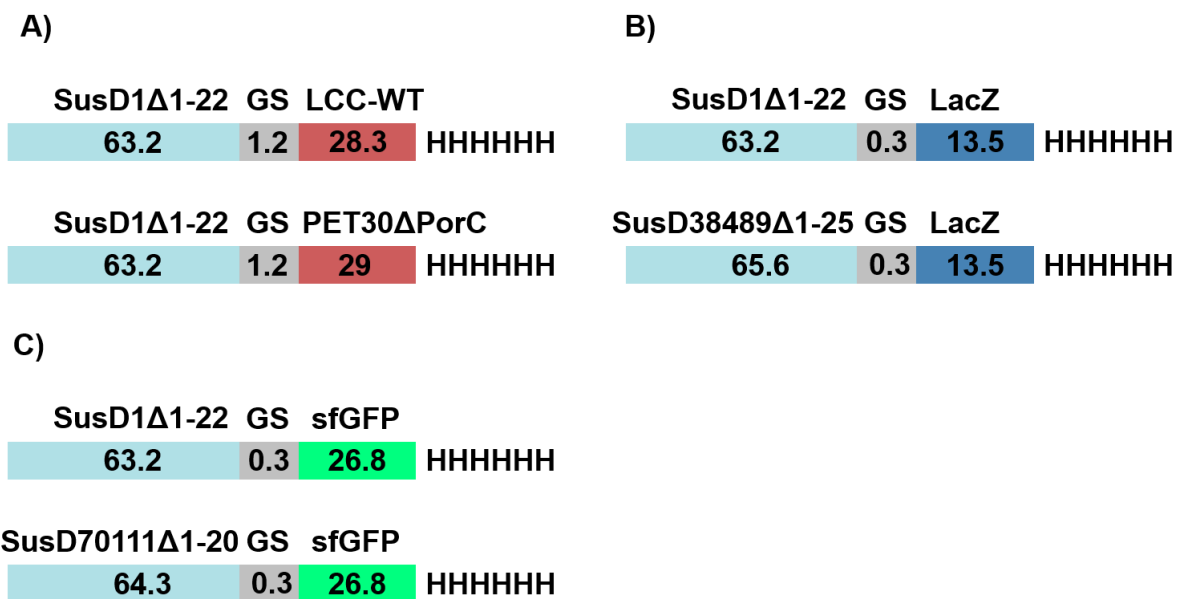


Figure 4: Structure of the final chimeras produced by translational fusion, with protein sizes (kDa) indicated. A) Fusion of *susD1Δ1-22* with the enzymes *lcc-wt* (Sulaiman et al., 2012) and *pet30ΔporC* (Zhang et al., 2021). A (GS)₁₇ linker (51 bp) was used. The His₆-tag was positioned to the C-terminus of the enzyme. This cloning was performed by Tabea Neumann as part of her Master thesis. **B)** Fusion of *susD1Δ1-22* and *susD38489Δ1-25* with *lacZ*. A GGGGS linker (15 bp) was used, and the His₆-tag was positioned to the C-terminus of *lacZ*. *SusD70111Δ1-20* was not fused to *lacZ* due to low protein yield. **C)** Fusion of *susD1Δ1-22* and *susD70111Δ1-20* with *sfGFP*. A GGGGS linker (15 bp) was used, and the His₆-tag was positioned to the C-terminus of *sfGFP*. *SusD38489Δ1-25* was fused to *sfGFP* as part of another study and, therefore, it will not be displayed here.

Another approach consisted of the fragmentation of *susD70111*. A search for conserved domains (Lu et al., 2020; Marchler-Bauer et al., 2017; Marchler-Bauer & Bryant, 2004; Marchler-Bauer et al., 2015; Marchler-Bauer et al., 2011) helped to design suitable primers. Four fragments flanked by the restriction sites *NdeI/SalI* were cloned and successfully expressed in *E. coli* BL21(DE3).

Heat-shock transformation was performed in accordance with the book “Molecular cloning: A laboratory manual” (Maniatis, 1982). Sanger sequencing was performed by Microsynth Seqlab (Göttingen, Germany). The sequences were trimmed and aligned using Chromas Pro v.2.1.10.

2.3.2 Polymerase Chain Reaction (PCR)

2.3.2.1 Touchdown PCR

Touchdown PCR (Don et al., 1991) was carried on for the amplification of single genes from other plasmid sources. In this error-proof PCR, the first cycle starts with the highest temperature and decreases in the first 15 cycles. Once the final temperature is reached, 15 more cycles are repeated. Table 4 shows the pipetting calculation scheme.

Table 4: PCR pipetting calculation.

Component	Volume (μL)
DNA [5 U/ μL]	1
10x Buffer B/BD (5x HF/GC Buffer)	2 (4)
MgCl ₂ [25 mM]	1
dNTPs [2 mM each]	1
Primers [5 pmol/ μL]	1
DMSO [1 M]	1
Polymerase	0.2 (0.5)
H ₂ O	<i>ad 20</i>

II. Materials and Methods

DCS polymerase (DCS, Hamburg, Germany) was used for most of the reactions. DNA-polymerase Phusion™ High-Fidelity (Thermo Fisher Scientific, Massachusetts, USA) was used for the fusion of the constructs and the values in brackets are indicative of this enzyme.

To calculate the annealing temperature (T_{ann} ; °C), the following equation was used:

$$T_{ann} = ((T_{m1} + T_{m2})/2) - 5$$

Where T_{m1} and T_{m2} represent the melting temperature (°C) of each primer. T_m average minus five equals T_{ann} . In the “**V. Supplementary Material**” section, it is possible to find each T_{ann} used in this work. Table 5 displays the standard touchdown PCR program used.

Table 5: Touchdown PCR conditions.

Step	Temperature (°C)	Time (min:sec)
Initial denaturation	95	3:00
Denaturation	95	0:30
Annealing	T_{ann}	0:45
Elongation	72	*
Denaturation	95	0:30
Annealing	T_{ann}	0:45
Elongation	72	*
Final elongation	72	3:00
Incubation	10	End

T_{ann} : annealing temperature. Light grey: 15 cycles; dark grey: 20 cycles.

*Elongation time for the DCS polymerase: 1 kb/60 sec.; Phusion™: 1 kb/30 sec.

2.3.2.2 Colony PCR

Colony PCR is a three-step PCR used to check for the correct insert size in *E. coli* DH5 α . Enough of each colony was suspended in 20 μ L of H₂O_{dd} and cooked at 95 °C for 10 min. The cell debris was separated by spinning the microtubes for 30 sec at maximum speed, and 1 μ L of the DNA suspension was used as the template in each

reaction. PCR pipetting calculation followed the same scheme displayed on Table 4, while Tables 6 and 7 show the cycling conditions and primer sequences, respectively.

Table 6: 3-step PCR conditions.

Step	Temperature (°C)	Time (min:sec)
Initial denaturation	95	3:00
Denaturation	95	0:30
Annealing	T _{ann}	0:45
Elongation	72	*
Final elongation	72	3:00
Incubation	10	End

Grey represents a repetition of 30 times of each cycle.

*Elongation time for the DCS polymerase: 1 kb/60 sec.

Table 7: Universal primer pair for the colony PCR.

Name	Sequence (5'-3')	T _m (°C)	Reference
T7 promotor	TAATACGACTCACTATAGGG	53	Eurofins (Germany)
T7 terminator	CTAGTTATTGCTCAGCGGT	55	Eurofins (Germany)

2.3.3 Electrophoresis

DNA gel with 0.8% of agarose ran at 100 V for 25 min. 1x TAE buffer (prepared from the stock solution 10x TAE buffer pH 8: 40 mM Tris-acetate and 2 mM EDTA) was used for the agarose gel preparation and for the run. The gel stained for 15 min in the dark, with ethidium bromide, and documented with Chemidoc™ MP Imaging System (BIO-RAD, California, USA) using the Blot/UV/Stain-Free Tray. The picture was printed with a Mitsubishi electric printer (North Rhine-Westphalia, Germany). The ladders used were GeneRuler™ 1 kb DNA ladder or GeneRuler™ 100 bp DNA ladder, manufactured by Thermo Fisher Scientific (Massachusetts, USA) and displayed on Supplementary Figure S1.

2.4 Working with protein

2.4.1 Protein expression

Heterologous protein expression was carried on using either autoinduction medium (Studier, 2005) (Table 8) or IPTG induction. A proportion of 1/1000 of bacterial preculture was added to the medium. The cultures were kept at 37 °C with vigorous shaking, until the OD₆₀₀ reached 0.7, and transferred to 28 °C overnight (16-18h). In the case of IPTG induction, a final concentration of 0.5 mM or 1 mM of IPTG was added when the OD₆₀₀ reached 0.7.

Table 8: Recipe of the autoinduction medium (Studier, 2005).

Solution	Recipe	Amount (mL)
ZY medium	10 g Tryptone 5 g Yeast extract <i>ad.</i> 1 L H ₂ O _{dd}	960
5052-SL (50x)	25% Glycerine 2.5% Glucose 10% α-lactose monohydrate	20
M-SL (50x)	1.25 M Na ₂ HPO ₄ • 2 H ₂ O 1.25 M KH ₂ PO ₄ 2.5 M NH ₄ Cl 0.25 M Na ₂ SO ₄	20
MgSO ₄ -SL	1 M MgSO ₄ • 7 H ₂ O	1
Antibiotics	100 mg/mL Ampicillin	1

On the next morning, the OD₆₀₀ was measured again, and the cultures were kept on ice. The cultures were harvested in a Beckmann Coulter Avanti JXN-30; Rotor JLA-12.500 (Krefeld, Germany), at 13,445 x g, 4 °C. To avoid salt and organic contamination, the pellets were washed with NPI-10 lysis/equilibration buffer pH 8 (50

mM NaH₂PO₄, 300 mM NaCl and 10 mM Imidazole) and stored at -20 °C until further use.

2.4.2 French press

The pellet was resuspended in NP-10 (ratio of 4 ml of buffer to 1 g of cells) and disrupted with a French Pressure Cell Press (American Instrument Company) at a maximal pressure of 1250 psi. The suspension was centrifuged for 20 min at 39,312 x g, 4 °C (Beckmann Coulter Avanti JXN-30, Rotor JA25-50; Krefeld, Germany) and the cell debris was discarded.

2.4.3 Protein purification

One bed volume of NiNTA agarose (Macherey Nagel, Düren, Germany) was mixed with approximately 50 mL of crude cell extract and the suspension incubated for 1 h at 4 °C on the roller shaker (IKA roller 6 basics; Thermo Fisher Scientific, Massachusetts, USA). Afterwards, the suspension was added to a gravity-flow polypropylene column (Qiagen, Hilden, Germany) and a gradient of imidazole was used for the wash and elution steps. The agarose bed was washed twice with NPI-20 pH 8 and the protein was collected in fractions after the elution with NPI-250 pH 8. NPI-20 and NPI-250 buffers were prepared as described for NPI-10, except for the addition of 20 mM and 250 mM of imidazole, respectively.

The buffer was changed to potassium phosphate buffer 0.1 M pH 7 (61.5 mL of K₂HPO₄ (1 M) and 38.5 mL of KH₂PO₄ (1 M); ad. 900 mL H₂O_{dd}). The dialysis took place with a Sartorius Vivaspin column (Sartorius, Göttingen, Germany), using the appropriate column cut-off to each protein size. The column was centrifuged at 4,332 x g 4 °C

(Eppendorf centrifuge 5804R, Rotor A-4-44, Hamburg, Germany) until the protein was concentrated to a small volume (200 up to 500 μ L). The protein concentration was measured using the feature “Protein UV” in the NanoPhotometer® (Implemen, California, USA). The molecular weight and the extinction coefficient (“assuming all pairs of Cys residues form cystines”) were collected using the Expasy ProtParam tool (available at [Expasy - ProtParam](#), accessed on 07/06/2023) (Gasteiger E., 2005).

The protein was stored at 4 °C for a maximum of one week. Every step of the protein purification and dialysis was collected and evaluated with SDS PAGE and Western Blot.

2.4.4 SDS PAGE

The samples were normalized (one part of loading dye to four parts of sample) and diluted with SDS 5x loading dye. 10 μ L of each sample was carefully applied on the gel. The gel was placed on a 1x SDS running buffer and the run took place at 120 V for 1 h. The gel stained overnight with Coomassie staining solution and destained for 1 h with destaining solution at 15 rpm. Unless otherwise stated, the ladder PageRuler™ Unstained Protein Ladder #26614 (Supplementary Figure S2; Thermo Fisher Scientific, Massachusetts, USA) was used. Tables 9 and 10 display the recipe for all the required reagents.

Table 9: Recipe used for the preparation of SDS PAGE gels.

Solution	12% separating gel (mL)	7% stacking gel (mL)
H ₂ O _{dd}	4.5	2.34
Separating gel buffer pH 8.8	2.5	-
Stacking gel buffer pH 6.8	-	0.96
40% Acrylamide/Bis-Solution (37, 5:1)	3	0.7
10% Ammonium persulfate solution (APS)	0.1	0.03
Tetramethylethylenediamine (TEMED)	0.01	0.004

Table 10: Recipe of the other reagents required to run the SDS PAGE.

Solution	Recipe
SDS 5x loading dye (10 mL)	50% Glycerol (v/v) 100 mM Dithiothreitol (DTT) 4% SDS (w/v) 0.02% Bromphenol blue (w/v) 150 mM Tris-HCl pH 6.8 1 mM EDTA 30 mM NaCl H ₂ O _{dd} <i>ad.</i> 5 mL
10x SDS running buffer pH 8.4	30.3 g TRIS 144.1 g Glycine 10 g SDS H ₂ O _{dd} <i>ad.</i> 1 L
(Staining) and destaining solutions	(1 g Coomassie Brilliant Blue R-250) 400 mL Ethanol 96% 100 mL Acetic acid 500 mL H ₂ O _{dd}

Values in brackets represent only the Coomassie staining solution.

2.4.5 Native and affinity PAGE

This assay was inspired by previously described affinity PAGE assays (Larsbrink et al., 2016; Tamura et al., 2019; Walker et al., 2015) with modifications. Polyacrylamide gels, 10x running buffer and protein loading dye were prepared without denaturing

compounds (Tables 11 and 12). Staining and destaining solutions were prepared as described previously in Table 10.

Table 11: Recipe used for the preparation of native and affinity polyacrylamide gels.

Solution	12% separating gel (mL)	7% stacking gel (mL)
H ₂ O _{dd}	4.5	2.34
Polymer substrate	4.5	-
1.5 M Tris-HCl buffer pH 8.8	2.5	-
0.5 M Tris-HCl buffer pH 6.8	-	0.96
40% Acrylamide/Bis-Solution (37, 5:1)	3	0.7
10% Ammonium persulfate solution (APS)	0.1	0.03
Tetramethylethylenediamine (TEMED)	0.01	0.004

The color grey represents each polymer substrate tested for the observation of putative affinity (carboxymethylcellulose (CMC); PET; polyamide 6 (PA6) and low-density polyethylene (LDPE)). In this case, the suspension containing each polymer replaced the H₂O_{dd} in the preparation of a 12% separating gel, resulting in a third additional layer.

Table 12: Recipe of 5x protein loading dye and 10x native running buffer pH 8.3.

Solution	Recipe
5x loading dye (10 mL)	50% Glycerol (v/v) 0.02% Bromphenol blue (w/v) 150 mM Tris-HCl pH 6.8
10x Native running buffer pH 8.3	30.3 g TRIS 144.1 g Glycine H ₂ O _{dd} ad 1 L

The substrates tested were carboxymethylcellulose (CMC) and semi-crystalline PET (GoodFellow, Cambridge, UK). CMC was diluted in H₂O_{dd}, to a final concentration of 0.1 mg/ml. Meanwhile, 1 g of synthetic powder was dissolved in 10 ml of dimethyl sulfoxide (DMSO) at over 100 °C. When the solution was homogenous, approximately 3 ml was dispensed in 100 ml of H₂O_{dd} with constant shaking. From top to bottom, the

affinity gels were prepared accordingly: 2 ml of stacking gel, 2 ml of substrate gel and 2 ml of separating gel (Figure 5).

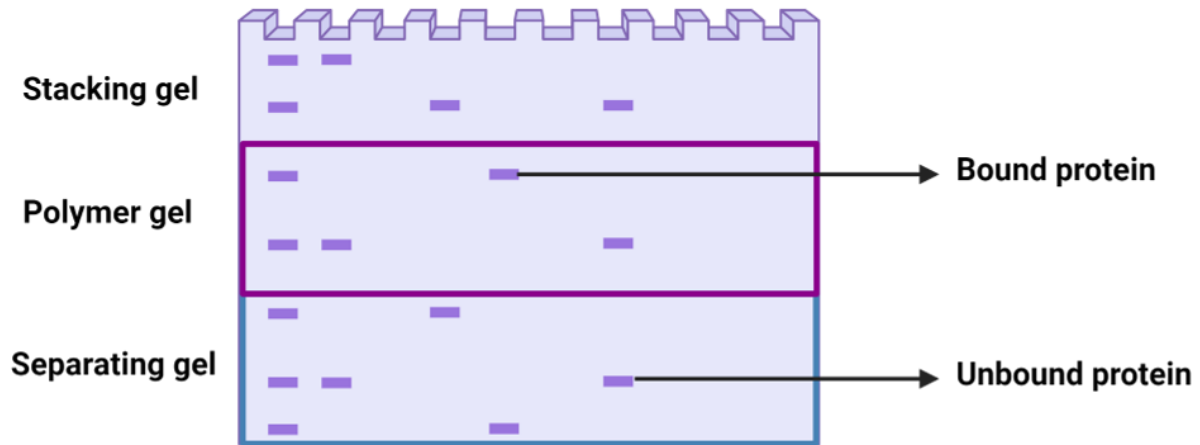


Figure 5: Schematic representation of the affinity gel. From the bottom to the top: 12% separating gel was prepared as described on Table 11, and 2 mL was dispensed between the glasses. Next, the polymer gel was prepared, replacing the H_2O_{dd} by the substrate. 2 mL of this suspension was added to the top of the separating gel (after the polymerization). The stacking gel was prepared according to Table 11 and dispensed on the top of the polymer gel, after the complete polymerization. The final result was a gel with 3 layers. Created in BioRender.com.

Only SusD1 Δ 1-22 and SusD38489 Δ 1-25 were evaluated, once they represented the best candidates in terms of recombinant protein expression and putative binding. 20 μ M of each protein was prepared shortly before being loaded in the gel, without the denaturation step. The negative control consisted of the native gel without the addition of any polymer. Each gel ran simultaneously at 120 V for approximately 2 hours. A protein that ran until the separating gel meant no substrate affinity. Bovine serum albumin (BSA; 20 μ M) could not be used as a non-interacting protein (negative control), once the protein completely ran out of each affinity gel.

2.4.6 Western Blot

The SDS gel run was carried on as previously described, except for the protein ladders. In this case, the ladders PageRuler™ Prestained Protein Ladder #26616 or PageRuler™ Plus Prestained Protein Ladder #26619 (Supplementary Figure S2; Thermo Fisher Scientific, Massachusetts, USA) were used.

Enough layers of Whatman paper (Gel blotting paper GB003, Schleicher & Schuell BioScience GmbH, Dassel, Germany) and nitrocellulose membrane (Roti®-NC transfer membrane, Roth, Karlsruhe, Germany) were soaked with transfer buffer and the gel was “sandwiched”. The blotting was conducted in a TransBlot Turbo Transfer System (BIO-RAD, California, USA), at 25 V and 1.0 A for 30 min.

Afterwards, the membrane was washed twice with a TBS buffer and blocked with 1% (w/v) of milk powder for 1 h. The membrane was washed 3 times with TBST buffer and incubated overnight at 4 °C with the primary antibody (α -His tag 6x, diluted 1:5,000 in TBST buffer). On the next day, the membrane was again washed 3 times with TBST buffer and incubated for 1 h with the secondary antibody (α -rabbit IgG-AP, diluted 1:10,000 in TBST buffer; 5% (w/v) of milk powder was added). After washing 3 more times with TBST, the membrane was equilibrated for 3 min in the detection buffer. The staining solution was added and the membrane incubated in the dark until the appearance of the protein bands (approximately 10 min). The documentation was prepared with a Canon 9000F MarkII scanner (Canon, Tokyo, Japan).

Every step of the Western Blot was performed with incubation at 15 rpm. Table 13 shows the recipe for the buffers and other reagents.

Table 13: Amount of each reagent required for the preparation of solutions used for Western Blot.

Solution	Recipe
Transfer buffer pH 8.6	125 mM Tris 192 mM Glycine 20% (v/v) Methanol <i>H₂O_{dd} ad 800 mL</i>
TBS(T) buffer pH 7.5	125 mM Tris 0.9% (w/v) NaCl (0.1% (v/v) Tween 20) <i>H₂O_{dd} ad 1 L</i>
Detection buffer pH 9.5	125 mM Tris 0.9% (w/v) NaCl <i>H₂O_{dd} ad 1 L</i>
Staining solution	66 μ L nitro blue tetrazolium chloride (NBT; stock solution 75 mg/mL in 70% (v/v) Dimethylformamide (DMF)) 33 μ L 5-Bromo-4-chloro-3-indolyl phosphate (BCIP; stock solution 50 mg/mL in 100% DMF) 10 mL Detection buffer

Values in brackets refer to the TBST buffer. The pH was measured using a pH meter (HI 221 Calibration Check Microprocessor pH Meter; HANNA Instruments, Rhode Island, USA) and the desired pH was achieved using a stock solution of 2 M of NaOH or 1 M HCl.

2.5 Protein activity screening

2.5.1 Pull-down assay of insoluble substrates

The qualitative assay was performed similarly to (Larsbrink et al., 2016; Moser et al., 2008; Tamura et al., 2019; Tauzin et al., 2016) with modifications. One representant of a natural polymer (microcrystalline cellulose (MC); Sigma-Aldrich, Missouri, USA) and three synthetic polymers (PET, low-density polyethylene (LDPE) and polyamide 6 (PA6); GoodFellow (Cambridge, UK)) were tested. To mimic weathering effects, PET was also incubated under UV-C light for 30 days with constant shaking.

The three SusD-homologs, as well as SusD70111 fragments, were tested. Each mixture of 0.1 g powder plus protein incubated for 1 h at room temperature (22 °C) on the roller shaker. The amount of protein required varied according to their concentration and purity, as observed in distinct rounds of protein expression and purification (Table 14).

Table 14: Average values obtained during protein purification and considered for the pull-down assay.

Protein	Purification		Pull-down assay
	Concentration (mg/mL)	Purity (%)	Concentration (mg/mL)
SusD1(Δ 1-22)	20	83.39	0.4
SusD70111(Δ 1-20)	3	50	CCE
SusD38489(Δ 1-25)	70	77.95	1
SusD70111 _{F3}	ND	NA	CCE

The SusD-homologs are represented with and without the N-terminal Sec/SPII signal peptide (in brackets). Protein concentration values, after protein purification, represent an average of several protein expression and purification experiments. The purity was accessed with SDS gel analysis using ImageJ v.1.53k (Wayne Rasband and contributors, National Institutes of Health, USA). The final concentration of protein used on the pull-down assay was calculated based on the observed protein

purity. In the case of proteins with low purity, for instance SusD70111(Δ 1-20) and SusD70111_{F3}, only the crude cell extract was tested. SusD70111_{F3}: Fragment 3; ND: not defined; NA: not applied; CCE: crude cell extract.

When pure protein was used for the assays, a final volume of 10 mL of protein diluted in potassium phosphate buffer 0.1 M pH 7 was calculated. In the case of low protein concentration or quick testing, crude cell extract was used.

Like the protein purification, each mixture was added to a gravity-flow Qiagen polypropylene column (Hilden, Germany). After the polymer formed a bed, it was washed twice with PBS 1x (prepared from the stock solution PBS 10x pH 7.4: 1.37 M NaCl; 27 mM KCl; 100 mM Na₂HPO₄ and 18 mM KH₂PO₄). The protein was eluted with 2% Triton X-100 (v/v) and the fractions analyzed with Western Blot. When the protein band on the first elution was stronger than the one on the last washing step, it represented that the protein bound to the substrate. Triton X-100 (v/v) interfered with the Bradford reagent (Bio-Rad Laboratories, California, USA), and the protein quantification using the NanoPhotometer® (Implen, California, USA) was also not possible.

2.5.2 Fluorescence assay

The proteins tagged with sfGFP were diluted to a final concentration of 20 μ M. Amorphous foils of PET, PA6 and LDPE (GoodFellow, Cambridge, UK) were cut with the hole punch to a diameter of 6 mm. Citrate buffer 0.1 M (45,95 mM C₆H₉Na₃O₉ and 54.05 mM of C₆H₈O₇; pH 4 and 5) and potassium phosphate buffer 0.1 M (prepared as described on the “**2.4.3 Protein purification**” section; pH 6 and 7) were used for the protein dilutions and negative controls.

II. Materials and Methods

Twenty micromolar of each protein in a final volume of 200 μL were used in the first step, during which a plastic foil was completely immersed in the liquid suspension (Figure 6). The incubation took place at room temperature (22 $^{\circ}\text{C}$) during 1 h, with constant shaking at 300 rpm. The foil was washed twice with the same buffer used for the incubation and transferred to a 96-well flat bottom plate, with black walls and transparent bottom (Thermo Fisher Scientific, Massachusetts, USA). For optimal measurements, 200 μL of fresh buffer was added to the well and fully covered the foil. sfGFP fluorescence and mean RFU were measured on a plate reader (Synergy H1 microplate reader, BioTek, Agilent Technologies, California, USA), with excitation at 485 nm and emission of 510 nm. The plate was shaken for 0.03 sec before each measurement, and measurement values from the top and the bottom were collected.

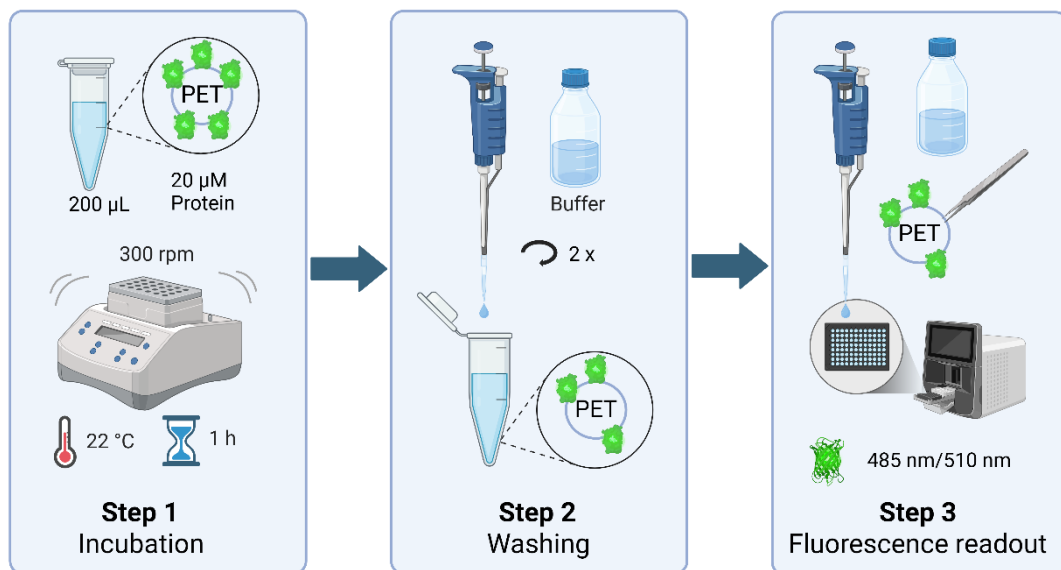


Figure 6: Schematic representation of the fluorescence assay, divided in three steps. Created in BioRender.com.

Likewise, 0.02 g of MC incubated with 20 μM of each protein. The powder was carefully resuspended in a fresh buffer before transferring to the 96-well plate. The experiments were conducted in triplicate and the negative controls were sfGFP and buffer plus each substrate.

2.5.3 Surface plasmon resonance (SPR) spectroscopy

SPR performed with Biacore™ systems (Cytiva, Massachusetts, USA) displays the real-time interaction between the analyte and ligand. When the analyte attaches to the ligand, the refractive index at the sensor chip surface changes. For this reason, this technique is highly sensitive, with no minimum analyte molecular weight required.

The SPR response is proportional to the adsorption of analyte to the ligand. The SPR detection unit consists of the optical unit pressed against the sensor chip, via an interface named “opto-interface”. The light source, illumination and imaging optics, glass prism and detector form the optical unit. When a molecule attaches to the surface of the gold layer, the reflection of light from the light source within the optical unit is affected. When the complex interaction between analyte and ligand (association) reaches an equilibrium, followed by a decrease in response due to the dissociation of the analyte.

The gold-coated sensor chip “CM5” with carboxymethyl dextran on the surface, to provide ligand attachment. In this work, the sensor chips were coated with anti-His antibody (Biacore, His-capture kit, Cytiva, Massachusetts, USA). Afterwards, the chips were equilibrated with HBS-EP buffer (10 mM HEPES pH 7.4, 150 mM NaCl, 3 mM EDTA, 0.005 % (v/v) detergent P20) and the flow cells were activated by the injection of 1:1 N-ethyl-N-(3-dimethylaminopropyl) carbodiimide hydrochloride and N-hydroxysuccinimide, using the standard amine-coupling protocol. The flow cells were loaded with 50 µg/mL of anti-His₆ in 10 mM acetate (pH 4.5) with a contact time of 420 sec until the surfaces contained approximately 8.500 response unit (RU) of antibody density. Free binding sites were saturated by the injection of 1 M ethanolamine/HCl pH 8.

15 µg/mL of each His₆-tagged protein was captured with HBS-EP buffer for 600 sec at a flow rate of 10 µL/min, reaching a final response of 600-1.800 RU. The substrates were injected over the chip with single cycle kinetics, at a flow rate of 30 µL/min. CMC and bis(2-Hydroxyethyl) terephthalate (BHET) at increasing concentrations of 1 nM, 10 nM, 100 nM, 1.000 nM, and 10.000 nM were injected without regeneration, using a contact time of 180 sec. and a final dissociation of 1200 sec. The chip was regenerated by the injection of 10 mM glycine pH 1.5 for 60 sec, at a flow rate of 30 µL/min.

Blank single cycle kinetics were recorded by the injection of buffers instead of increasing concentrations of the polymers. Single kinetics were performed four times at 25 °C and the sensorgrams were recorded using the Biacore T200 Control software v.3.2 and analyzed with Biacore T200 Evaluation software v.3.2 (Cytiva, Massachusetts, USA). The bulk refractive index background was subtracted to each sample with the blank and the drifts on the surface were normalized by the subtraction of the respective polymers plus buffer. The reference sensorgrams were normalized to a baseline of 0 and the peaks at each injection represented the runtime differences between the flow cells. R_{max} was calculated using the formula:

$$R_{max} = (MW_{analyte}/MW_{ligand}) \times RU_{immobilized\ ligand}$$

In which the maximal binding response for a 1:1 interaction is measured. Binding stoichiometry (n) was calculated with the formula:

$$n = RU_{max}/R_{max}$$

2.5.4 β -galactosidase (*lacZ*) reporter

The translational fusion proteins SusD1 Δ 1-22::LacZ and SusD38489 Δ 1-25::LacZ were diluted to a final concentration of 20 μ M in potassium phosphate buffer 0.1 M pH 6. Afterwards, 200 μ L of each was added to 1.5 mL microtubes with PET, LDPE and PA6 amorphous foils. The incubation was performed for 1 h at 22 °C and 300 rpm. LacZ was also diluted to 20 μ M and incubated under the same conditions, to be compared as a negative control. Each experiment was performed in triplicate.

The foils were washed twice in potassium phosphate buffer 0.1 M pH 6 and transferred to a 96-well microtiter plate with flat bottom (Thermo Fisher Scientific, Massachusetts, USA). 20 mg/mL of X-GAL was added to each well and the enzymatic activity was monitored after 1, 3, 18, 24, 96 and 120 h of incubations at 22 °C, 300 rpm. The enzymatic activity was read at 420 nm on the plate reader.

2.5.5 Enzymatic screening on agar plates containing synthetic substrates

The following method was performed by Tabea Neumann, as part of her Master thesis.

LB agar plates were casted with the addition of 100 mg/mL of ampicillin, 500 mg/L of the synthetic and biodegradable polymer polycaprolactone (PCL) or 5 mM of BHET. This methodology led to a fast screening of enzymatic activity and comparison between the WT and the translational fusion enzymes. PCL stock solution was solved in acetone at 60 °C, while BHET was solved in DMSO. 10 μ L of each crude cell extract was added into the plates. The negative control included the WT proteins, and the plates incubated at 37 °C. For the documentation, the plates were observed after 24 h and further, being scanned with a Canon 9000F MarkII (Tokyo, Japan).

2.5.6 Ultra-high-performance liquid chromatography (UHPLC) analysis

The following method was performed by Tabea Neumann, as part of her Master thesis.

With UHPLC, it is possible to detect the degradation products of PET (BHET; mono-2-hydroxyethyl-terephthalate (MHET) and terephthalic acid (TPA)). Amorphous PET foil with 0.25 mm of thickness (GoodFellow, Cambridge, UK) was cut with a hole puncher, washed with ethanol 70% (v/v) and dried. Each foil was immersed in a 1.5 mL microtube alongside 200 μ L of protein in potassium phosphate buffer 0.1 M pH 8. The protein concentrations were as follows: 11.5 μ M of PET30 Δ PorC and its translational fusion with SusD1 Δ 1-22; 65.9 μ M of LCC-WT and its respective protein fusion. The experiment was in triplicates and the negative controls included the buffer (with and without substrate) and each protein without substrate. The incubations took place at 30 °C, 450 rpm for 72 and 120 h. Afterwards, 50 μ L of each sample was collected and mixed with 200 μ L of acidified acetonitrile +1 % (v/v) of trifluoroacetic acid (TFA). The microtubes were centrifuged at 13,200 rpm, for 3 min at room temperature. The supernatant was collected, mixed with 600 μ L H₂O_{dd} and stored at -20 °C until further use. The UHPLC analysis was performed in an UltiMate 3000 (Dionex, Thermo Fisher Scientific, Massachusetts, USA), in which an injection of 15 μ L was collected by the autosampler. The separation of fractions was performed with YMC-Triart C18 column with 2 x 100 mm, 1.9 μ m of particle size and 120 Å of pore size (YMC Europe, Dinslaken). The constant rate was 0.4 mL/min and isocratic elution of 20 % (v/v) acetonitrile in H₂O_{dd} (also acidified with 1 % (v/v) TFA). The UV detection was performed at 254 nm and the calibration curve of TPA, and acetonitrile gradient were created (Figure 7).

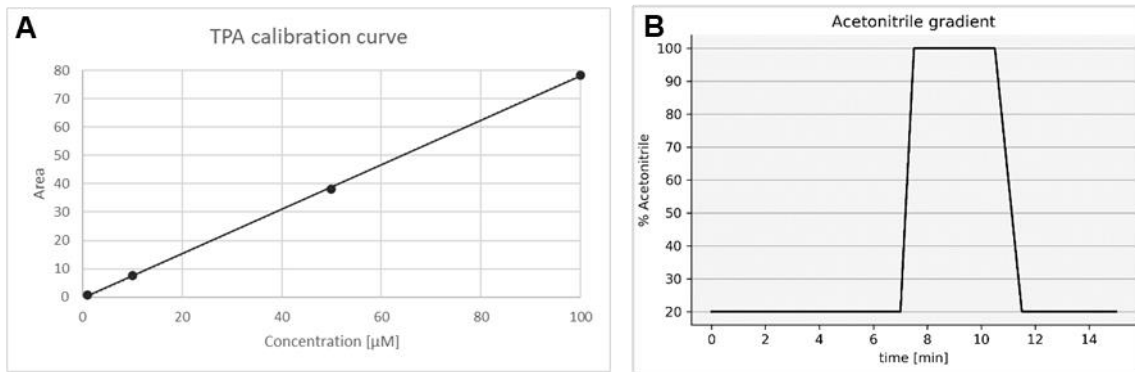


Figure 7: UHPLC control curves. A) Calibration curve of terephthalic acid (TPA). **B)** Acetonitrile gradient. The assays for SusD1Δ1-22 were conducted by Tabea Neumann during her Master thesis.

2.6 Bioinformatics

2.6.1 Phylogenetic analysis

The conserved domains of SusD70111 were identified with [NCBI Conserved Domain Search](#) (accessed on 14/06/2020) using the database CDD v.3.21 and default parameters.

[Protein BLAST](#) (BLASTp; accessed on 17/05/2023) was performed using the NCBI “Non-redundant protein sequences” Database. Sequences with 90% of coverage, at least 70% identity and from defined species were selected.

SusD-homologs from hot springs and RagB from *P. gingivalis* were found in the [NCBI protein Database](#) (accessed on 16/01/2024). The terms “SusD”, “hot spring”, “NOT hypothetical”, “NOT putative”, “NOT partial”, “RagB” and “Bacteroidota” were applied to the search. The search for RagB retrieved thousands of hits and, for this reason, the sequences were randomly selected based on their availability in the literature (Acuna-Amador et al., 2018; Hall et al., 2005; Hanley et al., 1999; Nagano et al., 2007; Nelson et al., 2003; Watanabe et al., 2011).

The proteins were aligned using T-coffee structural alignment v.11.00 (expresso) (Armougom et al., 2006; Di Tommaso et al., 2011; Notredame et al., 2000; O'Sullivan et al., 2004; Poirot et al., 2004) and the neighbour-joining tree with Bootstrap adjusted to 1000 was built with MEGAX v.10.2.4. The tree was colored using iTOL v.6 (Letunic & Bork, 2024). This structural alignment was also performed for SusD70111 with the chitin binding SusD-homologs named CusDI and CusDII (Larsbrink et al., 2016). SusD1 and SusD38489 were aligned with cellulose binding SusD-homologs (named SusD1† and SusD2 (Mackenzie et al., 2012). The cross indicates that the protein was not the same as the one evaluated in this work).

2.6.2 Structural analysis

2.6.2.1 AlphaFold v.2.3.2

The amino acid sequence of the proteins, with or without signal peptide, were submitted for structure predictions using the server [Alphafold](#) v.2.3.2 (accessed on 20/05/2023) (Jumper et al., 2021). AlphaFold was also used for folding the translational protein fusions and fragments, as well as the selected SusD-homologs from hot springs and RagB from oral pathogens (identified with the cut off described at the **2.6.1 Phylogenetic analysis** section). This server was employed using default parameters.

2.6.2.2 Structural studies using Chimera

The proteins were visualized with Chimera v.1.16 (Pettersen et al., 2004) or ChimeraX v.1.3 (Goddard et al., 2018; Pettersen et al., 2021) when indicated. The tool “MatchMaker” was used for structure comparison. The substrates were converted to mol2 using Chem3D® Professional v.22.0.0.22. Each substrate and protein were

submitted to a DockPrep (Shapovalov & Dunbrack, 2011) and the Docking was performed with Autodock Vina (Trott & Olson, 2010). The search was adjusted to show only the five most stable binding sites.

The protein pockets were characterized using [GeoMine](#) (Diedrich, 2021) (accessed on 15/11/2023, using default parameters).

2.6.2.3 Prediction of tetratricopeptide repeat using TPRpred

The Webserver [TPRpred](#) (Gabler et al., 2020; Karpenahalli et al., 2007; Zimmermann et al., 2018) was accessed on 27/09/2023, using default parameters. This tool uses P-value-dependent scores to calculate the probability that a protein has TPR or pentatricopeptide repeat.

III. Results

3.1 Main characteristics of SusD

SusD38489 (NCBI nucleotide accession number OQ616754) and *susD70111* (OQ616753) were found in elephant feces metagenomes, from an Asian elephant that was 6 years old and breastfeeding (Ilmberger et al., 2014). She was living in the Zoo (Hagenbecks Tierpark, Hamburg, Germany) and mainly fed with grass, hay, leaves and twigs, in addition to fruits and vegetables (Ilmberger et al., 2014). The samples were collected aseptically by the Zoo staff and the study did not involve protected or endangered species (Ilmberger et al., 2014). *SusD70111* WT had 588 amino acids (64.5 kDa) and *SusD38489* WT had 603 amino acids (67.3 kDa).

susD1 (AGH14103.1) belonged to cow rumen metagenome (fosmid *Sc00044*) (Rosewarne et al., 2014) and it was found in the Hidden Markov Model by Voss group (University of Stuttgart, Germany). Briefly, rumen samples were collected from cattle (*Bos indicus*) mainly fed with Rhodes grass (*Chloris gayana*) in Rockhampton (QLD, Australia) (Rosewarne et al., 2014). Besides, the sampling was in accordance with the protocols approved by the Rendel Laboratory Animal Experimentation and Ethics Committee (Rosewarne et al., 2014). *SusD1* WT had 580 amino acids (64.8 kDa).

Using the CDD Database, a “SusD superfamily” conserved domain (accession number cl21747) was identified for each protein. For example, in *SusD1* this conserved domain ranged between the positions 106 to 589 aa, in *SusD38489* between 114 and 509 aa and 23 to 214 aa in *SusD70111*. Additionally, *SusD70111* presented another conserved domain, named “SusD_RagB superfamily” (cl19983; between the amino acids 297 and 513).

Figure 8 shows the upstream-downstream operon map of each protein.

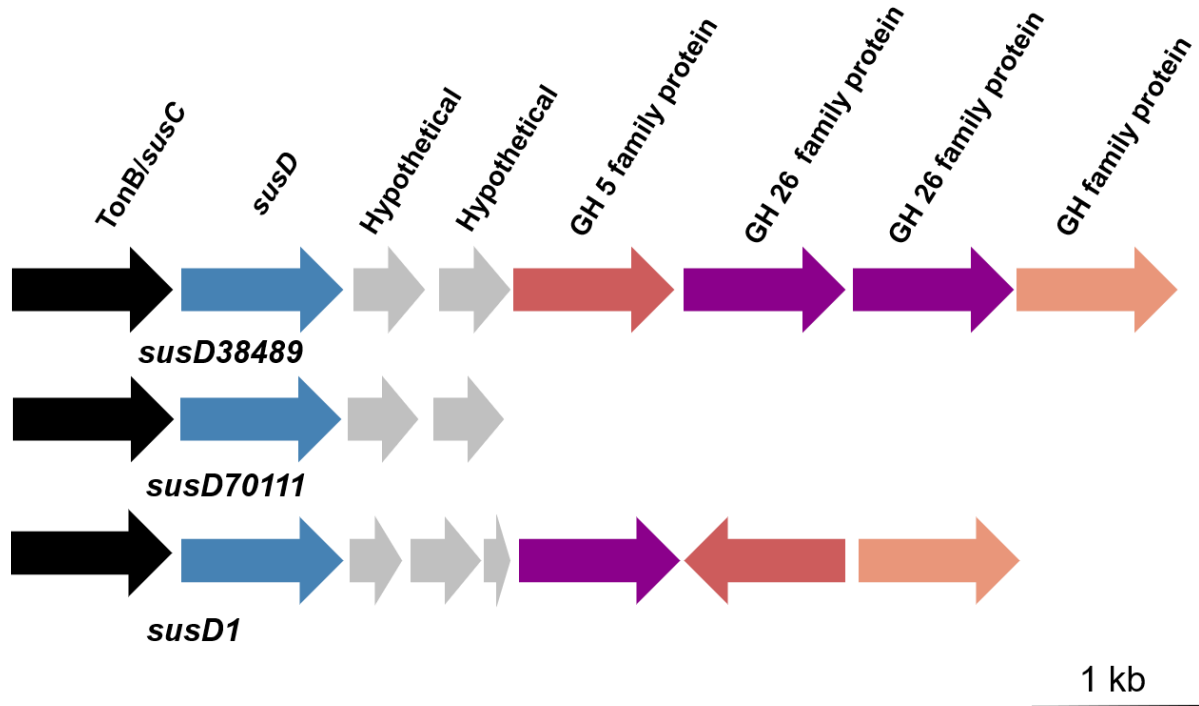


Figure 8: Upstream-downstream map of *susD38489*, *susD70111* and *susD1*. As expected, the neighbour analysis revealed the presence of *susC* (in black) positioned upstream *susD*. Downstream of *susD*, it was possible to identify genes encoding hypothetical proteins (grey) and glycoside hydrolases (GH) of distinct families (red, purple and salmon). Adjacent to *susD70111*, genes encoding GH were not found. This data was retrieved from the metagenome analysis of elephant feces (Ilmberger et al., 2014) and cow rumen (Rosewarne et al., 2014). *SusD70111* and *susD38489* presented contigs with sizes 11 and 16 kb, respectively. *SusD1* contig size was not identified.

The N-terminal signal peptide ranging from 19 to 23 aa residues was previously identified in several *SusD*-homologs and it was very conserved (Bolam & Koropatkin, 2012). Previously, Koropatkin *et al.* described a *susD* from *B. thetaiotaomicron* that included an outer membrane signal peptide and a lipidated cysteine at position 25, responsible for tethering the protein to the outer membrane (Koropatkin et al., 2008). A cysteine residue was also identified in *susD1*, *susD70111* and *susD38489* at the positions 23, 20 and 25, respectively.

SusD70111, SusD38489 and SusD1 presented a N-terminal lipoprotein signal peptide (Sec/SPII), which was removed and generated SusD70111 Δ 1-20, SusD38489 Δ 1-25 and SusD1 Δ 1-22 respectively (Figure 9).

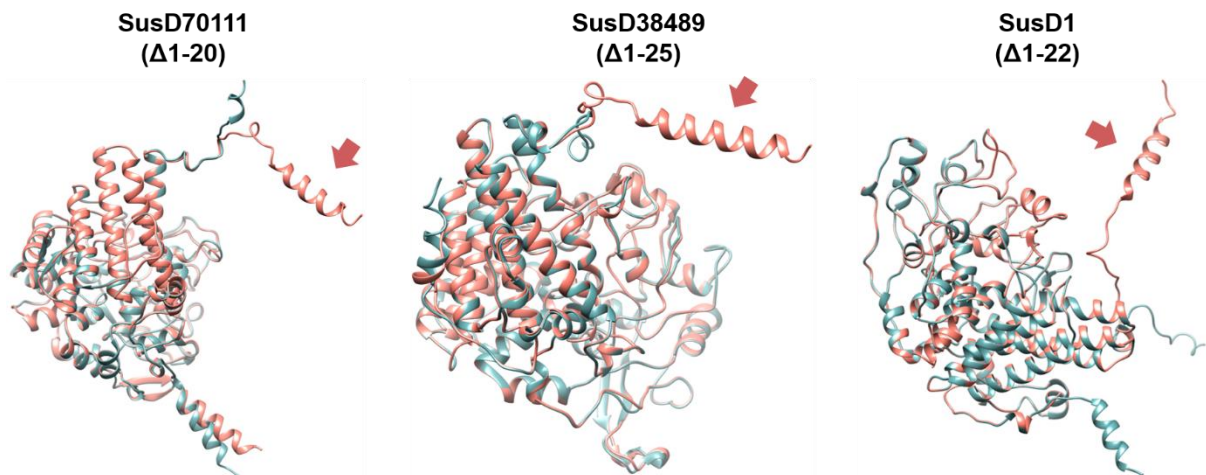


Figure 9: Side view of the predicted structure of SusD70111, SusD1 and SusD38489 WT (green) and their respective mutants lacking the N-terminal signal peptide Sec/SPII (salmon). The signal peptide (red arrow) of SusD70111 has 57 bp (19 aa), while SusD1 and SusD38489 have 60 bp (20 aa) and 71 bp (24 aa) respectively.

3.2 Phylogenetic analysis

SusD70111 shared a recent common ancestor with the SusD-homologs from hot springs and clustered with SusD from *Raineyia orbicola* (NCBI accession number PKQ69315.1). Structural analysis showed that SusD-homologs from hot springs presented a conserved structure, mostly composed of α -helices that overlapped with SusD70111, SusD1 and SusD38489.

III. Results

SusD1 and SusD38489 clustered with the proteins from a similar niche (gut or feces metagenomes), which also presented a conserved structure. Because of the structural similarity with SusD (Goulas et al., 2016), RagB proteins from the oral pathogen *P. gingivalis* were included as an external group (Figure 10).

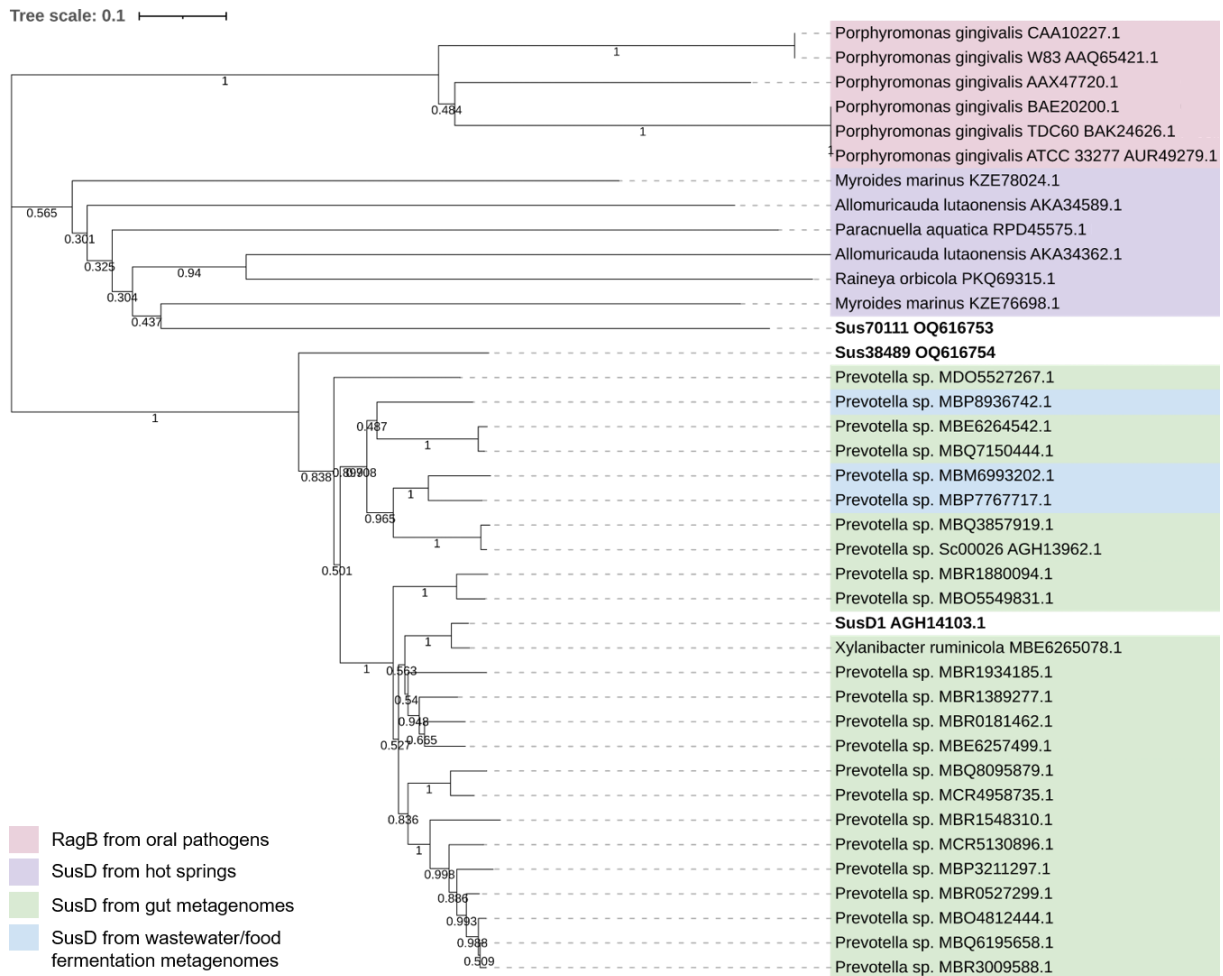


Figure 10: Phylogenetic tree of SusD1, SusD38489 and SusD70111. A bootstrap tree of proteins from the family of binding modules SusD and RagB was constructed. The tree was rooted at the RagB proteins from the oral pathogen *Porphyromonas gingivalis*, which was considered the external group (Acuna-Amador et al., 2018; Hall et al., 2005; Hanley et al., 1999; Nagano et al., 2007; Nelson et al., 2003; Watanabe et al., 2011). SusD-homologs from gut (Gharechahi et al., 2022; Rosewarne et al., 2014) and feces (green), wastewater and food fermentation metagenomes (blue) (Crognale et al., 2021) were found by BLASTp, using the NCBI “Non-redundant protein sequences” Database. RagB proteins are identified in pink. The SusD-homologs from hot springs (Wang et al., 2019) (purple) were included, because they represent a distinct niche. The branch lengths and NCBI accession numbers can be found in the tree.

3.3 Protein purification and concentration

In terms of concentration and purity, there was no difference between each protein and their respective mutants lacking the signal peptide. *SusD1Δ1-22* had the best purity percentage (83.39% *versus* 77.95% of *SusD38489Δ1-25*), while *SusD38489Δ1-25* had the highest protein yield (70 mg/mL *versus* 20 mg/mL of *SusD1Δ1-22*, in 5 g of cells) (Figure 11). *SusD70111Δ1-20* usually displayed the weakest performance (50% of purity, 3 mg/mL, in 5 g of cells). Besides, fractions from the supernatants were also collected and loaded onto SDS gels. Within this approach, it was observed that no protein was lost in the supernatant.

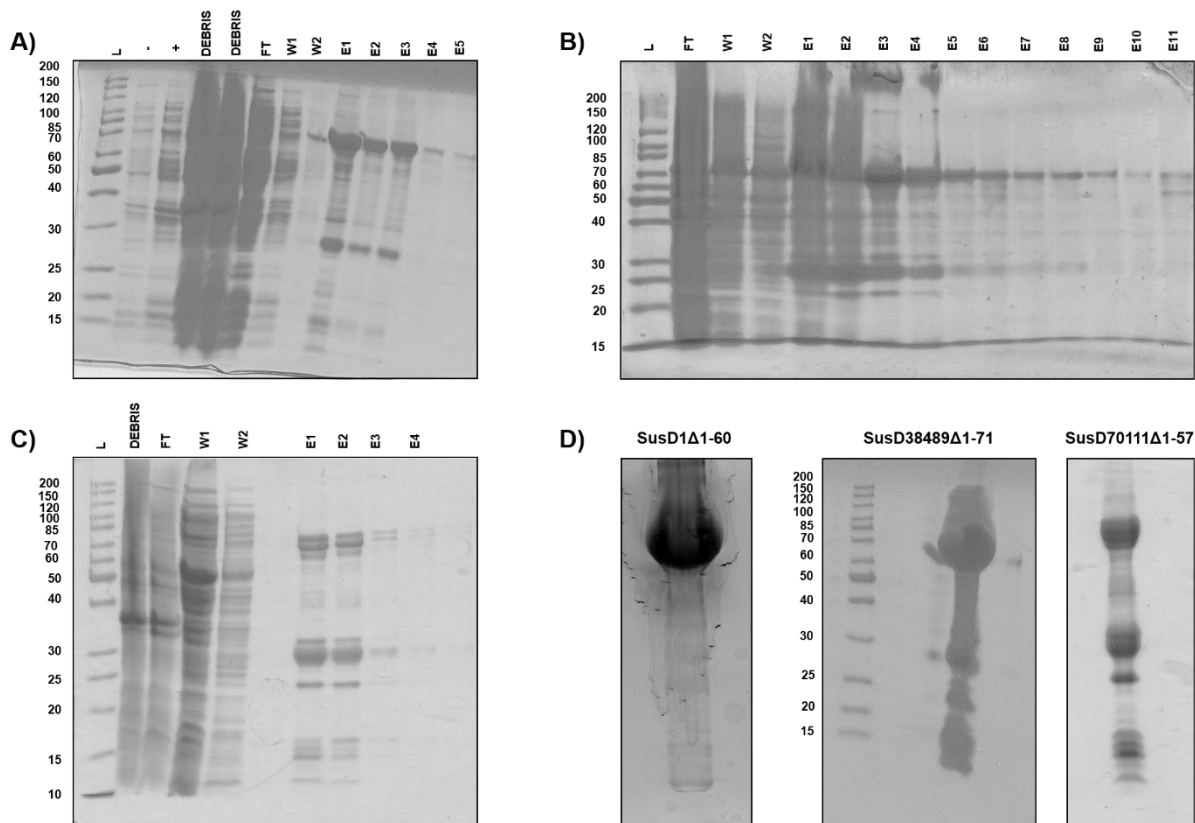


Figure 11: Polyacrylamide gels from each protein purification. A) *SusD1Δ1-22* (63.2 kDa); **B)** *SusD38489Δ1-25* (65.6 kDa); **C)** *SusD70111Δ1-20* (64.3 kDa); **D)** Proteins after buffer exchange to potassium phosphate buffer 0.1 M pH 7. From left to right: *SusD1Δ1-22*, *SusD38489Δ1-25* and *SusD70111Δ1-20*. The ladder used was PageRuler® unstained protein ladder #26614 (Thermo Fisher Scientific, Massachusetts, USA). L: protein ladder; -: cell culture before protein expression; +: cell culture after protein expression; DEBRIS: cell debris; FT: flow through; W1: 1st wash; W2: 2nd wash; E1: 1st

elution; E2: 2nd elution; E3: 3rd elution; E4: 4th elution; E5: 5th elution; E6: 6th elution; E7: 7th elution; E8: 8th elution; E9: 9th elution; E10: 10th elution; E11: 11th elution.

3.4 Pull-down assay

In this qualitative assay, protein fractions were loaded in SDS gels and evaluated with Western Blot. When a protein band appeared to be stronger in the elution than in the last washing step, it meant that the protein presented putative binding to the substrate and could be eluted with the detergent. SusD1 Δ 1-22 and SusD70111 Δ 1-20 showed putative adsorption to MC and PET, but not PET after 30 days under UV-C light (Figure 12A). SusD1 Δ 1-22 was also tested with LDPE and PA6, which suggested better affinity to PA6 than LDPE (Figure 12B). In some cases, it is possible to identify two protein bands at distinct sizes in kDa, which is likely due to protein degradation.

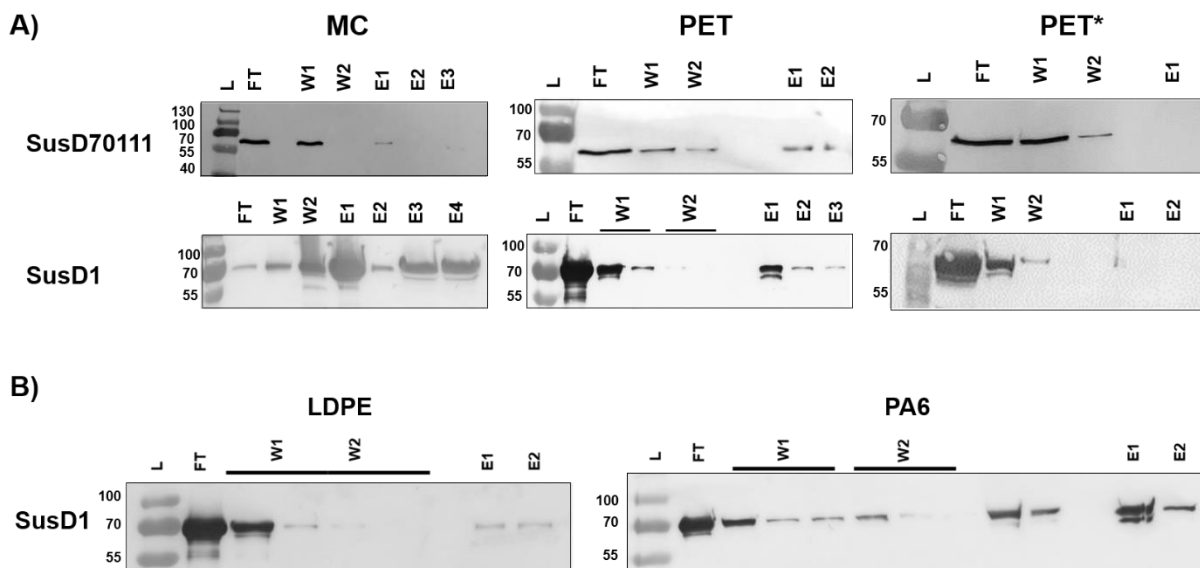


Figure 12: Nitrocellulose membrane of the Western Blot performed for the fractions collected from each pull-down assay. The ladders PageRuler™ prestained protein ladder (#26616) or PageRuler™ Plus prestained protein ladder (#26619) from Thermo Fisher Scientific (Massachusetts, USA) were applied onto the gels. **A)** SusD70111 Δ 1-20 (64.3 kDa) and SusD1 Δ 1-22 (63.2 kDa), could be detected from microcrystalline cellulose (MC) and PET powder after the elution with Triton 2% (v/v). However, no protein could be detected from PET after 30 days of incubation under UV-C light (PET*). **B)** SusD1 Δ 1-22 was also tested with the synthetic polymers LDPE and PA6. The putative adsorption of

this protein towards LDPE appeared to be the weakest, when compared to the other substrates. L: ladder; FT: flow through; W1: washing fraction 1; W2: washing fraction 2; E1: elution fraction 1; E2: elution fraction 2; E3: elution fraction 3. The assays for SusD1 were conducted by Tabea Neumann during her Master thesis. *SusD38489Δ1-25* was evaluated as part of another work and it will not be displayed here.

3.5 Affinity PAGE

The main features of the proteins were kept, once the protein was not denatured and the experiment was performed under native conditions. The negative control consisted of a polyacrylamide gel without substrate, comprising only two layers (stacking and separating gel). In the preparation of gels with substrates, a thin layer of 2 mL was added between the stacking and separating gels.

The substrates tested were CMC and semi-crystalline PET powder. Polyacrylamide and native buffer (1.5 M Tris-HCl), as well as the polymerizing reagents (APS 10% and TEMED), were added to each substrate respecting the same concentrations of the separating gel (Table 11). Only *SusD1Δ1-22* and *SusD38489Δ1-25* (20 μM each) were evaluated, once they represented the best candidates in terms of recombinant protein expression and putative binding. Figure 13 shows that both proteins ran slower in the presence of CMC, in comparison to the negative control and PET. This finding suggests that both proteins interacted better with CMC than with PET. Furthermore, thin protein bands could be detected interacting with the PET layer, which suggests a residual binding.

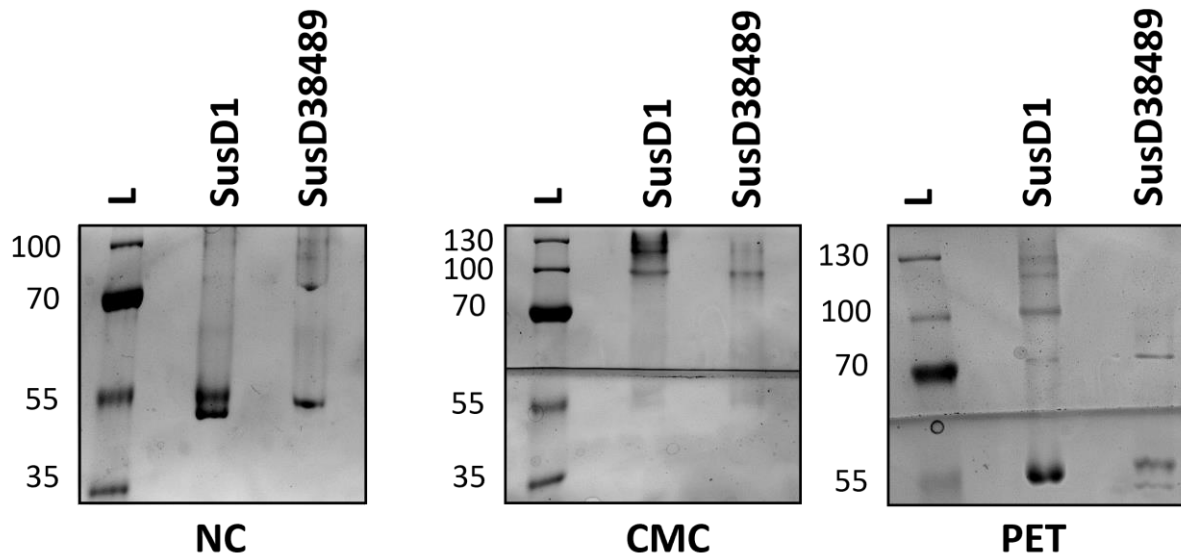


Figure 13: Native gel and affinity PAGE performed for the proteins SusD1 Δ 1-22 (63.2 kDa) and SusD38489 Δ 1-25 (65.6 kDa). The ladder PageRuler™ Plus prestained protein ladder (#26619, Thermo Fisher Scientific, Massachusetts, USA) was used as a “ruler”, ensuring that each protein would run similarly. Although native gels are not ideal for determining protein size in kDa, they are well-suited for identifying dimers, as demonstrated by the detection of SusD1 dimers in the negative control (NC; gel without substrate). CMC and PET: affinity PAGE, with a layer containing the substrates carboxymethylcellulose and PET, respectively.

As the negative control consisted of native PAGE, two bands of the same size in kDa were identified for SusD1. Each gel was repeated as three independent experiments and, in every case, these two bands were visible. A previously-described SusD was reported to be predominantly monomeric, with only a small fraction appearing as dimers (Koropatkin et al., 2008). This finding suggests that our Data is in accordance with other SusD-homologs.

3.6 Screening of the fluorescence signal

Translational fusions of SusD and sfGFP were produced in the expression vector *E. coli* BL21(DE3). The colonies were grown in LB agar plus ampicillin and IPTG, previously described in the “II. Materials and Methods” section. After overnight incubation at 37 °C, the colonies were green and fluorescent glowing under UV-C light (Figure 14).

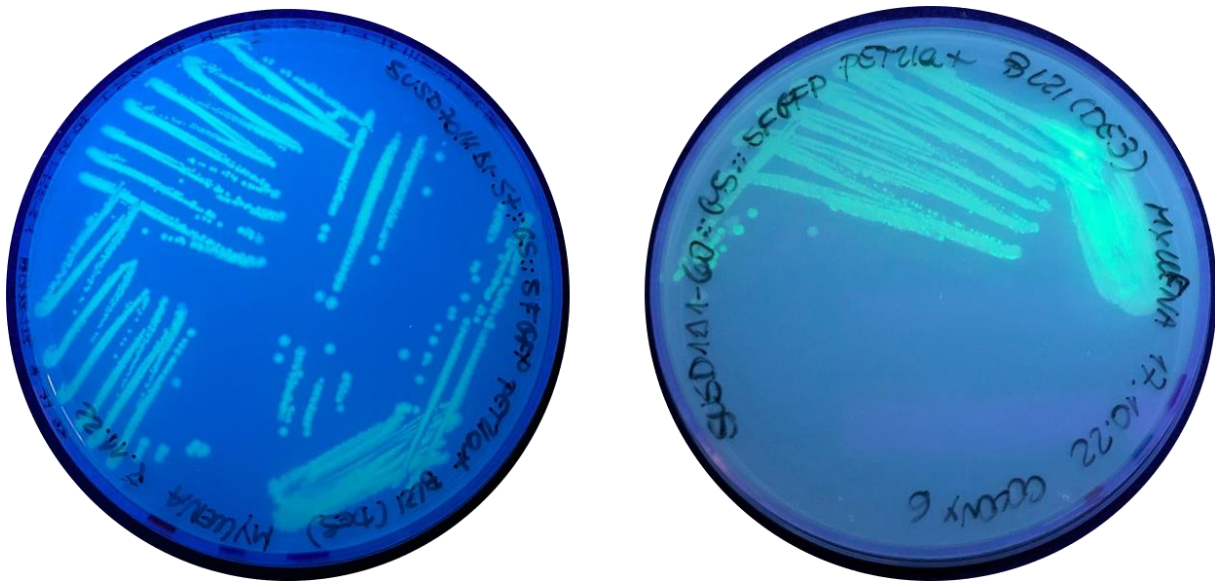


Figure 14: *E. coli* BL21(DE3) carrying genes that encode the translational protein fusions with sfGFP. A neon green color is visible under UV-C light and in the presence of 100 mg/mL of ampicillin and 1 mM of IPTG. SusD38489Δ1-25 was performed as part of another work, and it will not be presented here.

3.6.1 Natural polymers

The main objective of this assay was to quantify the fluorescent signal on each substrate as a measurement of bound protein. The measurements were collected from the top and bottom of the plates, with a subtle difference. For this reason, the measurements collected from the bottom were used for each natural and synthetic

polymer tested. The fluorescence measurements of natural polymers were performed with the insoluble substrates MC and chitin (Figures 15 and 16).

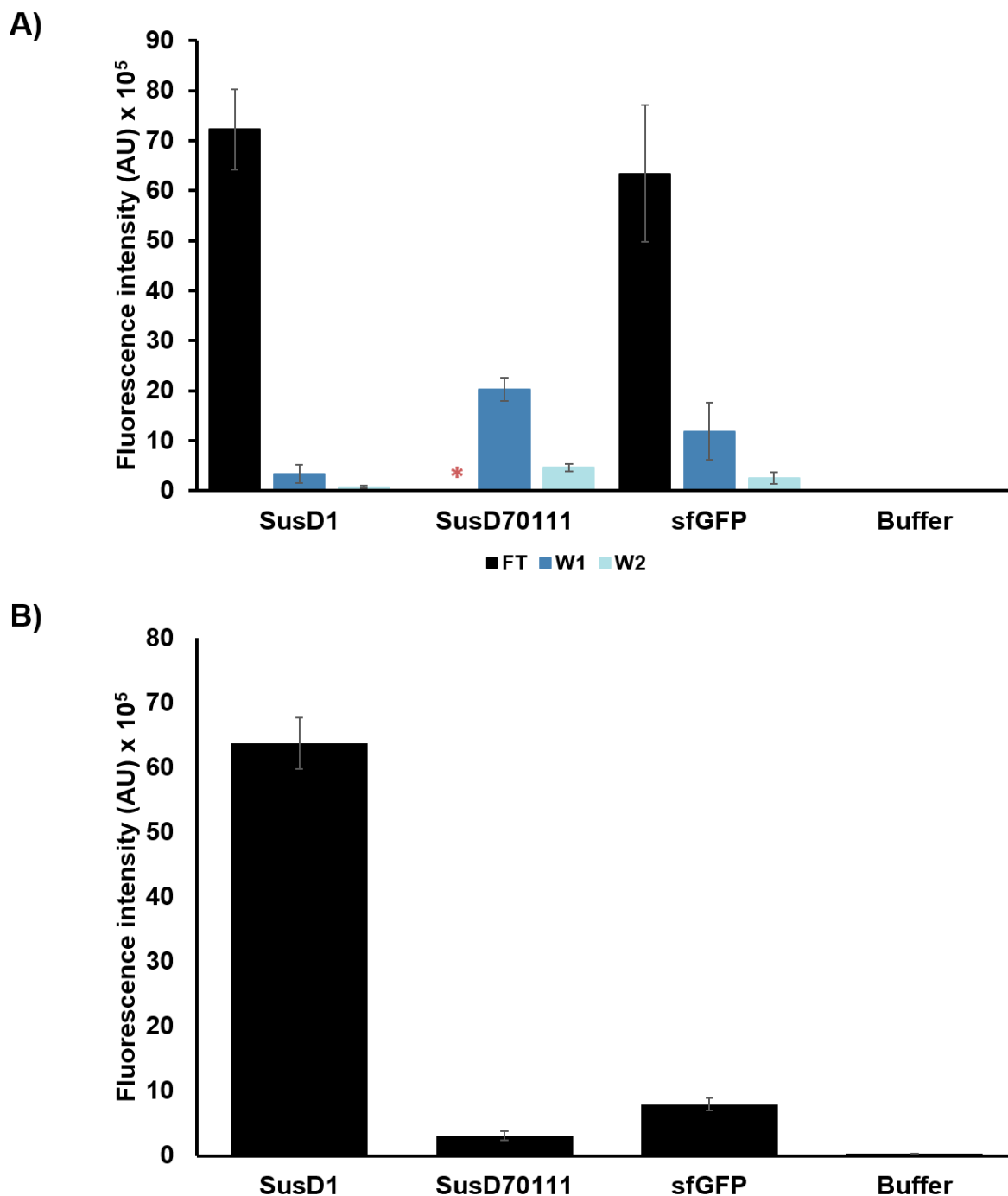


Figure 15: Protein adsorption captured by fluorescence measurements. A) Fractions of the flow through (FT), first and second washes (W1 and W2, respectively). 200 μ L of each was transferred to a 96-well microtiter plate, with transparent flat bottom and black walls. After gently shaking the plates for 3 sec, the fluorescence measurements were collected from the bottom at excitation of 485 nm and emission of 510 nm. The bars represent the mean value of the measurements collected in triplicates. Error bars represent the standard deviation. Red star represents a measurement indicated as “overflow”,

meaning that most of the protein was already lost in that step. The incubations were carried out with 20 μM of protein. sfGFP or the buffer used for each incubation (potassium phosphate buffer, 0.1 M pH 6) plus the substrate were the negative controls. **B)** Following the procedure mentioned above, microcrystalline cellulose (MC) was resuspended in 200 μL of fresh buffer and transferred to the plates.

SusD70111 Δ 1-20 is proposed to be the weakest cellulose binding protein. However, this protein might have preference for chitin (Figure 16).

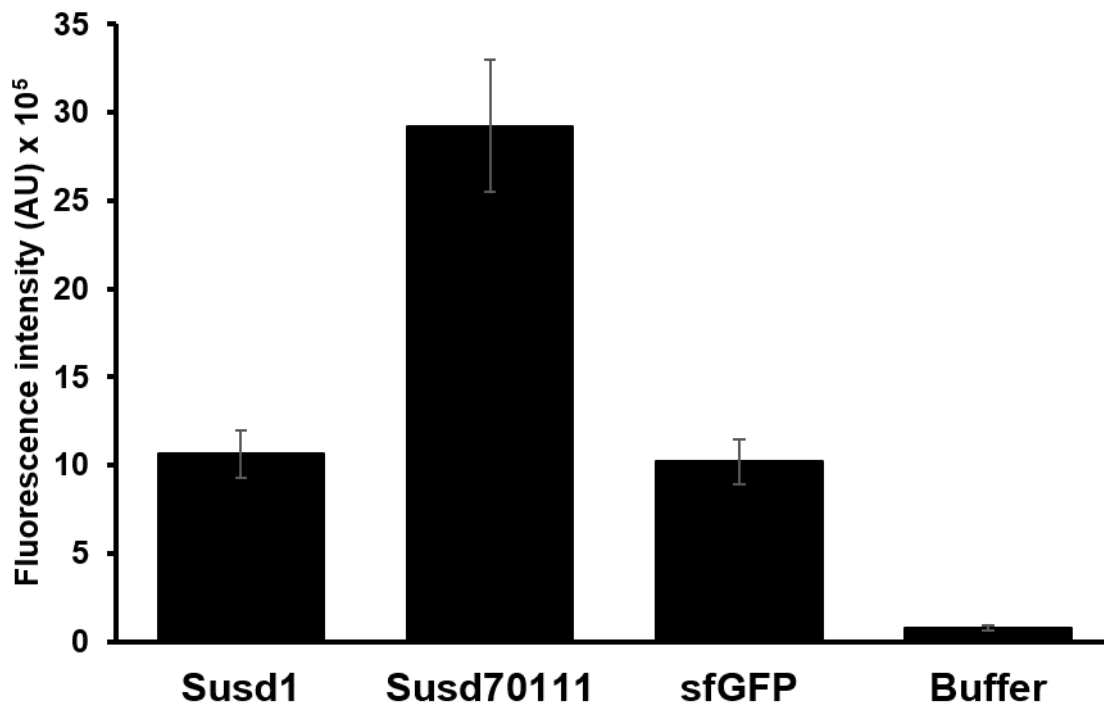


Figure 16: Fluorescence measurements after protein incubation with chitin. Each protein at a final concentration of 20 μM incubated with 0.01 g of chitin. After removing the flow through and washing the substrate twice with potassium phosphate buffer 0.1 M pH 6, chitin powder was resuspended in fresh buffer and transferred to a 96-well microtiter plate, with transparent flat bottom and black walls. The plate was mixed for 3 sec and sfGFP measurements were collected from the bottom, at excitation of 485 nm and emission of 510 nm. The bars represent the mean value calculated from triplicates, while the error bars represent the standard deviation. The negative controls were sfGFP or buffer plus chitin.

Natural polymers such as starch, xylan and algae compounds could not be successfully tested. The limitations included a high sfGFP background for starch and xylan, as well as the consistency of the algae powder, with the retention of most of the liquid.

3.6.2 Synthetic polymers

Many challenges were encountered with the sfGFP reporter towards synthetic polymers. First, PET foil presented a high autofluorescence background when analyzed with the plate reader (Figure 17A). Second, sfGFP appeared to interact with each synthetic polymer tested (PA6, PET and LDPE) (Figure 17A and B). An attempt to overcome the problem was to test the most promising substrate (which was PA6 foil, due to the lowest affinity to sfGFP and buffer background), at pHs ranging from 7 to 4 (Figure 17B). For the pHs 6 and 7, potassium phosphate buffer 0.1 M was used on each protein dilution, as well as on the negative controls. For the pHs 4 and 5, citrate buffer 0.1 M was used. Therefore, it was observed that sfGFP alone had the strongest performance at pH 7, and that every protein denatured at pHs 4 and 5. For this reason, further tests and repetitions were carried out with pH 6, but the attempts were not successful. Additionally, only the flow through presented a visible light green color, especially for SusD70111 Δ 1-20, suggesting that most of it was already lost in this fraction.

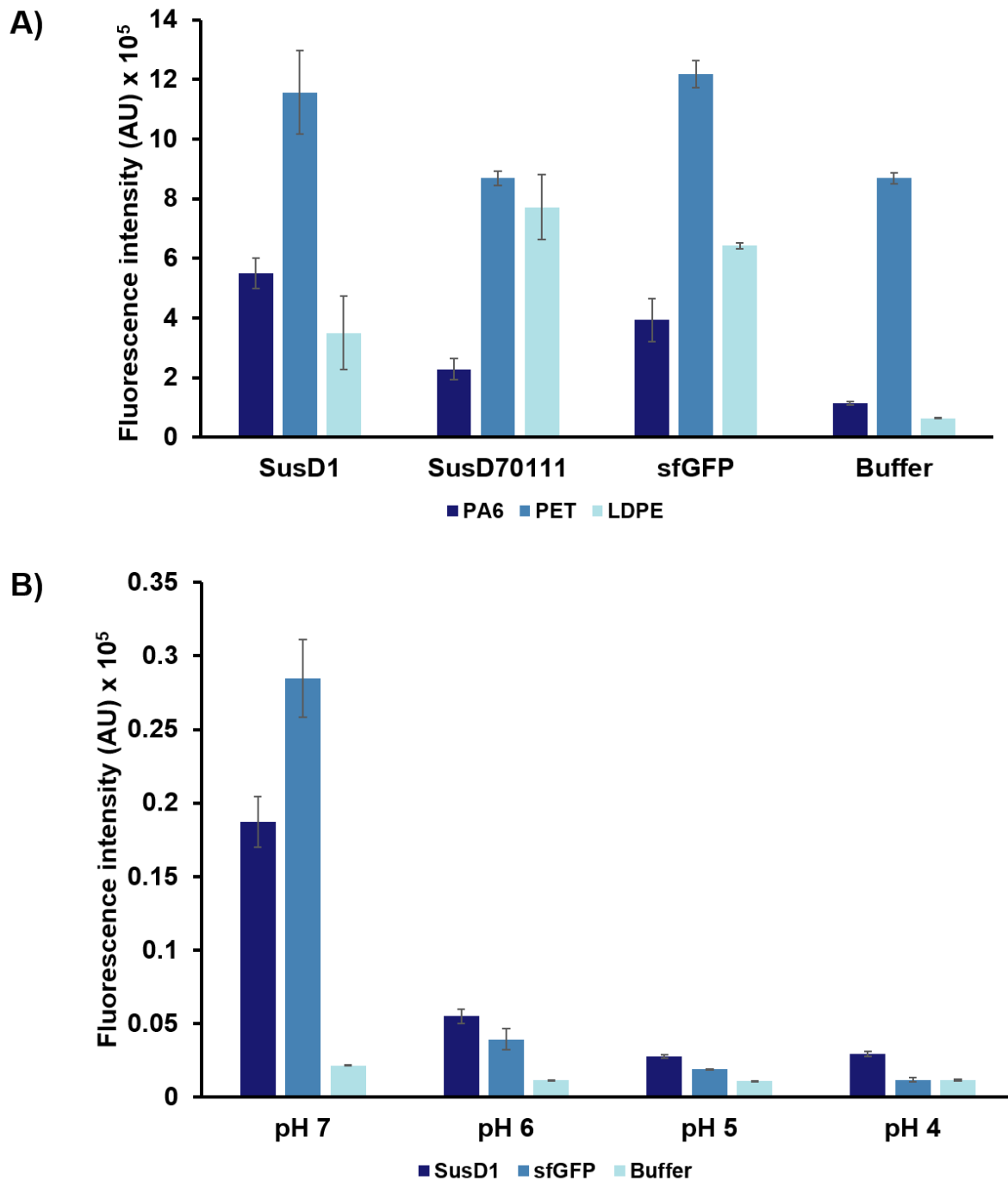


Figure 17: Fluorescence measurements after protein incubations with synthetic polymers. A) The synthetic polymers PA6, PET and LDPE were incubated with 20 μ M of each protein. The negative control consisted of potassium phosphate buffer 0.1 M pH 6 with each substrate. Besides, sfGFP was also used as a negative control. PET foil had a very high background in the negative controls and the measurements were not significant. sfGFP bound PA6 and LDPE, but SusD1 Δ 1-22 and SusD70111 Δ 1-25 bound PA6 and LDPE slightly better, respectively. **B)** An attempt to remove the background caused by sfGFP was testing distinct pHs, ranging from 4 to 7. PA6 was the substrate selected for this trial, once it presented the general lowest background for sfGFP. At pH 7, sfGFP presented the strongest background. At pHs 5 and 4, all the proteins denatured. Therefore, the selected pH for the tests were pH 6. The bars represent mean values obtained from tests performed in triplicates, while the error bars

represent standard deviation. In each test, the substrate measured was the foil resuspended in 200 μ L of fresh buffer and transferred to the 96-well microtiter plates with transparent flat bottom and black walls. The measurements were performed after gently shaking the plates for 3 sec, from the bottom of the microtiter plate at excitation of 485 nm and emission of 510 nm.

3.7 Characterization of SusD70111_{F3}

A fragment of 25.4 kDa, cloned from the region between 1102 and 1767 bp of *susD70111*, displayed preliminary binding towards PET (Figure 18A and B). This truncated protein was named SusD70111_{F3} and comprises two predicted conserved domains in the C-terminus region of SusD70111 (Figure 18C).

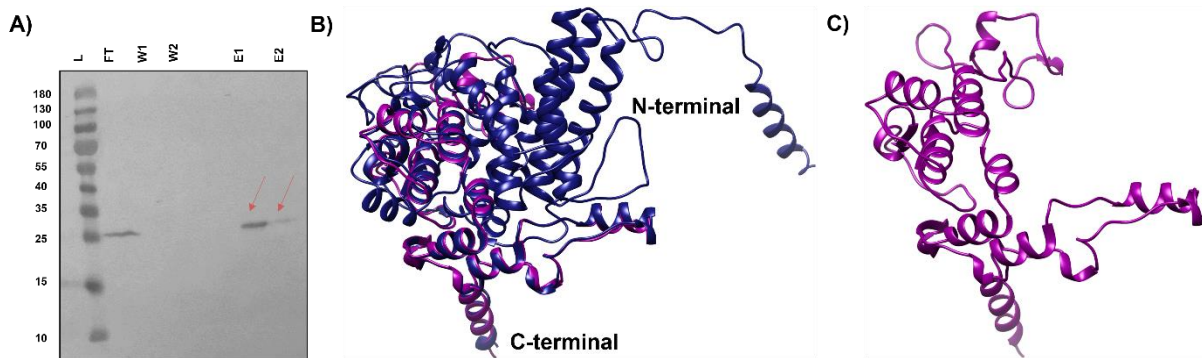


Figure 18: Main features of the truncated protein SusD70111_{F3}. **A)** Pull-down assay performed with the crude cell extract of SusD70111_{F3} showed putative binding towards PET, since the protein band could be detected after the elution with Triton X-100 2% (v/v). There was no visible protein band on the washing fractions. L: PageRuler™ prestained protein ladder (#26616, Thermo Fisher Scientific, Massachusetts, USA); FT: flow through; W1 and W2: washes 1 and 2, respectively; E1 and E2: elution 1 and 2, respectively. **B)** Predicted structure of SusD70111 (64.5 kDa; dark blue) and SusD70111_{F3} (25.4 kDa; dark magenta). The protein structure was mainly composed of α -helices, which is in accordance with previously-described SusD-homologs (Koropatkin et al., 2009). Six β -strands were present within the structure of SusD70111, in which four of them form β -hairpins. **C)** Predicted structure of SusD70111_{F3} in evidence. Four out of six β -strands were present in SusD70111_{F3}, because they were positioned near the C-terminus of SusD70111.

SusD70111_{F3} was also fused to sfGFP. In the future, further tests could be performed with chitin.

3.8 Binding kinetics with SPR analysis

SusD1 Δ 1-22, SusD38489 Δ 1-25 and SusD70111_{F3} were evaluated. However, SusD70111 Δ 1-20 could not bind to the analytical chip (possibly due to the low protein concentration). CMC is water-soluble and it was selected as a representative of cellulose. For comparison, Figure 19 shows the structure of the natural polymers used in this work.

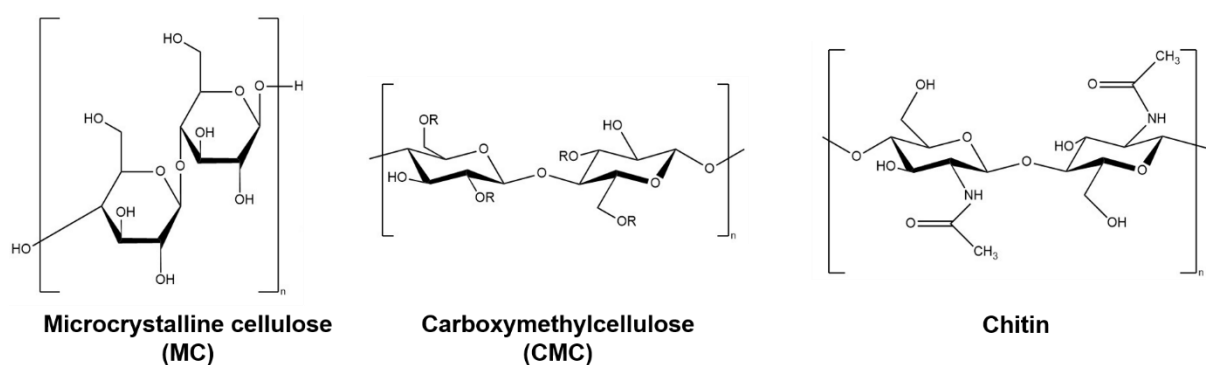


Figure 19: Chemical structure of microcrystalline cellulose (MC), carboxymethylcellulose (CMC) and chitin, the natural polymers evaluated in this work. Designed with ChemDraw Professional© v.22.0.0.22.

Due to the structure similarity, PETases are usually able to degrade BHET (Guo et al., 2023). For this reason, this substrate was a suitable candidate for the synthetic polymer testing. Other degradation products include MHET, TPA and ethylene glycol (EG; Figure 20), which were not evaluated during this work.

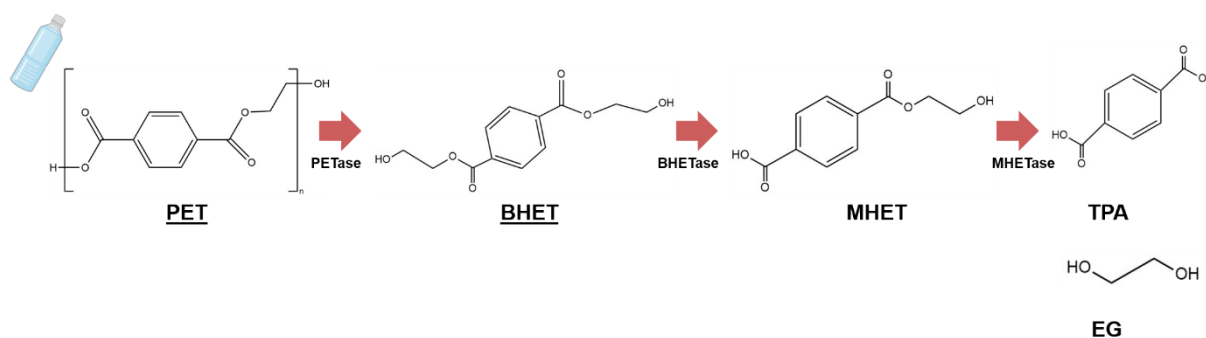


Figure 20: Chemical structure of PET and its constituents bis(2-Hydroxyethyl) terephthalate (BHET), mono-2-hydroxyethyl-terephthalate (MHET), terephthalic acid (TPA) and ethylene glycol (EG). Figure adapted from (A. Li et al., 2023). Designed with ChemDraw Professional© v.22.0.0.22.

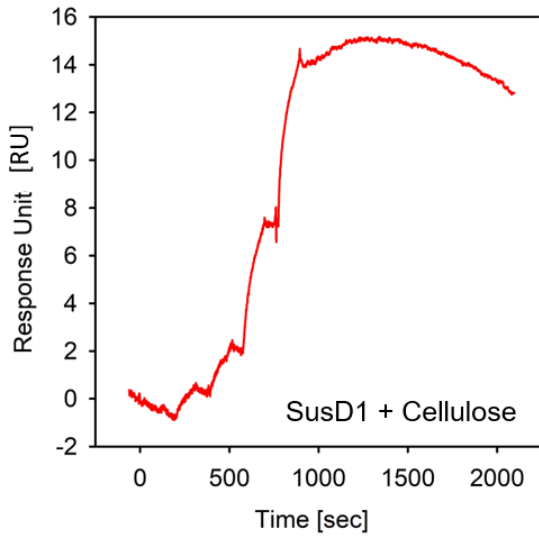
Each protein was captured through the C-terminal His₆-tag onto a CM5 sensor chip immobilized with anti-His₆ antibody. Afterwards, increasing concentrations of the polymers were injected over the chip without regeneration steps. The sensorgrams were analyzed using the 1:1 binding algorithm. The interaction of SusD1Δ1-22 with CMC resulted on an association rate of $5.2 \times 10^3/\text{M}^*\text{s}$ (k_a) and dissociation rate of $7.0 \times 10^{-5}/\text{s}$ (k_d), with an overall affinity of ($K_D=14$ nM) (Figure 21A). Besides, the shape of the sensorgrams and the R_{\max} of 2.5 RU suggest that SusD1Δ1-22 presented more than one binding site to CMC, with varied affinity towards this substrate. When higher concentrations of the analyte were injected, the R_{\max} increased, which suggests that SusD1Δ1-22 presented binding sites with high and low affinity to CMC. With BHET, the association rate was higher $k_a=5.0 \times 10^5/\text{M}^*\text{s}$ and the dissociation rate $k_d=1.2 \times 10^{-4}/\text{s}$, with an overall affinity of 0.3 nM (Figure 21B). Here, the binding stoichiometry was 1:1, meaning that a single binding site was detected.

Similar trends were observed for SusD38489Δ1-25, indicating that this second protein might also present more than one binding site to CMC ($R_{\max}=7$ RU) and one to BHET. SusD38489Δ1-25 presented an association rate of $k_a=5.0 \times 10^3/\text{M}^*\text{s}$ and a dissociation rate ten-fold lower ($k_d=6.3 \times 10^{-4}/\text{s}$) than SusD1Δ1-22 towards CMC. The lower affinity ($K_D=124$ nM) indicated a less stable interaction (Figure 21C). SusD38489Δ1-25 and

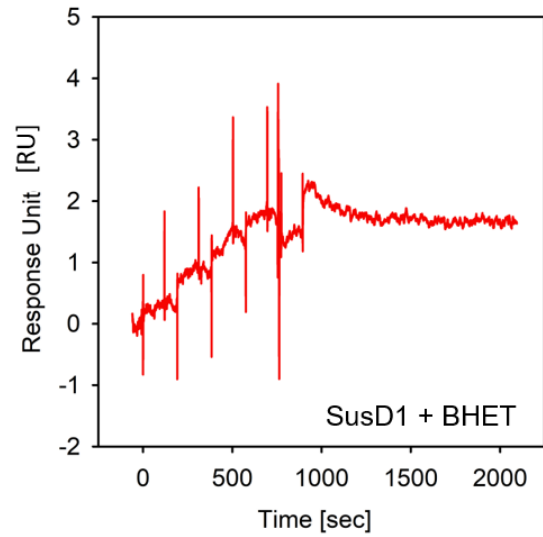
BHET also displayed low affinity, with an association/dissociation rate of $k_a=1.2 \times 10^5/\text{M}\cdot\text{s}$ and $k_d=1.0 \times 10^{-3}/\text{s}$, respectively. Therefore, the affinity of SusD38489 Δ 1-25 to BHET was 10 nM (Figure 21D).

SusD70111_{F3} interacted with CMC with a considerably high affinity ($K_D=0.3$ nM), which resulted from the association rate of $6.6 \times 10^3/\text{M}\cdot\text{s}$ and dissociation rate of $2.0 \times 10^{-4}/\text{s}$ (Figure 21E). Altogether, the R_{max} of 3 RU and the sensorgram shape indicated that only one binding site was detected for CMC. A similar trend was observed for the interaction with BHET ($k_a=9.4 \times 10^4/\text{M}\cdot\text{s}$; $k_d=1.5 \times 10^{-4}/\text{s}$; $K_D=1.6$ nM) (Fig. 21F). Due to the high dissociation rates, the interactions were stable and comparable to SusD1 Δ 1-22. Therefore, the results suggest that SusD70111_{F3} bound cellulose with higher affinity, followed by SusD1 Δ 1-22 and SusD38489 Δ 1-25. On the other hand, SusD1 Δ 1-22 bound BHET better, followed by SusD70111_{F3} and SusD38489 Δ 1-25.

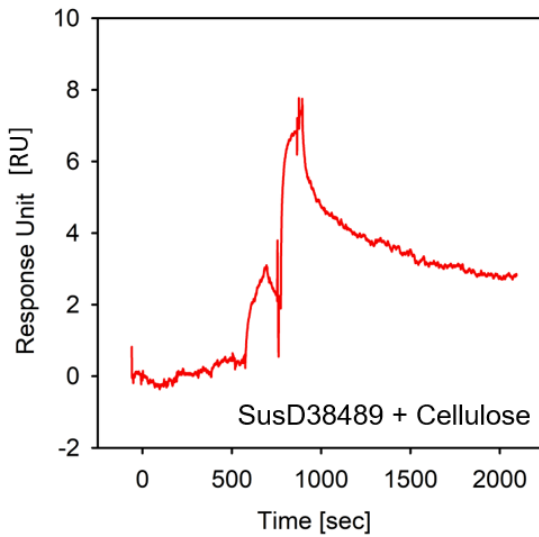
III. Results



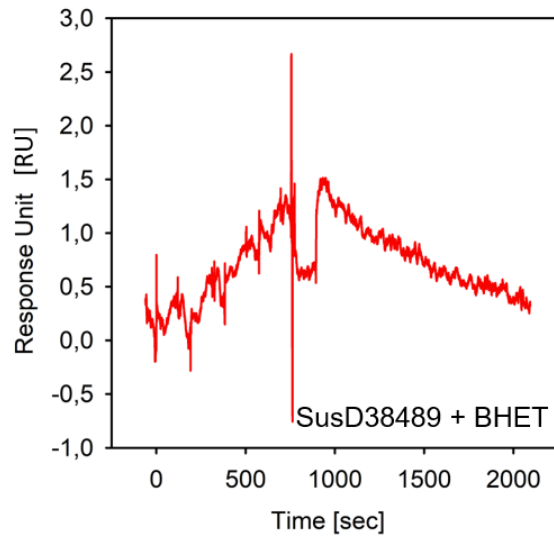
A $k_a = 5.2 \times 10^3 / M \cdot s$; $k_d = 7.0 \times 10^{-5} / s$; $K_D = 14 \text{ nM}$



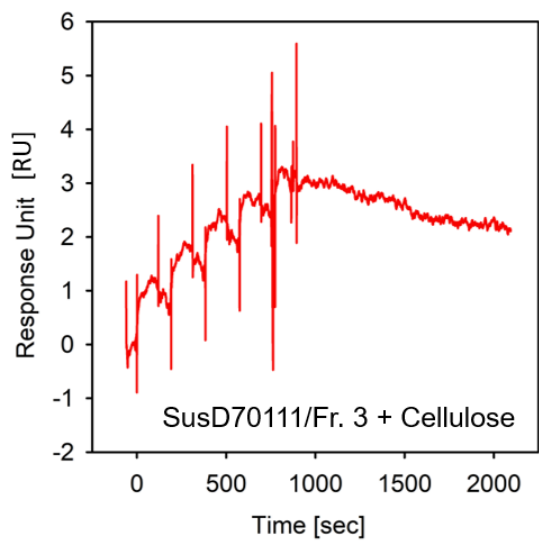
B $k_a = 5.0 \times 10^5 / M \cdot s$; $k_d = 1.2 \times 10^{-4} / s$; $K_D = 0.3 \text{ nM}$



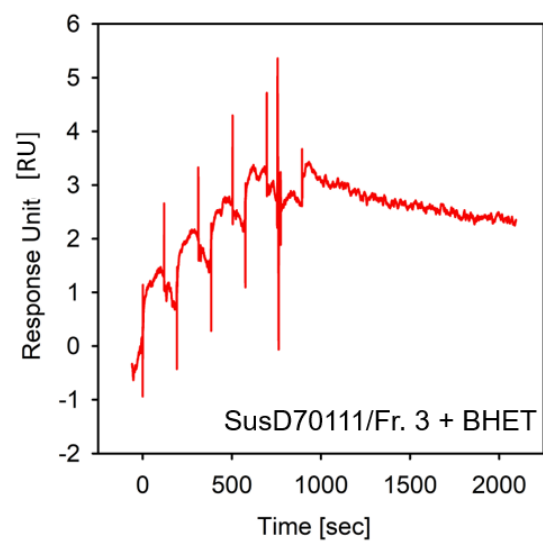
C $k_a = 5.0 \times 10^3 / M \cdot s$; $k_d = 6.3 \times 10^{-4} / s$; $K_D = 124 \text{ nM}$



D $k_a = 1.2 \times 10^5 / M \cdot s$; $k_d = 1.0 \times 10^{-3} / s$; $K_D = 10 \text{ nM}$



E $k_a = 6.6 \times 10^5 / M \cdot s$; $k_d = 2.0 \times 10^{-4} / s$; $K_D = 0.3 \text{ nM}$



F $k_a = 9.4 \times 10^4 / M \cdot s$; $k_d = 1.5 \times 10^{-4} / s$; $K_D = 1.6 \text{ nM}$

Figure 21: Sensorgrams obtained from the Surface Plasmon Resonance (SPR) spectroscopy. SusD70111 Δ 1-20 could not be evaluated with this approach, since the protein did not bind to the analytical chip. **A)** SusD1 Δ 1-22 and carboxymethylcellulose (CMC). Association rate: $5.2 \times 10^3/\text{M}^*\text{s}$ (k_a); dissociation rate: $7.0 \times 10^{-5}/\text{s}$ (k_d); overall affinity: $K_D=14$ nM. **B)** SusD1 Δ 1-22 and bis(2-Hydroxyethyl) terephthalate (BHET). Association rate: $k_a=5.0 \times 10^5/\text{M}^*\text{s}$; dissociation rate: $k_d=1.2 \times 10^{-4}/\text{s}$; overall affinity: $K_D=0.3$ nM. **C)** SusD38489 Δ 1-25 and CMC. Association rate: $k_a=5.0 \times 10^3/\text{M}^*\text{s}$; dissociation rate: $k_d=6.3 \times 10^{-4}/\text{s}$; overall affinity: $K_D=124$ nM. **D)** SusD38489 Δ 1-25 and BHET. Association rate: $k_a=1.2 \times 10^5/\text{M}^*\text{s}$; dissociation rate: $k_d=1.0 \times 10^{-3}/\text{s}$; overall affinity: $K_D=10$ nM. **E)** Truncated protein SusD70111 $_{F3}$ and CMC. Association rate: $k_a=6.6 \times 10^3/\text{M}^*\text{s}$; dissociation rate: $k_d=2.0 \times 10^{-4}/\text{s}$; overall affinity: $K_D=0.3$ nM. **F)** SusD70111 $_{F3}$ and BHET. Association rate: $k_a=9.4 \times 10^4/\text{M}^*\text{s}$; dissociation rate: $k_d=1.5 \times 10^{-4}/\text{s}$ and overall affinity: $K_D=1.6$ nM. Each curve was subtracted by the reference curve, used as a negative control.

3.9 Enzymatic activity of *lcc-wt* and *pet30 Δ porC* fused with *susD1*

One well-described cutinase with PETase activity, named LCC-WT (Sulaiman et al., 2012), and one enzyme from the phylum Bacteroidota with moderate activity on PET (PET30 Δ PorC) (Zhang et al., 2021), were fused with SusD1. Unfortunately, both enzymes did not present any improvement on the activity towards BHET and PCL. Figure 22A shows the incubation of *E. coli* BL21(DE3) expressing LCC-WT and SusD1 Δ 1-22::LCC-WT on substrate agar plates, whereas Figure 22B shows the results for PET30 Δ PorC and its fusion on a BHET plate.

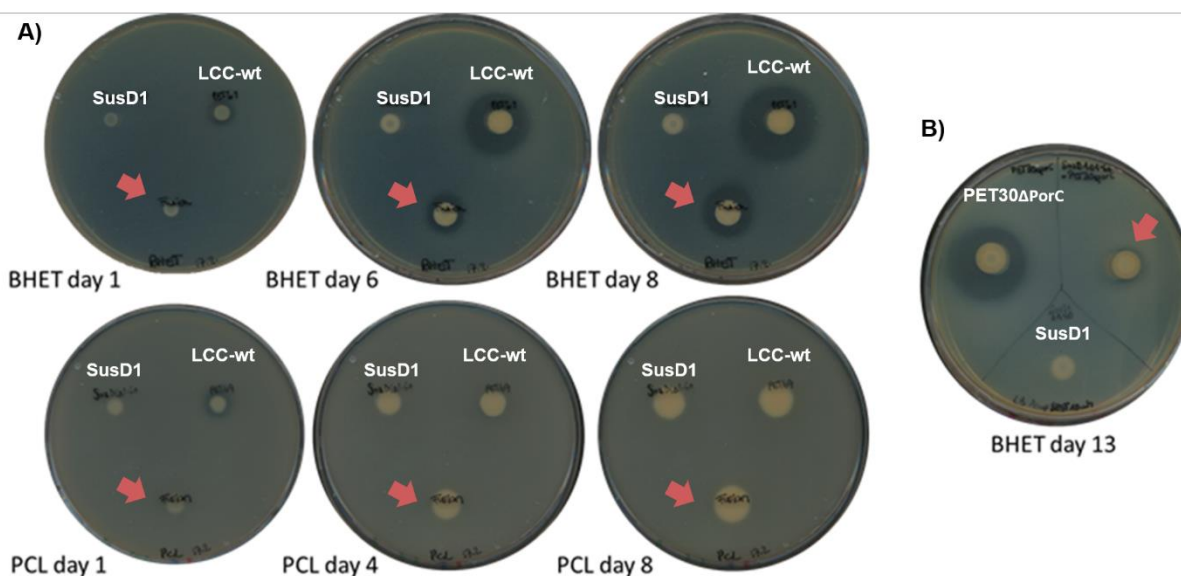


Figure 22: Enzymatic screening using agar plates with the substrates of interest. A) Activity plates of SusD1 Δ 1-22 fused with LCC-WT (Sulaiman et al., 2012) on bis(2-Hydroxyethyl) terephthalate (BHET; top) and polycaprolactone (PCL; bottom). **B)** SusD1 Δ 1-22 fused with PET30 Δ PorC (Zhang et al., 2021) on a BHET agar plate. The experiments were performed with 10 μ L of crude cell extract. Red arrows indicate the translational fusions.

Incubations with amorphous PET foil were also performed, to evaluate whether the enzymatic activity would improve when the substrate was in suspension with pure protein. After 72 and 120 h of incubation with constant shaking at 350 rpm, the samples were collected in six replicates for the UHPLC analysis. The concentration of TPA on each sample was calculated from the area of the peak around the retention time of 1.7 min. Negative controls included: 1) WT proteins or potassium phosphate buffer 0.1 M pH 8 (with and without substrate) and 2) translational fusion proteins without substrate. No peaks that could interfere with the analysis were detected on the negative controls. Besides, neither MHET nor BHET (with retention times of 2.1 and 2.6 min, respectively) were detected on any sample.

The six replicates did not present major differences, and Figure 23 compares the samples PET30 Δ PorC Fraction 2 (F2) and SusD1 Δ 1-22::PET30 Δ PorC fractions 1 and 5 (F1 and F5), after 72 and 120 h of incubation. For the WT enzyme, a peak could be

III. Results

detected at 1.7 min, which was proportional to the length of incubation time. However, no peak could be detected for the fusion protein, which means that probably there was an enzymatic impairment rather than improvement (Figure 23).

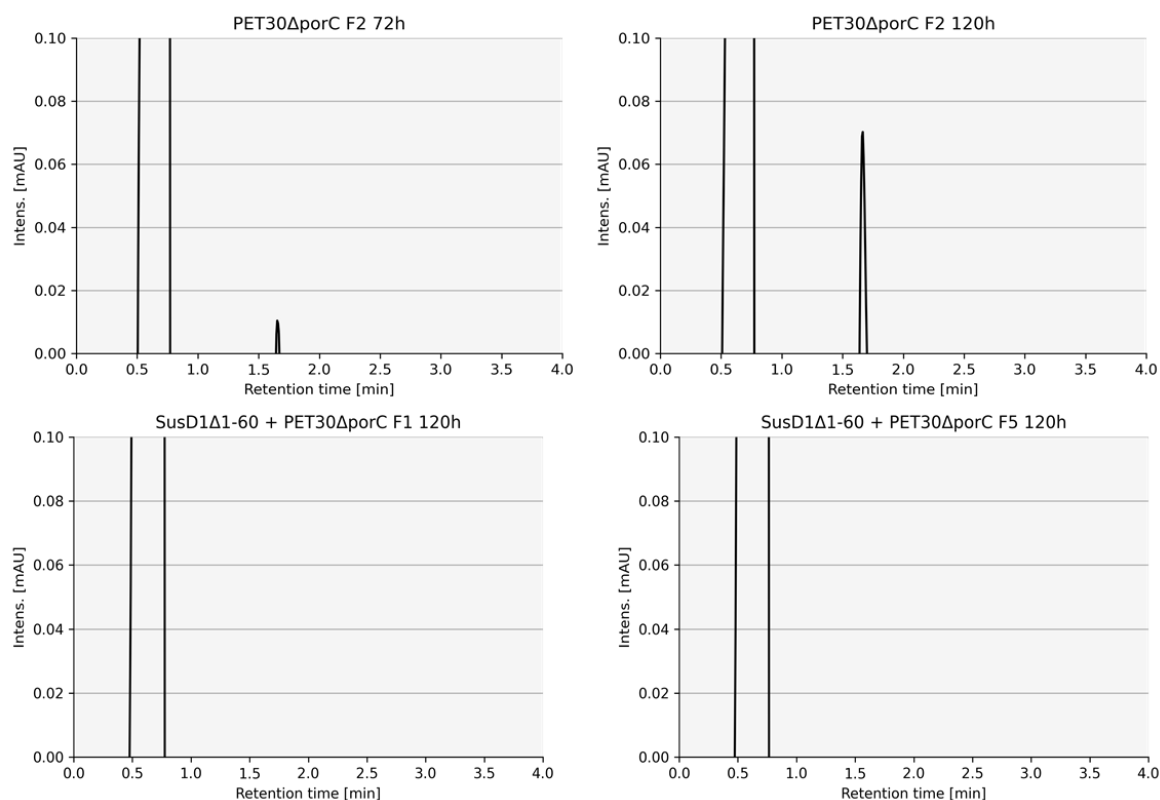


Figure 23: Chromatograms of PET30ΔPorC (top) (Zhang et al., 2021) and SusD1Δ1-22::PET30ΔPorC (bottom) after 72 and 120 h of incubation with amorphous PET foil. The 72-h incubation presented a peak with an area of 1.3692 (TPA concentration of 1.7543 μM), whereas the 120-h incubation had an increased area of 1.6601 (TPA concentration of 2.127 μM).

The incubation of LCC-WT and its respective fusion protein followed a similar trend. The negative controls did not interfere with the detection of PET degradation products. MHET and BHET at their respective retention times were not detected. For the WT, the average TPA concentration after 72 h was 17.734 μM , which increased to 55.391 μM after 120 h. The fusion enzyme presented inefficient activity when compared to the WT, with an average TPA concentration of 4.499 μM after 72 h and increased to only 4.559 μM after 120 h (Figure 24).

III. Results

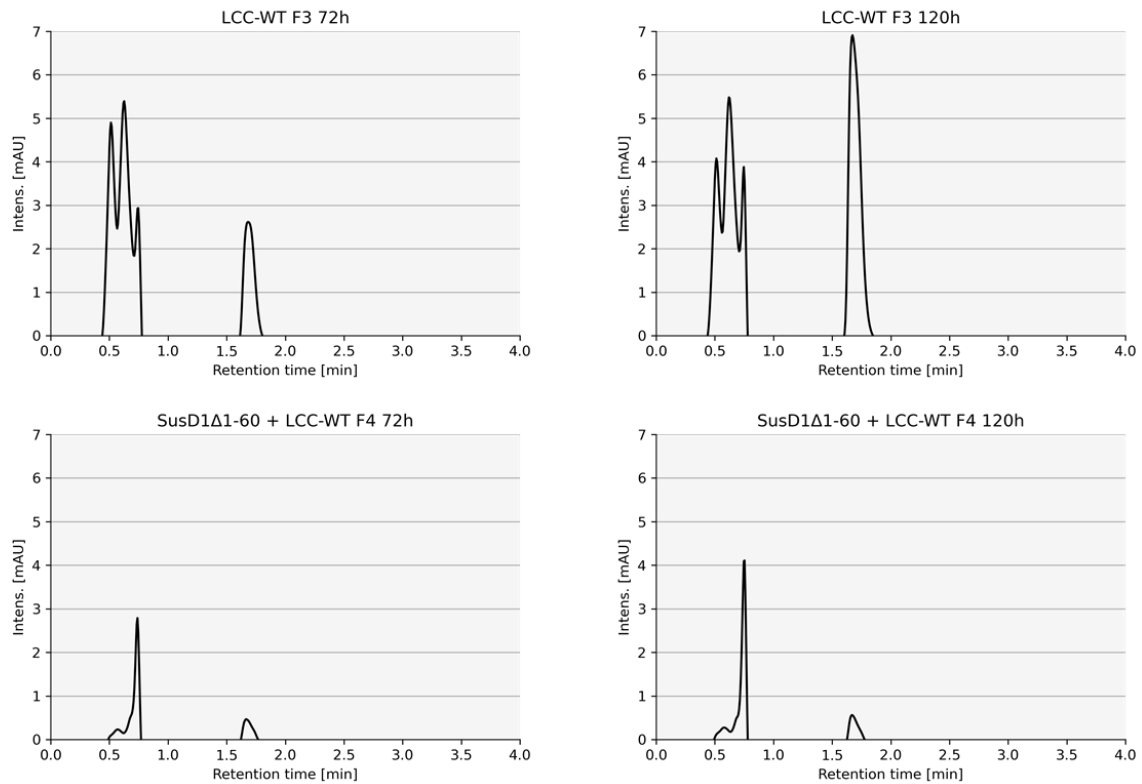


Figure 24: Chromatograms of LCC-WT (top) (Sulaiman et al., 2012) and SusD1Δ1-22::LCC-WT (bottom) after 72h and 120 h of incubation with amorphous PET foil. LCC-WT TPA concentration after 72 h: 17.734 μ M and after 120 h: 55.391 μ M. However, the TPA concentration of SusD1Δ1-22::LCC-WT decreased to 4.499 μ M after 72 h and 4.559 μ M after 120 h.

3.10 *lacZ* reporter

Each *susD* gene was fused to the β -galactosidase *lacZ*, using a flexible GGGGS linker (Figure 4). The final construct sizes were 2106 bp for *susD1Δ1-22* and 2139 bp for *susD38489Δ1-25* (Figure 25).

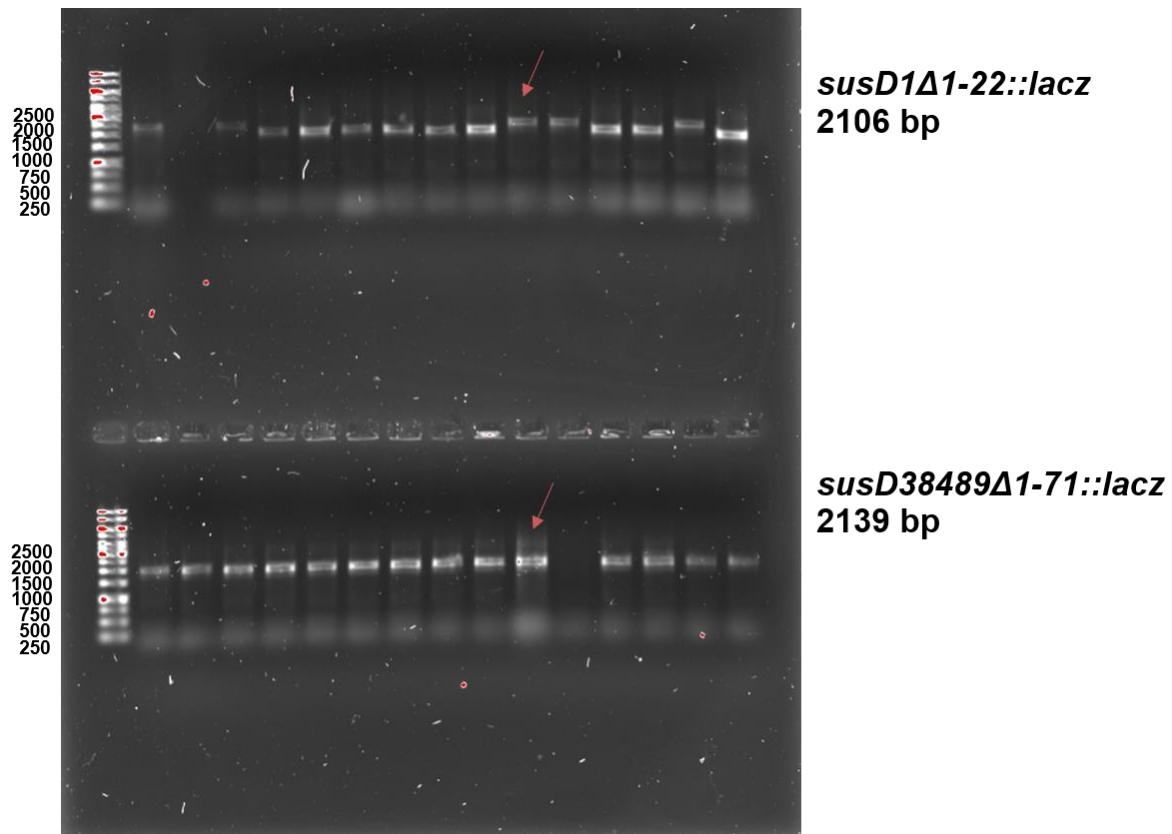


Figure 25: Colony PCR of the translational protein fusions of *susD1Δ1-22* and *susD38489Δ1-25* with *lacZ*. The *susD*-homologs had their N-terminal signal peptide removed and were fused to the C-terminal with the enzyme. The red arrows represent the clones with expected size that were randomly selected and further analyzed by Sanger sequencing. *SusD1Δ1-22* final construct had 2106 bp and *susD38489Δ1-25* had 2139 bp. A His₆-tag was positioned on the C-terminal of each construct. The ladder applied to the gel was GeneRuler™ 1 Kb DNA ladder (Thermo Fisher Scientific, Massachusetts, USA).

The idea behind the experiments was to characterize the affinity of SusD to the synthetic polymers PET, PA6 and LDPE (amorphous foils), considering that SusD would anchor LacZ to each substrate. For this purpose, each protein was diluted to 20 μM in potassium phosphate buffer 0.1 pH 6 and a final volume of 200 μL was added to each foil. After 1 h of incubation (22 °C, 300 rpm) and washing the foils twice with the same buffer, the foils were soaked in 20 mg/mL of X-GAL. This concentration was chosen because it was the same concentration used to produce agar plates, where the bacterial blue colonies were visible (Supplementary Figure S3).

To preserve X-GAL fluorescence, the plates were always kept in the dark. The enzymatic activity was monitored at distinct time points (1, 3, 18, 24, 96 and 120 h) and read at 420 nm, but the results were inconclusive since the protein measurements were very similar to the negative controls. Therefore, this observation suggests that X-GAL is not sensitive enough to capture LacZ activity as a reporter of plastic binding proteins. Further tests need to be performed with a more sensitive substrate, which could be 4-MU- β -D-galactopyranoside (MU-GAL). MU-GAL is described by the manufacturer (Abcam, Cambridge, UK) as a fluorescent substrate that can be used for the detection of β -galactosidase activity in cell extracts and pure enzymatic preparations. The substrate is water-soluble and yields to a blue, fluorescent fluorophore upon cleavage (excitation 360 nm and emission 450 nm).

On the other hand, it needs to be addressed that these reporters might not be stable and efficient enough for the quantitative adsorption assays. This awareness came from the observation that the negative control (*lacZ* in pET21a(+)) presented a continuous increase of dark blue color, due to the possible increase in the production of 5,5'-dibromo-4,4'-dichloro-indigo. On the other hand, the color of the competent cells carrying SusD1 Δ 1-22::*LacZ* and SusD38489 Δ 1-25::*LacZ* remained the same over the course of one week, suggesting that the production of chimeras might have impaired LacZ catalytic activity.

3.11 Structural comparison and docking

The structures were mostly composed of α -helices and a few β -strands, usually positioned near the C-terminus. Besides, the formation of β -hairpins appeared to be common in each structure. As observed on previous assays, the signal peptide was not involved with putative binding sites and, therefore, the removal did not impair the protein activity.

SusD1, SusD70111 and SusD38489 presented one single chain. As it was mentioned in the “II. **Materials and Methods**” section, docking studies were performed with Autodock Vina (Trott & Olson, 2010). The search was adjusted to show only the five most stable binding sites, which will be detailed below.

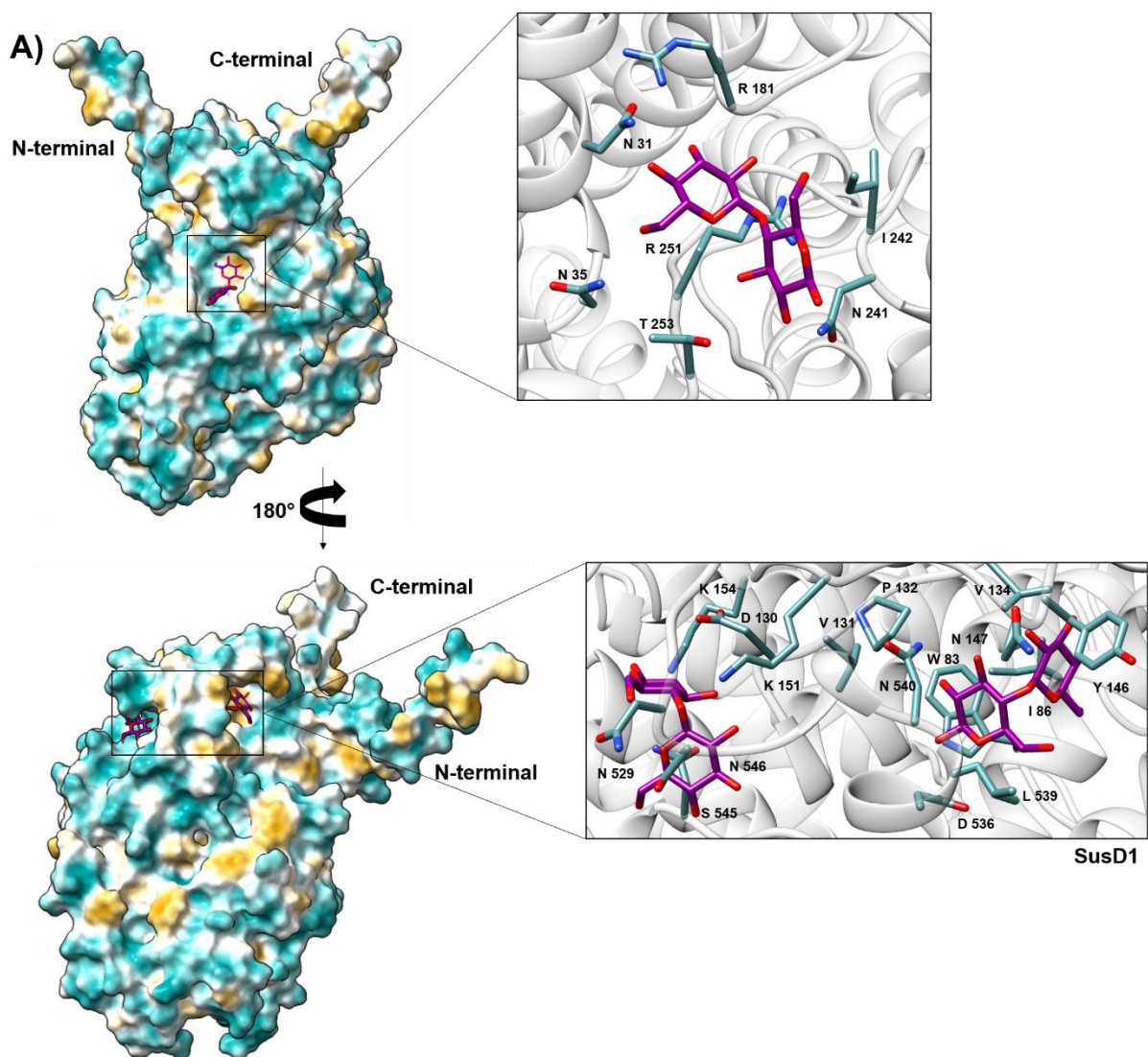
3.11.1 Docking with natural polymers

3.11.1.1 Cellulose

SusD1 and SusD38489 docking were performed with two cellulose derivatives (MC and CMC). SusD1 and SusD38489 presented three putative binding sites to MC, with similar Free Gibbs' values (ΔG -6,1 and -6,2, respectively). The lower the ΔG , the highest the expected stability.

III. Results

Apart from the residues D130 and V131, distinct amino acids were detected in both proteins' putative binding sites. The residues N540 and N546 of SusD1 were replaced by P540 and S546 in SusD38489. However, one of the putative binding sites was structurally located in the same position. Following on with the order SusD1/SusD38489, the amino acids N546/N566, S545/S565 and V131 were superimposed. It was also observed that the predicted binding sites formed pockets on the surface. Remarkably, the pockets mostly comprised hydrophilic residues (except for one pocket of SusD1, that presented highly hydrophobic characteristics; Figure 26).



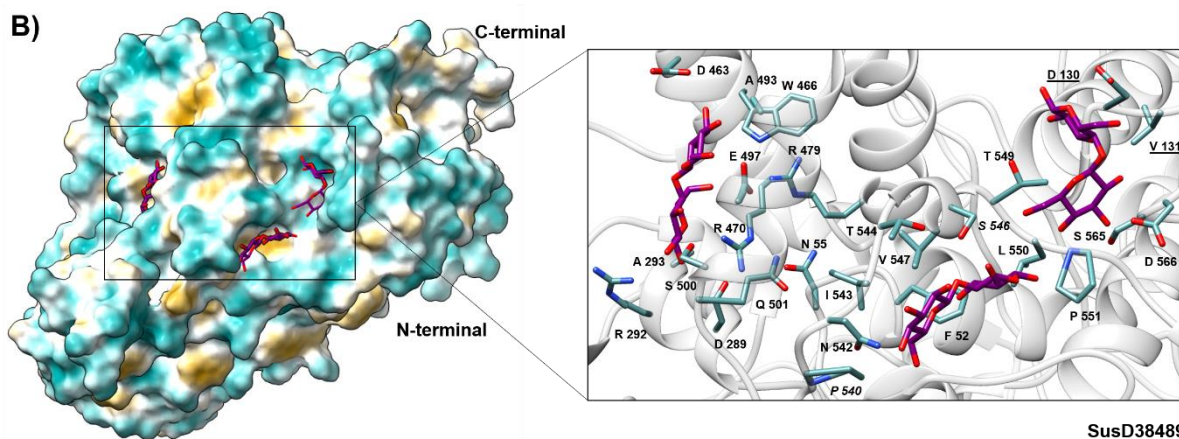


Figure 26: Structure of SusD1 and SusD38489 docking with microcrystalline cellulose (MC). A) Side view of SusD1 with 180° rotation. **B)** Bottom view of SusD38489 structure with the predicted binding sites. Both proteins presented three putative binding sites, formed by pockets on the proteins' surface. The surfaces were color-coded by hydrophobicity, where blue represents the most hydrophilic and yellow represents the most hydrophobic residues.

Regarding CMC, SusD1 and SusD38489 presented one and two putative binding sites, respectively. The ΔG values varied between -5,9 for SusD1 and -6,2 for SusD38489. The proteins had the amino acids T179, R251 and T253 in common. The amino acids I242 and R181 in SusD1 were replaced by T242 and H181 in SusD38489, respectively. Besides, these predicted binding sites were structurally located in the same region, with the residues T179, R181/ H181, I242/T242, R251 and T253 being superimposed.

The predicted binding sites followed similar patterns as previously observed for MC. SusD1 and SusD38489 presented hydrophilic sites, but the second predicted site of SusD38489 was mostly hydrophobic. Taking a closer look to SusD1, the protein presented many residues that were also present in MC docking (for example: N31, N35, R181, N241, I242, T253 and R251). SusD38489 predicted sites for MC and CMC appeared to be distinct, with only the residue V131 in common.

3.11.1.2 Chitin

SusD70111 and its truncated version named SusD70111_{F3} were analyzed with chitin, due to the protein's preference observed on the fluorescence assays (Figure 16). The ΔG values were similar, ranging from -7.9 to SusD70111 and -6.4 to SusD70111_{F3}. Three putative binding sites were identified for SusD70111 and two for SusD70111_{F3}, located in the two main pockets formed within the protein's surface (Figure 27 and Supplementary Figure S4). Color-coded hydrophobicity displayed similar attributes to SusD1 and SusD38489 docking with their natural polymer, where hydrophilic and hydrophobic residues appear to be similarly distributed.

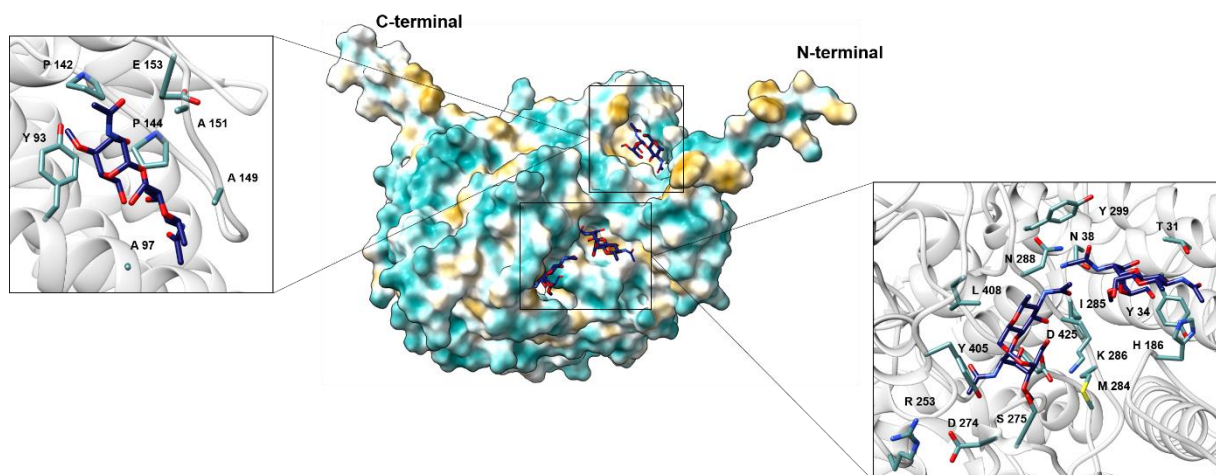


Figure 27: Side view of SusD70111 docking with chitin. The amino acids found in the putative binding site are shown in detail. Three putative binding sites were found, which appear to be in pockets. The surface was color-coded by hydrophobicity: blue represents the most hydrophilic and yellow the most hydrophobic residues.

Structural alignment of SusD1 and SusD38489 with two SusD-homologs previously described to bind strongly to cellulose (Mackenzie et al., 2012) revealed several conserved domains. Due to the demonstrated preference for chitin, SusD70111 was aligned with CusDI and CusDII (Larsbrink et al., 2016), displaying few conserved domains (Figure 28).

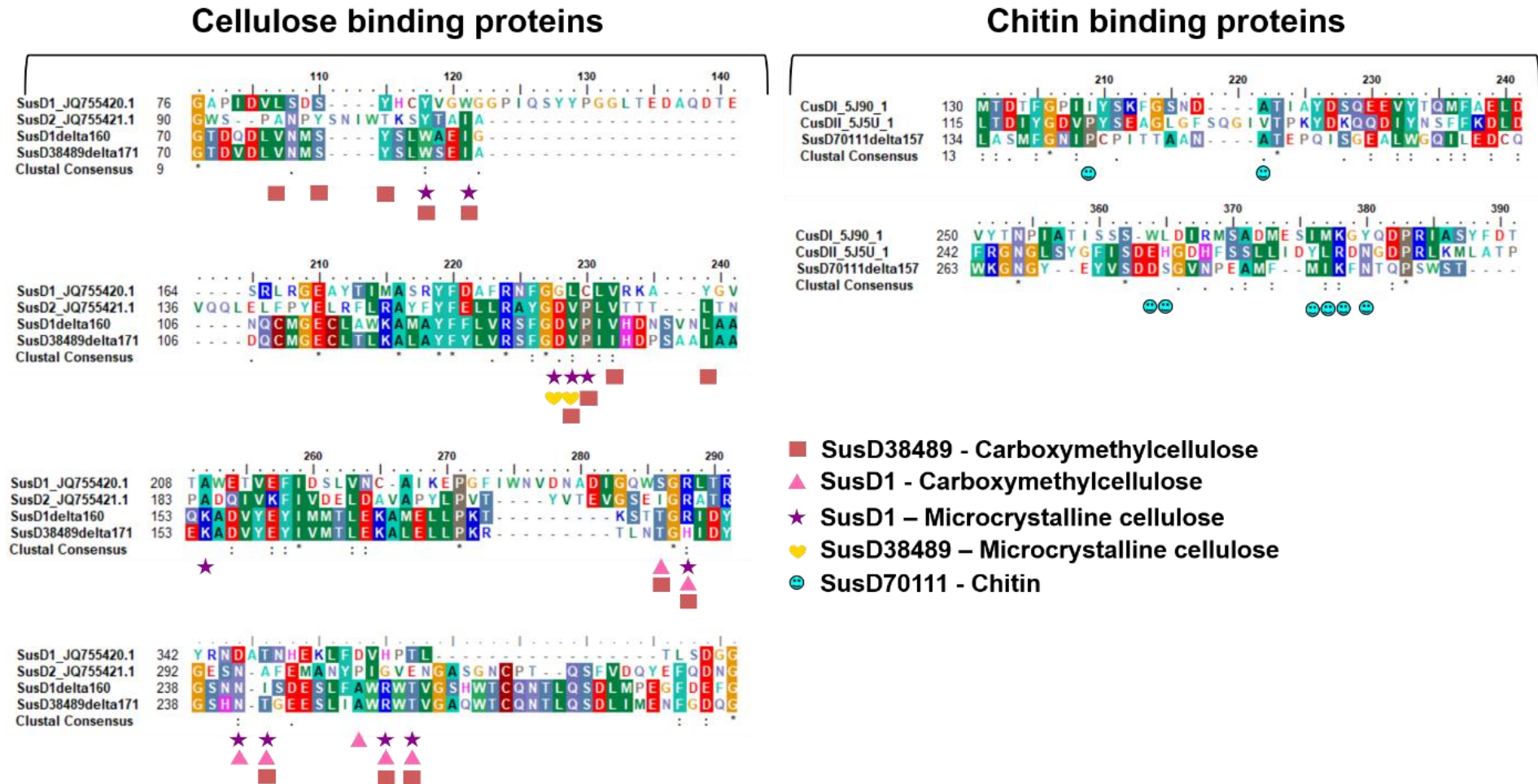


Figure 28: Structural alignment of SusD1 and SusD38489 with SusD1[†] and SusD2 (Mackenzie et al., 2012) and SusD70111 with CusDI and CusDII (Larsbrink et al., 2016). The NCBI or PDB accession numbers are provided. †: Not the same SusD1 as the one characterized in this work. Red square and pink triangle represent the amino acids found in the carboxymethylcellulose docking of SusD38489 and SusD1, respectively. Purple star and yellow heart are the residues found in the microcrystalline cellulose docking of SusD1 and SusD38489, respectively. Blue smiley represents the amino acids identified at the putative binding site of SusD70111 with chitin.

SusD70111_{F3} was also studied with CMC (ΔG -6.8), because of the experimental analysis conducted with SPR (see topic “**3.8 Binding kinetics with SPR analysis**” and Figure 21). Two putative binding sites were identified, and they were structurally the same as identified for chitin (Supplementary Figure S4). Since SusD70111_{F3} is a truncated version of SusD70111, alterations in protein folding may have enhanced this protein’s ability to bind cellulose. Further experiments using x-ray crystallography are necessary to investigate this hypothesis.

3.11.2 Docking with synthetic polymers

3.11.2.1 PET

One putative binding site was identified to SusD1 (ΔG -7.5) and SusD38489 (ΔG -7.2). The predicted binding sites of both proteins were structurally located in the same position. The following residues could be identified on both proteins: N147, W83, I86, H88, Y80 and Y146 (Figure 29A and B). A84 and L141 in SusD1 were replaced by S84 and I141 in SusD38489. Furthermore, surfaces colored by hydrophobicity showed that the putative binding sites form pockets mostly composed of hydrophobic residues (Figure 29C and D).

Regarding SusD translational fusion with sfGFP, the docking analysis showed that the putative binding sites remained the same ones as the WT, with no putative binding sites to PET trimer detected in sfGFP (Supplementary Figure S5).

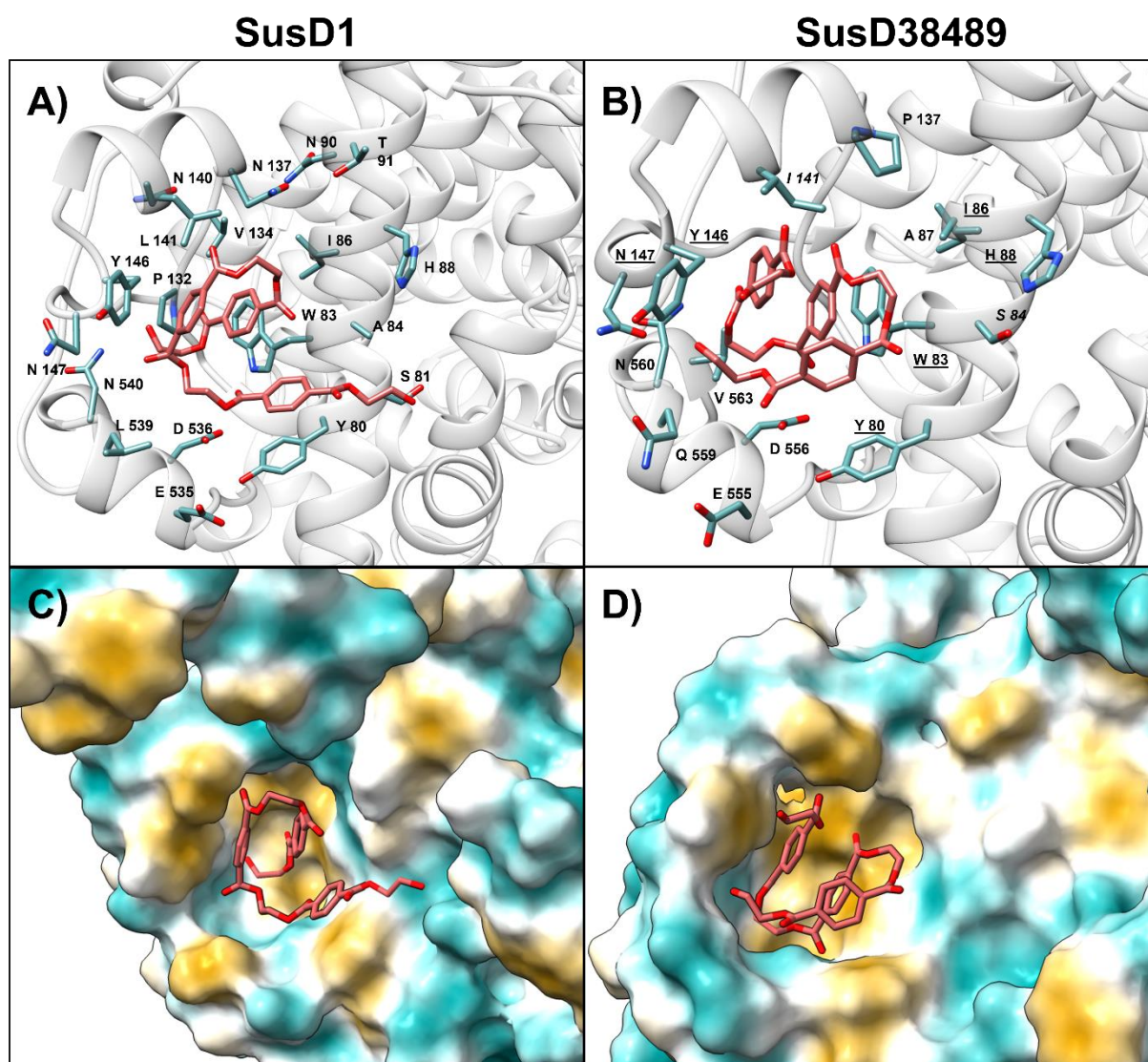


Figure 29: Docking of SusD with PET trimer. A) and B) SusD1 and SusD38489 with exposed amino acids around the putative binding site. In SusD38489, the underlined one-letter coded residues N147, W83, I86 and H88 were also identified in SusD1. The residues represented in italic show that the amino acids in the same structural position were replaced. Besides, V and Q at distinct positions were also identified on both proteins. **C) and D)** SusD1 and SusD38489, respectively, with surface color-coded by hydrophobicity. Yellow represents the most hydrophobic while blue represents the most hydrophilic residues.

On the other hand, SusD70111 presented two putative binding sites (ΔG -6.3; Figure 30). When the surface was color-coded by hydrophobicity, one of the predicted sites appeared to follow a similar trend of SusD1 and SusD38489: a pocket was formed in the protein's surface, predominantly composed of hydrophobic residues. However, the

second predicted site appeared to have similar ratio of hydrophilic and hydrophobic residues (Figure 30).

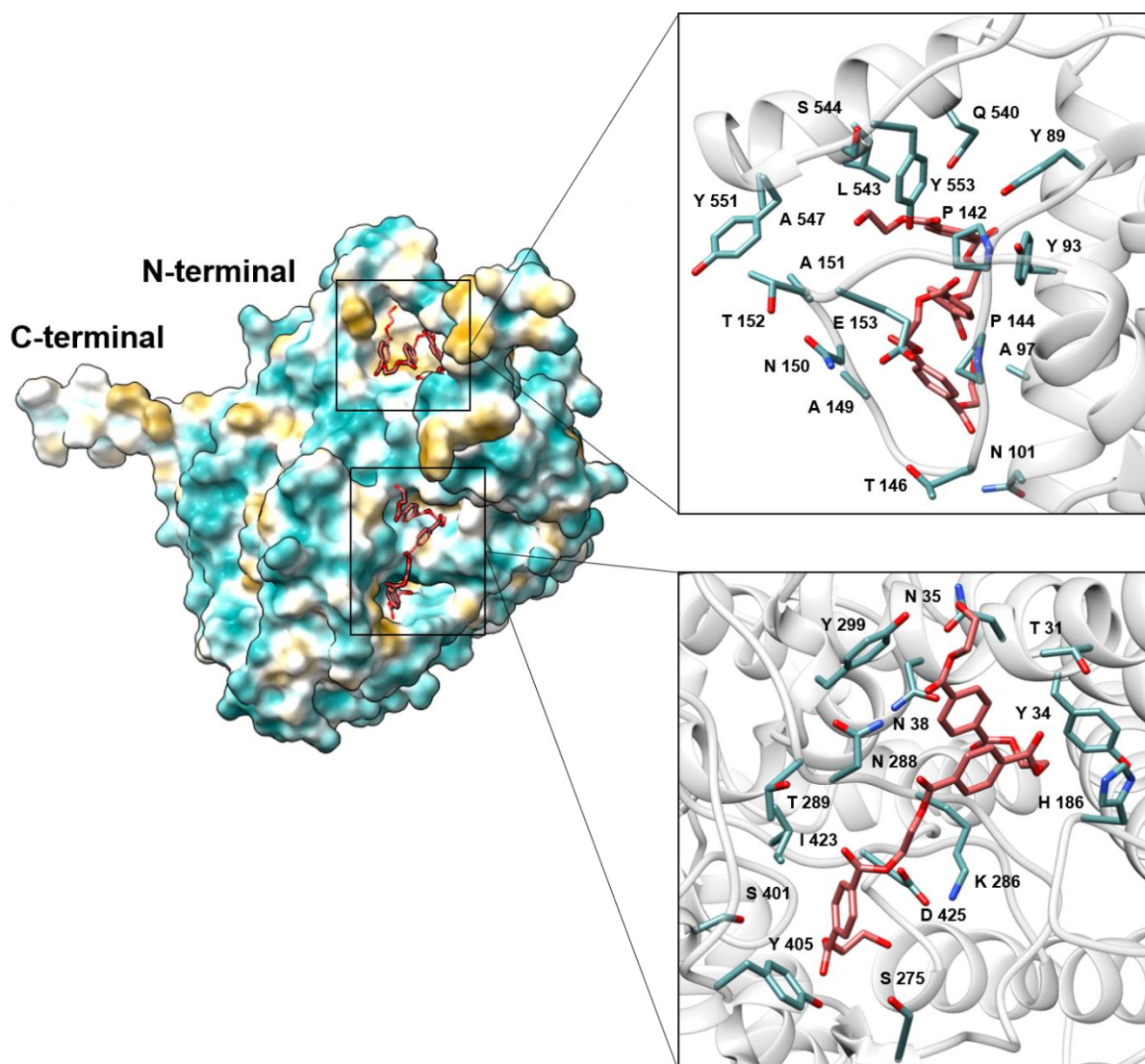


Figure 30: SusD70111 docking with PET trimer. Two putative binding sites were identified and the amino acids present in each region were exposed. The docking sites were structurally distinct to SusD1 and SusD38489 and the residues possible involved in protein binding were also not the same.

In the truncated protein SusD70111_{F3}, one putative binding site was found (ΔG -6.7). Remarkably, the residues were different from the ones identified in SusD70111's putative binding site, suggesting that the protein was probably flexible and able to fold distinctly. Overall, hydrophobic amino acids predominate in the putative binding site of SusD70111_{F3} (Figure 31).

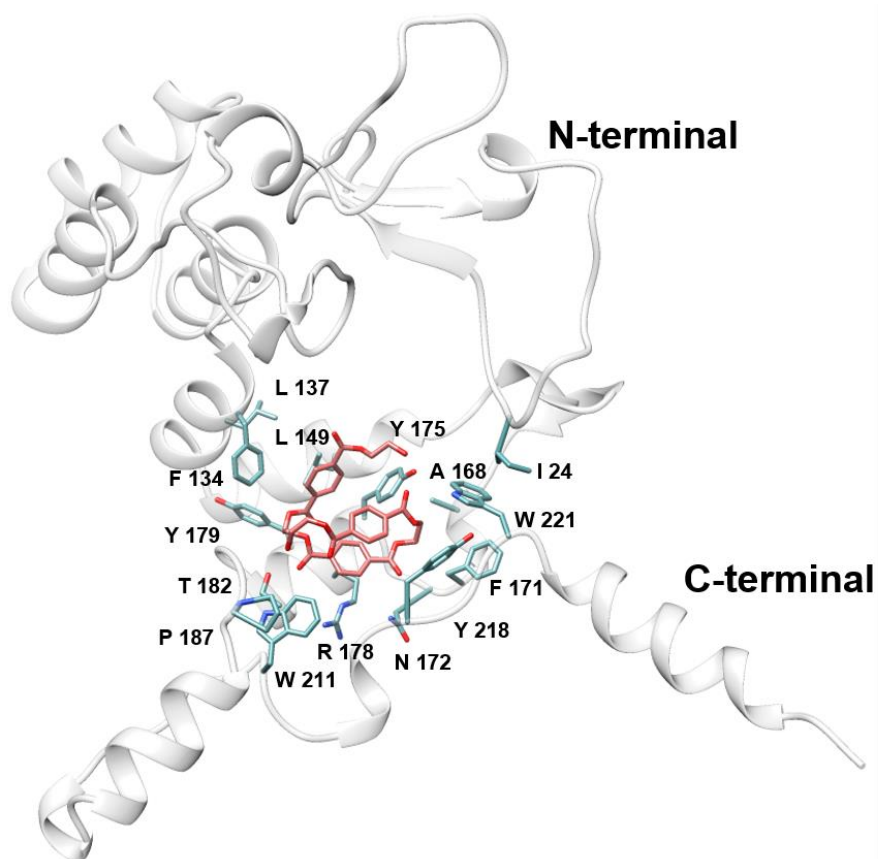


Figure 31: Structure of the truncated protein SusD70111_{F3}. The docking was performed with PET trimer and the residues located around the putative binding site were exposed.

SusD1, SusD38489 and SusD70111 pockets were further characterized using GeoMine (Diedrich, 2021). The data is displayed in Table 15.

Table 15: Characteristics of the protein pockets identified with GeoMine (Diedrich, 2021).

		Depth (Å)	Hydrophobicity	Surface (Å ²)	Volume (Å ³)
SusD1	Pocket 1	8.04 Å	0.82	201.03	126.98
	Pocket 2	9.73 Å	0.62	257.48	113.15
SusD38489	Pocket 1	14.71 Å	0.71	493.21	255.49
	Pocket 2	9.50 Å	0.66	419.01	125.95
SusD70111	Pocket 1	11.57 Å	0.75	234.19	145.92
	Pocket 2	8.20 Å	0.67	278.54	115.20

3.11.2.2 BHET

SusD1 and SusD38489 docking with BHET presented ΔG between -5.9 and -6.3, respectively. General features were similar as previously observed to PET trimer. For example, the amino acids Y80, I86, W83, Y146, N147 and P132 were also found in both SusD1 and SusD38489 predicted binding sites for BHET. Taking a closer look at SusD1 docking with PET trimer and BHET, this protein also displayed the residues L141, L539, D536 and N540. Additionally, SusD38489 docking with BHET presented the residues D556, N560, P137 and A87 in common with the predicted binding site of PET trimer. Overall, surface hydrophobicity matched the previously described PET trimer, with the formation of a pocket mostly composed of hydrophobic residues.

A second putative binding site was identified for both SusD1 and SusD38489. In SusD1, this site primarily involved residues near the C-terminus, whereas in SusD38489, it was located closer to the N-terminus (Supplementary Figure S6). In

both cases, this second predicted site appears to be formed in a shallow pocket with less hydrophobic residues.

SusD70111_{F3} presented a single putative binding site to BHET (ΔG -6.5), which was in accordance with the Data obtained with SPR. This site was predicted to be the same as the one identified for PET trimer.

Supplementary Table S6 provides a summary of the residues located in each predicted binding site.

3.11.3 Structural alignment and prediction of tetratricopeptide repeat

In this work, the predicted structures of SusD1, SusD70111 and SusD38489 as well as the proteins' size of 500 up to 600 residues are in accordance with previously described SusD-homologs (Bolam & Koropatkin, 2012; Koropatkin et al., 2008). However, the tetratricopeptide region, which is highly conserved in SusD and believed to be responsible for the interaction with SusC (Bakolitsa et al., 2010; Martens et al., 2009; Sonnenburg et al., 2005), was only identified in SusD70111. By using TPRpred (Karpenahalli et al., 2007) with default parameters, SusD70111 is likely to have a tetratricopeptide from the amino acid residues 70 to 104 (P-value 4.4e-02). The phylogenetic analysis suggests that SusD70111 had earlier evolutionary divergence than SusD1 and SusD38489 (Figure 10).

The proteins SusD1 and SusD38489 share sequence and structure similarity, with the identification of the residues S79, Y80, W83, I86, H88, Y146 and N147 in the putative binding sites described. Altogether, the alignment, phylogeny and tetratricopeptide prediction suggest that SusD1 and SusD38489 are variable SusD-homologs, as no

tetratricopeptide region was identified. For instance, two SusD structures previously characterized by Koropatkin *et al.* did not present a tetratricopeptide motif, and the authors suggested that the reason could be the lack of a conserved amino acid signature (Koropatkin *et al.*, 2009; Koropatkin *et al.*, 2008).

Figure 32 shows the structural alignment of SusD1, SusD38489 and SusD70111. The predicted tetratricopeptide region of SusD70111 is identified with a black bar, while the residues that SusD1 and SusD38489 present in common are marked with a star. For the putative binding site displayed here, the only residue that was present in each of the three proteins was I86 (Figure 32).

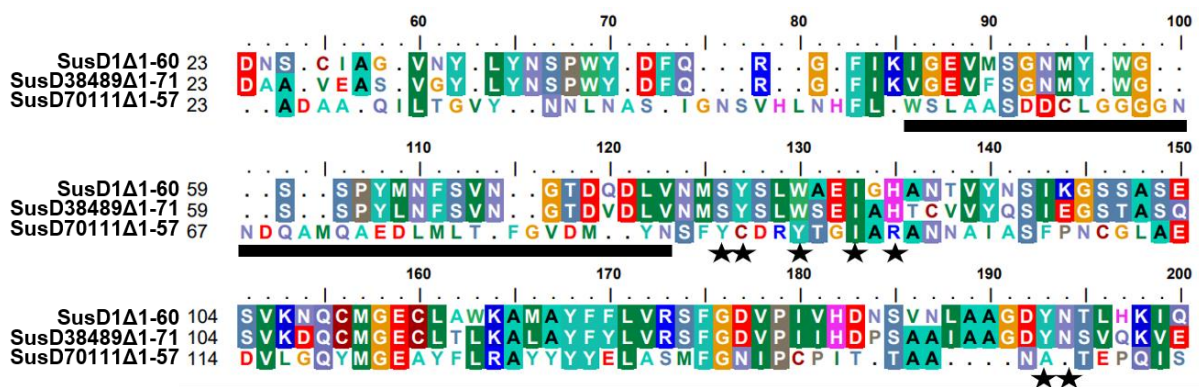


Figure 32: Structural alignment of SusD1, SusD38489 and SusD70111. The black bar indicates the region where the tetratricopeptide was predicted in SusD70111. However, SusD1 and SusD38489 did not present a tetratricopeptide region, suggesting that both proteins are non-conserved. These two proteins share structural and sequence similarity, with the residues S79, Y80, W83, I86, H88, Y146 and N147 being found in the putative binding sites (indicated with a star).

IV. Discussion & Outlook

4.1 SusD as part of the Bacteroidotal operon *sus* and their substrate in nature

There are several copies of *susD* within the Bacteroidotal cell, which are specialized on distinct substrates in accordance with the organism's lifestyle (for more information, see Table 1) (Bjursell et al., 2006; Bolam & Koropatkin, 2012). Recently, Qu *et al.* identified seven *B. fragilis* strains with over 200 copies of SusD-like proteins and shared identities between 21 and 100% (Qu et al., 2022). A SusD-like protein with no sequence similarity to other SusDs, yet retaining a conserved structure, was previously described, suggesting an early divergence from a common ancestor (Koropatkin et al., 2009). The versatility of these proteins is interesting, because it confers advantage on the competition with other bacteria, since the gene expression is regulated in response to the availability of a specific nutrient in the environment. In another work, the crystal structure of SusD with α -cyclodextrin presented a glycan-induced dimerization, possibly caused by the putative binding of more than one protein to a single ligand (Foley et al., 2016; Koropatkin et al., 2008). This event facilitates starch binding to the cell surface.

The surface hydrophobicity possibly plays a major role in the initial binding of the protein to starch and cellulose. A SusD described by Koropatkin *et al.* presented a shallow pocket with an arc of tryptophan residues (W96, W98 and W320) (Koropatkin et al., 2008). According to isothermal titration calorimetry (ITC) measurements with maltotriose, the tryptophan residues are responsible for the initial binding, but they are not enough for high affinity binding (Koropatkin et al., 2008). When a longer oligosaccharide binds, SusD moves two flexible loops and brings the residues Y296 and R81 to the binding site (Koropatkin et al., 2008). Afterwards, the residue D73 also

moves towards the binding pocket and interacts with Glc7 of maltoheptaose (Koropatkin et al., 2008). These findings highlight the plasticity of SusD binding pockets. Furthermore, the crystal structures revealed that the molecular interactions occur via hydrophobic (aromatic ring) stacking and hydrogen-bonding (Chaudet & Rose, 2016; Koropatkin et al., 2008). Interestingly, exposed tryptophan residues were also identified on the surface of a chitin binding domain (ChBD) from family 5 and are believed to be involved in the protein adsorption (Itoh et al., 2006; Uni et al., 2009, 2012). Regarding the hydrogen-bonding, Déjean *et al.* reported that a conserved asparagine residue (N136) and two glutamic acid residues (E137 and E220) were possibly engaging in the interactions with the substrate, which was further confirmed by site-directed mutagenesis (Dejean et al., 2020).

Overall, the protein structure of SusD characterized by Koropatkin *et al.* was flexible enough to accommodate the substrate, rather than interacting with the stereochemistry of glucose residues (Koropatkin et al., 2009; Koropatkin et al., 2008). In this work, we observed that SusD1 and SusD38489 presented three putative binding sites to MC (Figure 26). When the cellulose variant was CMC, SusD1 had one predicted binding site and SusD38489 had two. These regions appeared to be in pockets formed in the protein's surface, in which two (one pocket of SusD1 with predicted adsorption to MC and one of SusD38489 to CMC) were highly hydrophobic. Besides, the structural alignment of SusD1 and SusD38489 presented conserved residues with two previously described cellulose binding SusD-homologs (Mackenzie et al., 2012) (Figure 28). The residues D130 and V131 are located in one of the predicted docking regions to MC and T179, R251 and T253 to CMC (Table 6). The neighbour analysis revealed that SusD1 and SusD38489 were flanked by GH5 and GH26, which belong

to the families of cellulases and mannanases, respectively (Sanjaya et al., 2021; Sharma et al., 2018).

On the other hand, the experiments suggest that SusD70111 is a chitin binding protein (Figure 16). SusD70111 also displayed conserved residues with two chitin binding SusD-homologs (CusDI and CusDII) (Larsbrink et al., 2016) (Figure 27). Chitin is a polymer composed of $\beta(1,4)$ -linked N-acetyl-D-glucosamine, whereas cellulose is composed of $\beta(1,4)$ -linked D-glucose (Larsbrink et al., 2016) (Figure 19). Three binding sites were predicted for SusD70111 and two for the truncated protein SusD70111_{F3}. The amino acids were not the same ones as observed in SusD70111's putative binding site, which suggests that the protein is flexible and able to accommodate the substrate. Besides, these pockets comprised not only the predicted docking site of SusD70111_{F3} towards chitin, but also to CMC. SusD70111_{F3} was empirically evaluated with CMC by SPR analysis and only one binding site could be predicted due to the R_{\max} value and sensorgram shape. Because previous SusD characterizations pointed to a preference for cyclic substrates, such as β -cyclodextrin (Chaudet & Rose, 2016; Koropatkin et al., 2008), further SPR experiments can also be performed.

During the course of this work, SusD70111_{F3} was further fragmented and generated SusD70111_{F3a} (339 bp; 12.1 kDa), but this small module presented rapid denaturation. However, SusD70111_{F3} and SusD70111_{F3a} are successfully fused to sfGFP and could be expressed to reach desired protein levels (Table 2). The next step would be the investigation of SusD70111_{F3} and SusD70111_{F3a} adsorption towards chitin, to verify whether SusD70111's preference to this crystalline natural polymer is maintained.

In this work, we faced limitations on the experimental assays with other natural polymers (for example starch, xylan, lichenan (Icelandic moss) and algae (*Fucus* sp.) extract powder). Lichenan and algae extract retained most of the liquid assay. Besides, starch and xylan presented high backgrounds in their negative controls (substrate plus buffer) during the sfGFP assays. For these reasons, these assays were not validated. However, the finding that SusD1/SusD38489 behave as cellulose binding modules and SusD70111 as a chitin binding module is in accordance with the habitat and niche occupied by the bacteria, as cellulose and chitin are the most abundant polysaccharides on earth (Larsbrink et al., 2016) and can be easily acquired in an herbivore diet.

4.2 SusD adsorption to synthetic polymers

4.2.1 Structural characteristics

The main peptide-polymer binding interactions were previously identified as hydrogen bonding, hydrophobic, electrostatic and π - π stacking (Ejima et al., 2010; Ji et al., 2021; Sahihi et al., 2024; Serizawa et al., 2007; Serizawa et al., 2005; Swaminathan, 2012). For example, aromatic amino acids could possibly bind to aromatic polymers due to the ring interaction (Anni et al., 2001; Qiang et al., 2017; Serizawa, 2011). Using molecular dynamics simulations of a CBM from family 2 originally from *Bacillus anthracis* (BaCBM2) with PET, Weber *et al.* identified an aromatic triad (W9/W44/W63) on the protein surface, stabilized by π -stacking and hydrogen bonds (Weber et al., 2019). Tryptophan quenching and alanine point mutations further confirmed the hypothesis. Furthermore, PET binding strength was determined by the hydrophobic/polar ratio at the surface (Weber et al., 2019).

The predicted binding sites of SusD1/SusD38489 towards small synthetic polymers, such as PET trimer and BHET, appear to be in pockets (Figure 29). These pockets were characterized with GeoMine (Diedrich, 2021), in which it was noticed that they have similar sizes and they are mostly composed of hydrophobic residues (Table 15). SusD1/SusD38489 predicted binding site to PET trimer is in the same structural position, and the proteins share many amino acids in common (Figure 29 and Figure 32). For example, W83 was found in both SusD1/SusD38489 predicted binding sites. Despite the absence of a tryptophan triad, the aromatic residues Y80 and Y146 were found in the same location in both proteins and appeared to form a triad shape alongside W83. Additionally, the proteins could be eluted from the substrate with a high concentration of Triton X-100 (v/v) (Figure 12). This non-ionic and amphipathic detergent is known to disrupt hydrophobic interactions (Makino et al., 1973), thus suggesting that the hydrophobic portions of both the detergent and the protein interacted, causing the disruption of protein's binding to the substrate.

Regarding the most distinct SusD-homolog described in this work, named SusD70111, two binding sites were predicted for PET trimer. These binding sites appear to follow the same patterns as SusD1/SusD38489: they were in surface pockets, but slightly less hydrophobic (Figure 30 and Table 15). Tyrosine residues were abundant and could be important for the protein adsorption, increasing the surface hydrophobicity alongside other residues (Supplementary Table S6). Likewise, SusD70111_{F3} presented putative adsorption to PET (Figure 31) and BHET. Structural analysis showed that SusD70111_{F3} presented two main pockets, in which the most hydrophobic pocket was predicted to be responsible for the adsorption to PET and BHET (Supplementary Table S6).

The inspiration to produce truncated modules came from previous works. With the removal of the first 71 residues at the N-terminus of the esterase from *Clostridium botulinum* (Cbotu_EstA), Biundo *et al.* observed that this variant was able to degrade PET. Interestingly, the WT enzyme was not able to degrade PET, because the residues formed a lid and covered a hydrophobic path on the protein's surface (Biundo *et al.*, 2017). In a later study, the same enzyme was submitted to site-directed mutagenesis on the zinc binding domain, resulting in the increase of the enzymatic activity (Biundo, Reich, *et al.*, 2018).

SusD70111 and SusD70111_{F3} do not share the predicted binding site, which suggests that the protein might be versatile and able to accommodate the substrate. In previous publications, two *susD*-homologs from *B. thetaiotaomicron* (BtSusD and BT1043) were co-crystallized with glycan ligands and it was observed that the substrates also shaped the binding sites (Koropatkin *et al.*, 2009; Koropatkin *et al.*, 2008). BtSusD has a flexible binding site that recognizes preferably cyclic maltooligosaccharide molecules due to the 3D structure recognition, rather than the monosaccharide components (Anderson & Salyers, 1989; Koropatkin *et al.*, 2008). Due to SusD70111's low protein concentration and purity, it was not possible to perform x-ray crystallization studies. Further experiments using a competent Bacteroidotal strain are necessary, since this phylum is the original source of the SusD proteins. For instance, Guo *et al.* stated that *E. coli* BL21(DE3) was probably not a suitable chassis to produce a PETase (OQN32_06240) from Gram-positive bacteria, because low enzymatic activity was observed (Guo *et al.*, 2023).

4.2.2 Translational fusion of SusD1 and known PETases

The translational fusion of SusD1 with known PETases was also performed during this work. However, the screening of the enzymatic activity of PET30ΔPorC (Zhang et al., 2021) and LCC-WT (Sulaiman et al., 2012) revealed an enzymatic impairment on the utilization of PET. Here, SusD was fused to the N-terminal of the enzyme, because both catalytic and non-catalytic sites appeared to be exposed and without interference of the C-terminal His₆-tag. While the non-catalytic binding domain of cellulases and chitinases is usually positioned at the N-terminal (Itoh et al., 2016; Kitamura & Kamei, 2006; Kuba et al., 2018), two synthetic constructs of a cutinase from *Thermobifida fusca* were fused to the C-terminal with CBM_{Cel6A} or CBM_{CenA} and showed improved enzymatic activity towards the natural substrate (Zhang et al., 2010). When it comes to PET, a previous work reported a reduced catalytic activity when the CBM cellobiohydrolase I from *Trichoderma reesei* was fused to the N-terminal of IsPETase (Dai et al., 2021).

On the other hand, Graham *et al.* reported the fusion of several CBMs to the C-terminal of a thermostable variant LCC (Graham, 2022). However, it was observed that the CBMs were not beneficial to the enzymatic turnover of PET at the industrial scale (Graham, 2022). Because of the uncertainty, the production of PETases with the C-terminal fused to SusD would be the next step on the evaluation of these chimeras. Besides, the size and type of linker might also influence protein stability and catalytic activity (Arai, 2021; Yu et al., 2015). This work represents the first time that a SusD-homolog was fused to PETases. In the future, SusD1 can be fused to a known cellulase and tested as a positive control.

The design of chimeras containing two or more catalytic and non-catalytic domains can also be explored in the future. Recently, the thermostability of a chitinase improved by 10 to 15 °C after the fusion with two CBM92, which confers great advantage at the industrial levels (H. Li et al., 2023). Chitinases can have two binding domains displayed in tandem and, in some cases, the catalytic domain can be positioned between two CBMs (Forsberg et al., 2016; Itoh et al., 2016; Kitamura & Kamei, 2003; Kuba et al., 2018; H. Li et al., 2023; Mine et al., 2014). Interestingly, Taira *et al.* described the structure of a GH18 chitinase from *Euglena gracilis*, which consisted of a N-terminus signal peptide, GH18, CBM18, GH18, CBM18 and transmembrane helix (Taira et al., 2018). Therefore, it would be interesting to analyze translational fusions of SusD-homologs and PETases with multi-domain architecture regarding their adsorption and activity towards non-natural substrates.

4.2.3 PET modifications

A report regarding the identification and engineering of anchor peptides with adsorption to diverse synthetic polymers was published in 2021 (Ji et al., 2021). External factors such as temperature and pH could affect the binding strength between anchor peptide and hydrophobic substrate (Ji et al., 2021; Tsai et al., 2012). This topic focuses on PET structural modifications caused by increased temperatures, prior to protein incubation. Within this framework, further incubations could also be performed prior SusD binding assays.

Solid PET typically exists in a semi-crystalline state, consisting of both highly ordered crystals and amorphous domains (Thomsen et al., 2023). This is usually challenging for the catalytic domains, because the increased crystallinity tends to reduce the enzymatic reaction rate (Biundo, Ribitsch, et al., 2018; Ronkvist, 2009; Thomsen et al., 2022). The structure of PET consists of repeating units of TPA and EG covalently linked by ester bonds, which are hydrolysed by PETases. Above the melting temperature (260 °C), PET adopts an amorphous and flexible random coil polymeric form. If the substrate is sufficiently cooled to temperatures below the glass transition of PET (approximately 65-75 °C for amorphous bulk PET, depending on the method (Jog, 1995; Thomsen et al., 2022; Wellen, 2011)), then the disordered random coil is preserved (Thomsen et al., 2023).

Interestingly, the UV-light causes a shortening of PET chains due to intra-chain scissions, which affects the crystallinity and hydrophobicity (Chow et al., 2022; Gotoh, 2011; Lin et al., 2020) (Figure 33). In this work, PET powder semi-crystalline was incubated under UV-C light during 30 days. After the incubation and washing steps, none of the proteins could be eluted from the substrate (Figure 12). The lack of protein being eluted, in comparison to untreated PET powder, suggests that the hydrophobicity changed, affecting the proteins' adsorption.

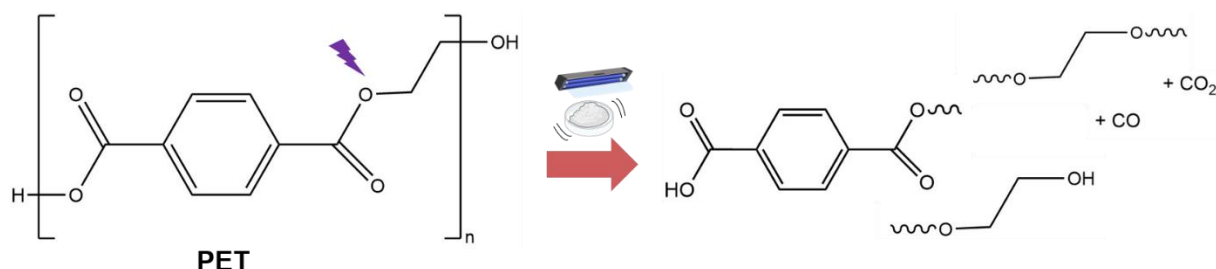


Figure 33: Proposed changes to PET chain after exposure to UV-C light. Figure adapted from (Falkenstein et al., 2020). Designed with ChemDraw Professional© v.22.0.0.22.

Recently, Rennison *et al.* published a detailed work regarding the adsorption of BaCBM2 to crystalline PET (Rennison et al., 2023). The affinity was observed to be dependent on the temperature and crystallinity, suggesting that it could be tuned to the desired level (Rennison et al., 2023). Type A CBMs present a well-known binding capacity to crystalline polysaccharides (for example, cellulose and chitin). Hydrophobic interactions through conserved aromatic residues are responsible for such affinity, making these CBMs good PET-binding candidates (Liu et al., 2023; Liu et al., 2022; Zhang et al., 2013).

4.3 Other promising plastic binding modules

4.3.1 SusE-G

Alongside SusD, SusE (42.7 kDa) and SusF (52.1 kDa) are putative glycan binding proteins encoded by the operon *sus* and partially homologous to SusD (Foley et al., 2016; Foley et al., 2018; Reeves et al., 1997). Tamura *et al.* reported that the conserved structure of SGBPs-A (SusD-homologs) overlaps with distinct SGBPs-B (sometimes referred as “SusE-homologs”). Curiously, SGBP-B from *B. fragilis* comprises a bimodular architecture with a β -barrel domain at the C-terminus that carries a “shallow binding canyon” (Tamura et al., 2021). Even though SusE and SusF are not essential for the starch acquisition of *B. thetaiotaomicron* (Cho & Salyers, 2001), they could be further assayed regarding their affinity towards plastics.

The GH named SusG is also part of operon *sus* and essential for starch binding (Cho & Salyers, 2001; Reeves et al., 1997; Shipman et al., 2000). SusG might not be significantly involved in starch binding (Reeves et al., 1997; Shipman et al., 2000), but a CBM58 is inserted in domain B (Foley et al., 2016; Koropatkin & Smith, 2010). Interestingly, this CBM58 does not interact with the catalytic domain (Foley et al., 2016). When a mutant lacking CBM58 was constructed, the enzyme had decreased activity towards insoluble substrates, but a three-fold increase on the activity towards soluble amylopectin (Foley et al., 2016). Therefore, these data suggest that SusG might sequester oligosaccharides released by the active site or transfer these substrates to the SusC/SusD complex (Foley et al., 2016). SusG with and without CBM58 could be further assayed with insoluble PET.

4.3.2 PilF

According to previous structural analysis using DALI server (Holm, 2022), the closest structural homolog of SusD was the inner membrane PilF from *Pseudomonas aeruginosa* (Kim et al., 2006; Koropatkin et al., 2008). PilF is an entirely α -helical protein involved in type IV pilus biogenesis (Kim et al., 2006). The C α of PilF residues 30-172 (PDB 2FI7) overlaid with a RMSD of 1.6 Å to the four tetratricopeptide units of SusD (Koropatkin et al., 2008). A structure comparison was conducted using UCSF Chimera tool “MatchMaker” (Pettersen et al., 2004), revealing that SusD1’s structure overlays with the chain B of PilF, while SusD70111 aligns with chain A. This finding indicates distinct levels of conserved protein structure (Figure 34).

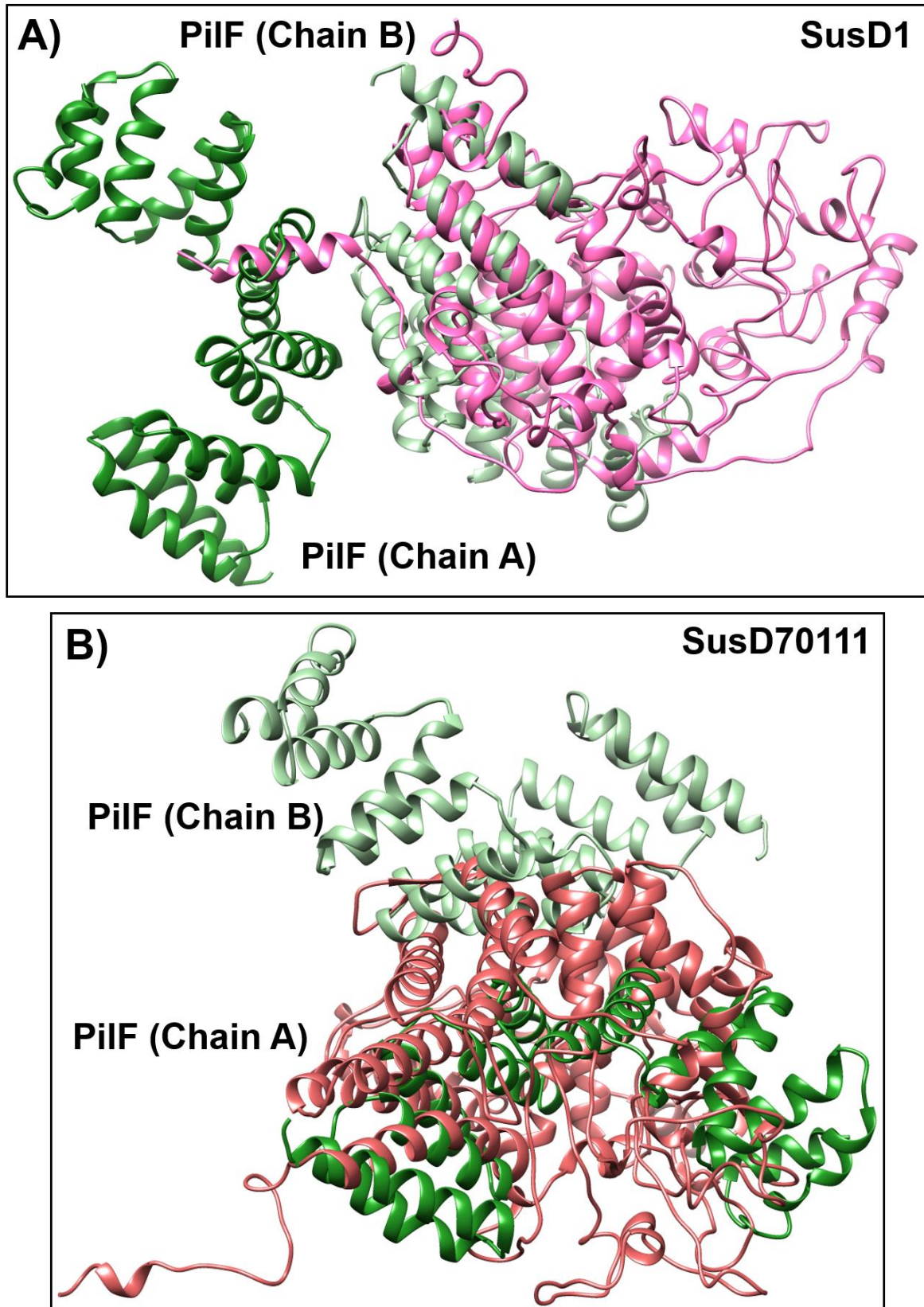


Figure 34: Structural analysis of SusD1, SusD70111 and PilF, a protein responsible for the type IV pilus biogenesis in *Pseudomonas aeruginosa*. PilF was previously identified as a structural homolog of SusD (Koropatkin et al., 2008). **A)** SusD1 (in pink) presented similarity with the chain B of PilF (light green). **B)** SusD70111 (red) was like chain A of PilF (forest green).

4.3.3 Hydrophobins

Hydrophobins could also potentially increase PETase activity, because they are surface-active and capable of spontaneous self-assembly at hydrophilic-hydrophobic interfaces. These small secreted fungal proteins contain eight conserved cysteine residues and are divided in two classes (Espino-Rammer et al., 2013). The class I hydrophobin RolA from *Aspergillus oryzae* and HGFI from *Grifola frondosa* were previously investigated, showing that PET pretreatment with each hydrophobin accelerated PETase hydrolysis (Puspitasari et al., 2021a). After the pretreatment, the weight loss of catalyzed PET increased from approximately 18% to 34%. However, when each hydrophobin and PETase were simultaneously added to the reaction, there was not a significant enhancement. RolA could also enhance the hydrolysis of a PET bottle, with the highest weight loss of approximately 26% after four days (Puspitasari et al., 2021b). A distinct trend was observed for class II hydrophobins, showing that the dosage of translational fusion proteins could stimulate catalytic activity on PET (Espino-Rammer et al., 2013).

Table 16 provides additional information regarding distinct putative binding modules that could also be tested with PET or other synthetic polymers. Furthermore, the substrate hydrophobicity and crystallinity need to be taken into consideration. Succeeding the discovery of IsPETase by Yoshida *et al.* (Yoshida et al., 2016), several researchers are focusing on finding bio-sustainable solutions for PET degradation. Due to the time-consuming work behind the production of fusion proteins and activity assays, it is fundamental to perform large-scale binding assays and structural analysis. The distinct binding assays presented in this work were performed in replicates and might be useful for the discovery of promising binding modules. Besides, the protein

characterized here (named SusD1) can be further fused to LCC-WT or PET30 Δ PorC applying distinct approaches or even fused to other well-known PETases.

Table 16: Binding modules that could be further tested regarding their adsorption to PET or other synthetic polymers.

Name	Microorganism	Description	Approximate size (kDa)
SusE-SusG	Phylum Bacteroidota	With these proteins from the operon <i>sus</i> , many testing possibilities are interesting. For example: A two-protein complex (SusE/SusF) (Cho & Salyers, 2001) or testing each protein individually, regarding their adsorption to PET and other synthetic polymers. On the other hand, SusG has a CBM58 inserted in domain B that does not interfere with the catalytic domain (Foley et al., 2016). If the results are promising, the proteins could be considered for further translational fusion with a catalytic domain.	SusE: 42.7; SusF: 52.1; SusG: 76 (Reeves et al., 1997).
PilF	<i>Pseudomonas aeruginosa</i>	Responsible for the pilus formation and entirely composed of α -helices and six and a half tetratricopeptide. Despite the distinct length and topology, this protein was found to be homologous to SusD (Kim et al., 2006; Koropatkin et al., 2008).	29 (Silveira et al., 2014).
Hydrophobins	Fungi	Small proteins secreted by fungi that contain eight cysteine residues, which are responsible for the adsorption to hydrophobic substrates (Biundo, Ribitsch, et al., 2018; Whiteford & Spanu, 2002). In the presence of class II hydrophobins (HFB4 and HFB7) from <i>Trichoderma</i> spp., the degradation of PET was enhanced 2.5 times (Biundo, Ribitsch, et al., 2018; Espino-Rammer et al., 2013). Besides, the fusion of hydrophobins to cutinase 1 from <i>T. cellulolytica</i> (Thc_Cut1) enhanced the enzymatic activity towards PET by releasing 16x higher concentrations of hydrolysis products, when compared to the WT (Biundo, Ribitsch, et al., 2018; Ribitsch et al., 2015).	Varies and usually depends on the source.
RagB	<i>Porphyromonas gingivalis</i>	Sugar-binding proteins, such as SusD and RagB, usually present low sequence identity but similar 3D structures (Goulas et al., 2016). These proteins are recognized to have tetratricopeptide, being very distinct from β -type carbohydrate binding moieties of cellulases and GHs (Hashimoto, 2006).	54 (Goulas et al., 2016).
PBM	<i>Alcaligenes faecalis</i>	Responsible for the adsorption to polyhydroxyalkanoate (PHA) (Pham et al., 2004). When fused to Cutinase 1 from <i>Thermobifida cellulolytica</i> (Thc_Cut1), led to a two-fold increase of the catalytic activity towards poly(1,4-butylene adipate) (PBA) (Perz et al., 2015) and an 11-fold increase on PET (Ribitsch et al., 2013).	6.3 (Ribitsch et al., 2013).
Zwitterionic polypeptides		Alternating-charged glutamic (E) acid and lysine (K) residues were fused to a PETase. Distinct lengths of polypeptides were evaluated and the fusion with EK(30 kDa)	5-30 (Chen, 2021).

presented 11-fold enhanced catalytic activity, when compared to the WT enzyme. This result was observed in PET film with high crystallinity (45.2%). After 5 days at 40 °C, the concentration of released products was 9.4-fold higher than that observed for the WT. The structural analysis showed that the molecule stability was enhanced and the substrate binding pocket was more open. Besides, the improved catalytic activity probably resulted from the exposure of hydrophobic residues (W185, I208 and W159), alongside the benzene ring rotation of Y87 and a shortened catalytic distance the substrate and the catalytic relevant residue S160 (Chen, 2021).

PBM: Polymer Binding Module; SusC/SusE/SusF: transmembrane protein (SusC) and accessory binding proteins (SusE and SusF) belonging to the operon *sus*. These proteins interact and form a complex with SusD (Cho & Salyers, 2001); PilF: protein responsible for the type 4 pilus biogenesis in *P. aeruginosa*; RagB: receptor antigen B; WT: wild-type.

V. Supplementary Material

5.1 Primers and Touchdown PCR cycles

Table S1: Primers and Touchdown PCR cycling conditions for the signal peptide removal and to produce *susD70111_{F3}*.

Program (Signal Peptide removal)	Forward primer (5'-3')	Reverse primer (5'-3')	Touchdown PCR cycles	Final product (bp)
<i>susD1Δ1-22</i>	GCGCATATGTGCGATGATTTTCTT GATAAACCTGTTG	CGGGTCGACATAAGCATATTCG GTAC	95°C – 3 min. 95°C – 30 sec. 62°C – 30 sec. 15* 72°C – 1 min 42 sec. 95°C–30sec. 50°C – 30 sec. 15 72°C – 1 min 42 sec. 72°C – 3 min. 10°C	1695
<i>susD70111Δ1-20</i>	GCGCATATGTGCGAGAAATTCCTT GATACAACC	ACAGCGGTCGACGTTCCAACCT GCATAAGCGG	95°C – 3 min. 95°C – 30 sec. 63°C – 30 sec. 15* 72°C – 1 min 44 sec. 95°C–30sec. 51°C – 30 sec. 15 72°C – 1 min 44 sec. 72°C – 3 min. 10°C	1731
<i>susD38489Δ1-25</i>	GCGCATATGTGTGAAGACTTCCTG GATCGTCCGAGC	GCAGGTCGACATGGATAGCCT GAGCATCCGAG	95°C – 3 min. 95°C – 30 sec. 70°C – 30 sec. 15* 72°C – 1 min 44 sec. 95°C–30sec. 60°C – 30 sec. 15 72°C – 1 min 44 sec. 72°C – 3 min. 10°C	1729

V. Supplementary Material

susD70111_{F3}

ACAGCGCATATGCGTGAGGCTTC
AATCATCCC

ACAGCGGTCGACGTTCCAACCT
GCATAAGCGG

95°C – 3 min.

95°C – 30 sec.

64°C – 30 sec.

72°C – 42 sec.

95°C–30sec.

53 – 30 sec.

72°C – 42 sec.

72°C – 3 min.

10°C

687

15*

15

SusD70111_{F3}: Fragment 3. Restriction enzyme binding sites are in italic and the spaces provided for the restriction enzyme cutting are in bold. *The temperature changes $x/15$ in each of the first 15 cycles, where x represents the difference between both annealing temperatures, until the final annealing temperature is reached. The elongation was calculated to DCS polymerase (DCS, Hamburg, Germany), where it takes 60 seconds to produce 1 Kb sequence.

V. Supplementary Material

Table S2: C-terminal *susD* fusion to superfolder GFP (*sfGFP*).

Program (<i>sfGFP</i> fusion)	Forward primer (5'-3')	Reverse primer (5'-3')	Touchdown PCR cycles	Final product (bp)
<i>susD1Δ1-22</i>	GAAATAATTTTGTTTAACTTTAAG AAGGAGATATACATATGTGCGAT GATTTTCTTGATAAACC	GTGAACAGCTCTTCGCCTTTACGGCTACC <u>GCCACCGCC</u> ATAAGCATATTCGGTACGAA CATC	95°C – 3 min. 95°C – 30 sec. 63°C – 30 sec. 15* 72°C – 53 sec. 95°C–30sec. 51°C – 30 sec. 15 72°C – 53 sec. 72°C – 3 min. 10°C	1756
<i>susD70111Δ1-20</i>	GAAATAATTTTGTTTAACTTTAAG AAGGAGATATACATATGTGCGAG AAATTCCTTGATACAAC	GTGAACAGCTCTTCGCCTTTACGGCTACC <u>GCCACCGCC</u> GTTCCAACCTGCATAAGCG	95°C – 3 min. 95°C – 30 sec. 64°C – 30 sec. 15* 72°C – 54 sec. 95°C–30sec. 53°C – 30 sec. 15 72°C – 54 sec. 72°C – 3 min. 10°C	1786
<i>susD70111_{F3}</i>	GAAATAATTTTGTTTAACTTTAAG AAGGAGATATACATATGCGTGAG GCTTCAATCATCCC	GTGAACAGCTCTTCGCCTTTACGGCTACC <u>GCCACCGCC</u> GTTCCAACCTGCATAAGCG GC	95°C – 3 min. 95°C – 30 sec. 71°C – 30 sec. 15* 72°C – 23 sec. 95°C–30sec. 58°C – 30 sec. 15 72°C – 23 sec. 72°C – 3 min. 10°C	767

V. Supplementary Material

<i>susD</i> fusion to <i>sfGFP</i> in pET21a(+)	PCR product from each reaction described above. Required concentration of 425 ng/μL to 73 ng/μL of sfGFP in pET21a(+).	95°C – 3 min. 95°C – 30 sec. 65°C – 30 sec. 15* 72°C – 4 min 30 sec. 95°C–30sec. 50°C – 30 sec. 15 72°C – 4 min 30 sec. 72°C – 3 min. 10°C	<i>susD</i> product plus 6017 bp**
---	---	--	---------------------------------------

SfGFP: superfolder GFP. Annealing sites with pET21a(+) vector in italic, while the GGGGS linker sequence (15bp) is underlined. *The temperature changes x/15 in each of the first 15 cycles, where x represents the difference between both annealing temperatures, until the final annealing temperature is reached. **6.017 bp stands for the plasmid size of *sfGFP* in pET21a(+). The elongation was calculated to Phusion™ High-Fidelity (Thermo Fisher Scientific, USA), considering that it takes 30 seconds to produce 1 Kb sequence.

Table S3: *SusD1* Δ 1-22 fusion to *pet30* Δ *porC* (Zhang et al., 2021) and *lcc-wt* (Sulaiman et al., 2012).

Program (<i>susD1</i> fusion to PETases)	Forward primer (5'-3')	Reverse primer (5'-3')	Touchdown PCR cycles	Final product (bp)
<i>susD1</i> Δ 1-22	GCG CATATGTGCGATGATTT TCTTGATAAACCTGTTG	GAAGCGGCCGCCCGGATCCCCGAAC CGGAGCCGCTGCCAGACCCACTCCC CGAACCGCTGCCGTCGACATAAGCA TATTCGGTACGAACATC	95°C – 3 min. 95°C – 30 sec. 69°C – 30 sec. 15* 72°C – 1 min 46 sec. 95°C – 30sec. 56°C – 30 sec. 15 72°C – 1 min 46 sec. 72°C – 3 min. 10°C	1754
<i>pet30</i> Δ <i>porC</i>	CAACGCGGCCGCAATGCAG TGTACCGGCGCC	CAGCGCCTCGAGCAGATTAACCGG GTTTTGCTATCCACAACGCC	95°C – 3 min. 95°C – 30 sec. 71°C – 30 sec. 15* 72°C – 52 sec. 95°C–30sec. 58°C – 30 sec. 15 72°C – 52 sec. 72°C – 3 min. 10°C	859
<i>lcc-wt</i>	GATGCGGCCGCAATGTCTAA CCCGTATCAGCG	CAGCCTCGAGCTGACAATGGCGATT ATTGG	95°C – 3 min. 95°C – 30 sec. 63°C – 30 sec. 15* 72°C – 48 sec. 95°C–30sec. 53°C – 30 sec. 15 72°C – 48 sec. 72°C – 3 min. 10°C	799

V. Supplementary Material

lcc-wt: leaf-compost cutinase wild type. Restriction enzyme binding sites are in italic and the spaces provided for the restriction enzyme cutting are in bold. Besides, the (GS)₁₇ linker sequence (51 bp) is underlined. *The temperature changes $x/15$ in each of the first 15 cycles, where x represents the difference between both annealing temperatures, until the final annealing temperature is reached. The elongation was calculated to DCS polymerase (DCS, Hamburg, Germany), where it takes 60 seconds to produce 1 Kb sequence.

V. Supplementary Material

Table S4: *SusD1* Δ 1-22 and *susD38489* Δ 1-25 fusion to *lacZ*. The negative control (*lacZ* in pET21a(+)) was also prepared following the conditions described.

Program (<i>susD1</i> fusion to <i>lacZ</i>)	Forward primer (5'-3')	Reverse primer (5'-3')	Touchdown PCR cycles	Final product (bp)
<i>lacZ</i> plus GS linker	<u>GCGGTCGACGGCGGTGGCGGT</u> <u>AGCATGACCATGATTACGCCAAG</u> CG	GCGGCGGCCGCCAATTT CCATTCGCCATTCAGGC	95°C – 3 min. 95°C – 30 sec. 65°C – 30 sec. 15* 72°C – 12 sec. 95°C – 30sec. 54°C – 30 sec. 15 72°C – 12 sec. 72°C – 3 min. 10°C	378
<i>lacZ</i> with vector overhangs (pET21a(+):: <i>susd1</i> Δ 1-22)	GCTCGAGTGCGGCCGCAAGCTT CAATTTCCATTCGCCATTCAGG	<u>TGTTTCGTACCGAATATGC</u> <u>TTATGTCGACGGCGGTGG</u> <u>CGGTAGCATG</u>	95°C – 3 min. 95°C – 30 sec. 68°C – 30 sec. 15* 72°C – 13 sec. 95°C – 30sec. 52°C – 30 sec. 15 72°C – 13 sec. 72°C – 3 min. 10°C	428
<i>lacZ</i> with vector overhangs (pET21a(+):: <i>susd38489</i> Δ 1-25)	GCTCGAGTGCGGCCGCAAGCTT CAATTTCCATTCGCCATTCAGG	<u>GGATGCTCAGGCTATCCA</u> <u>TGTCGACGGCGGTGGCG</u> <u>GTAGCATG</u>	95°C – 3 min. 95°C – 30 sec. 68°C – 30 sec. 15* 72°C – 13 sec. 95°C–30sec. 52°C – 30 sec. 15 72°C – 13 sec. 72°C – 3 min. 10°C	425

V. Supplementary Material

<i>lacz</i> without GS linker (NC)	<u>GCTCGAGTGCGGCCGCAAGCTT</u> CAATTTCCATTGCGCCATTGAGG	<u>TCCGAATTCGAGCTCCGT</u> CGACATGACCATGATTAC GCCAAGC	95°C – 3 min. 95°C – 30 sec. 63°C – 30 sec. 72°C – 15 sec 95°C–30sec. 49°C – 30 sec. 72°C – 15 sec. 72°C – 3 min. 10°C	487 15* 15
<i>lacz</i> fusion to <i>susD1Δ1-22</i> or <i>susD38489Δ1-25</i> in pET21a(+)	PCR product from the reactions described above. Required concentration of 102.7 ng/μL to 85.2 ng/μL of <i>susD</i> in pET21a(+).		95°C – 3 min. 95°C – 30 sec. 76°C – 30 sec. 72°C – 4 min 14 sec. 95°C–30sec. 66°C – 30 sec. 72°C – 4 min 14 sec. 72°C – 3 min. 10°C	487 15* 15 <i>lacz</i> product plus 7068 bp (<i>susD1Δ1-22</i>) or <i>lacz</i> product plus 7101 (<i>susD38489Δ1-25</i>)**
NC: <i>lacz</i> in pET21a(+)	PCR product from the reactions described above. NC: Required concentration of 97.7 ng/μL to 65.3 ng/μL of pET21a(+).		95°C – 3 min. 95°C – 30 sec. 76°C – 30 sec. 72°C – 3 min 95°C–30sec. 66°C – 30 sec. 72°C – 3 min. 72°C – 3 min. 10°C	487 15* 15 <i>lacz</i> product (NC) plus 5443**

NC: negative control. Annealing sites with pET21a(+) vector in italic, while the GGGGS linker sequence (15bp) is underlined. *The temperature changes x/15 in each of the first 15 cycles, where x represents the difference between both annealing temperatures, until the final annealing temperature is reached. **Plasmid size. The elongation was calculated to Phusion™ High-Fidelity (Thermo Fisher Scientific, USA), considering that it takes 30 seconds to produce 1 Kb sequence.

5.2 Structural analysis

Table S5: Amino acids identified in the putative binding sites of SusD1, SusD38489, SusD70111 and SusD70111_{F3}. Docking was performed with microcrystalline cellulose (MC), carboxymethylcellulose (CMC), chitin, PET trimer and bis(2-Hydroxyethyl) terephthalate (BHET).

	MC	CMC	Chitin	PET trimer	BHET
SusD1	R 181, N 31, R 251, N 35, T 253 , N 241, I 242 K 154, D 130, K 151, N 546, S 545, N 529, V 131 , N 540, P 132, W 83, N 147, V 134 , I 86 , Y 146 , L 539 , D 536	A 392, N 241, A 394, A 249, R 251, I 242 , T 179 , R 181, Y 84, N 31, N 35, T 253	ND	N 90, T 91 , N 137, N 140, V 134 , L 141 , Y 146 , P 132, N 147, N 540, L 539 , D 536, E 535, Y 80 , S 81, W 83 , A 84, H 88 , I 86	L 141 , Y 146 , I 86 , W 83 , Q 540, P 132 , F 128 , L 539 , D 536, S 79 , Y 80
SusD38489	D 463, A 493, W 466, R 479, E 497, R 470, Q 501, D 289, S 500, A 293, R 292, N 55, T 544, V 547, I 543, N 542, P 540, F 52, S 546, L 550, T 549, P 551, S 565, D 130, V 131 , D 566	T 253 , T 176, N 178, H 181, E 27, V 30, A 28, D 4, F 5, R 251, M 1, T 242, T 179 S 138, P 137, A 87, I 86, S 84, W 83, S 79, Y 80, V 131, V 76, P 553, F 552, E 555, V 563, N 560, P 132, V 149, Y 146, I 134, I 141	ND	P 137, I 141, A 87, I 86, H 88, S 84, W 83, Y 80, D 556, E 555, Q 559, V 563, N 560, N 147, Y 146	Q 257, L 6, R 8, Y 14, F 19, A 16, A 28, S 29, S 95, I 96, Y 32 A 87, P 137, I 86, I 134, Y 146, Y 80, S 79, W 83, P 132, N 147, N 560, D 556

V. Supplementary Material

SusD70111	ND	ND	P 142, E 153, P 144, <u>A 151</u> , <u>A 149</u> , <u>A 97</u> , <u>Y 93</u>	S 544, <u>Y 553</u> , N 540, <u>Y 89</u> , <u>L 543</u> , P 142, <u>Y 93</u> , P 144, <u>A 97</u> , N 101, <u>T 146</u> , <u>A 149</u> , N 150, E 153, <u>A 151</u> , <u>T 152</u> , <u>A 547</u> , <u>Y 551</u>	ND
			<u>Y 299</u> , <u>T 31</u> , N 38, <u>Y 34</u> , <u>H 186</u> , <u>I 285</u> , N 288, <u>K 286</u> , D 425, <u>L 408</u> , <u>M 284</u> , S 275, <u>Y 405</u> , R 253, D 274	N 35, <u>T 31</u> , <u>Y 34</u> , <u>H 186</u> , <u>K 286</u> , D 425, S 275, <u>Y 405</u> , S 401, <u>I 423</u> , <u>T 289</u> , N 288, N 38, <u>Y 299</u>	
SusD70111	ND	M 1, <u>A 4</u> , S 5, <u>Y 33</u> , R 2, <u>F 129</u> , <u>A 128</u> , R 82, <u>W 125</u> , E 126, R	<u>L 137</u> , <u>L 149</u> , <u>F 134</u> , <u>Y 179</u> , <u>T 182</u> , P 187, <u>W 211</u> , R 178, N 172, <u>Y 218</u> , <u>F 171</u> , <u>W 221</u> , <u>I 24</u> , <u>A 168</u> , <u>Y 175</u>		
	F3	<u>Y 218</u> , R 178, <u>W 211</u> , P 187, <u>A 186</u> , <u>T 182</u> , <u>F 185</u>			

Highlighted in yellow: hydrophobic amino acids; underlined: present in SusD1 and SusD38489; italic: replaced in SusD1 and SusD38489; ND: not defined.

5.3 Figures

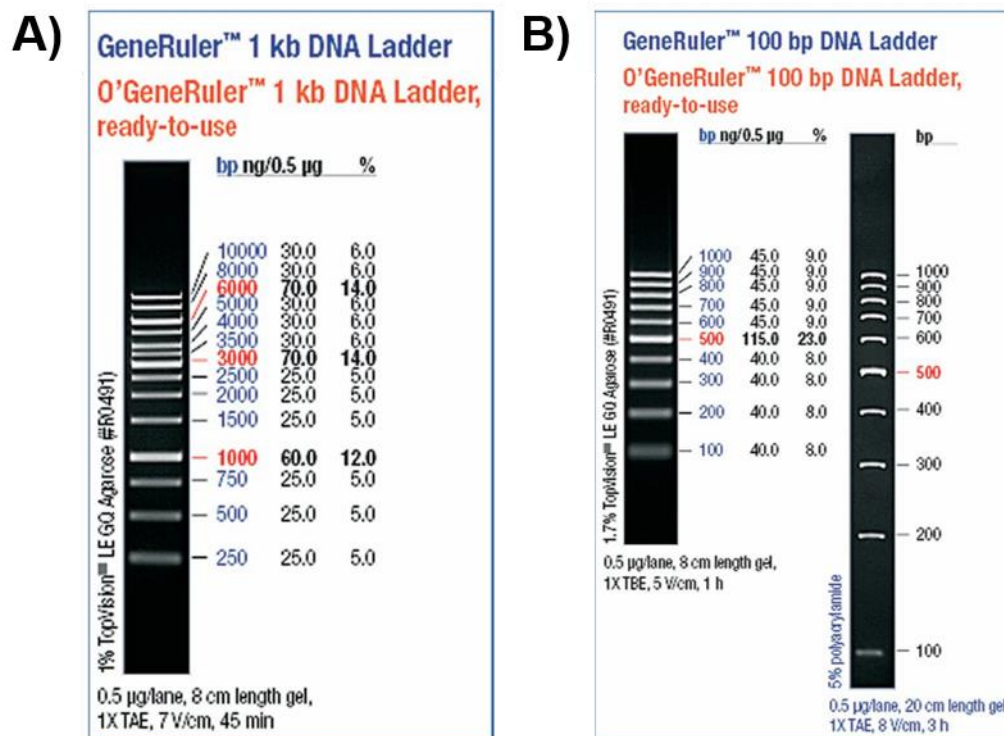


Figure S1: DNA ladders used for the 0.8% agarose electrophoresis. A) GeneRuler™ 1 kb DNA Ladder. B) GeneRuler™ 100 bp DNA Ladder. Both ladders were manufactured by Thermo Fisher Scientific (Massachusetts, USA).

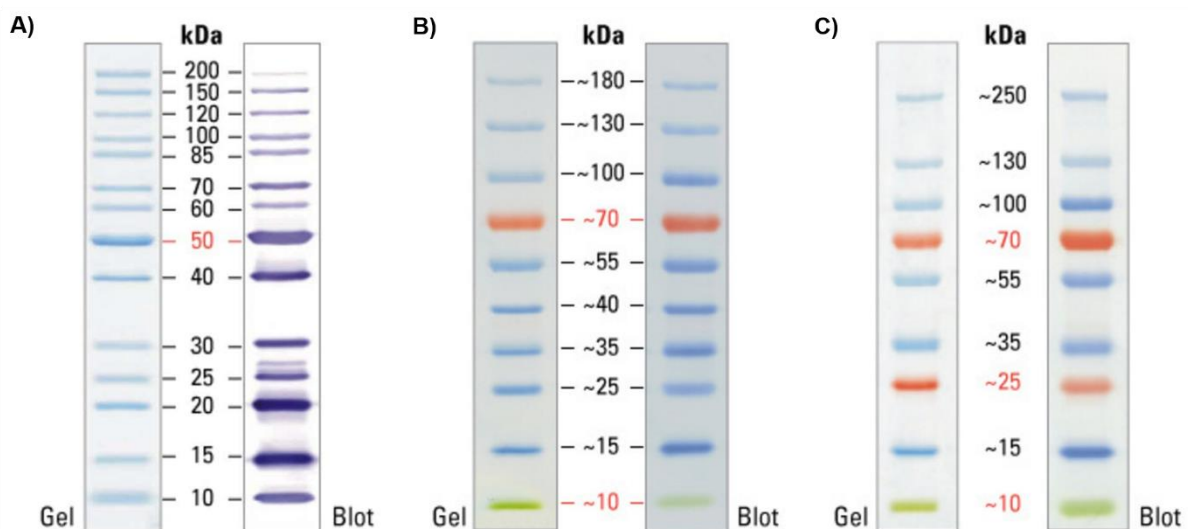


Figure S2: Protein ladders used for SDS PAGE and Western Blot. A) PageRuler™ unstained protein ladder (#26614) used for SDS PAGE. B) and C): PageRuler™ prestained protein ladder (#26616) and PageRuler™ prestained plus protein ladder (#26619), respectively. Both prestained ladders were used for Western Blot, affinity and native PAGE. All the protein ladders were manufactured by Thermo Fisher Scientific (Massachusetts, USA).

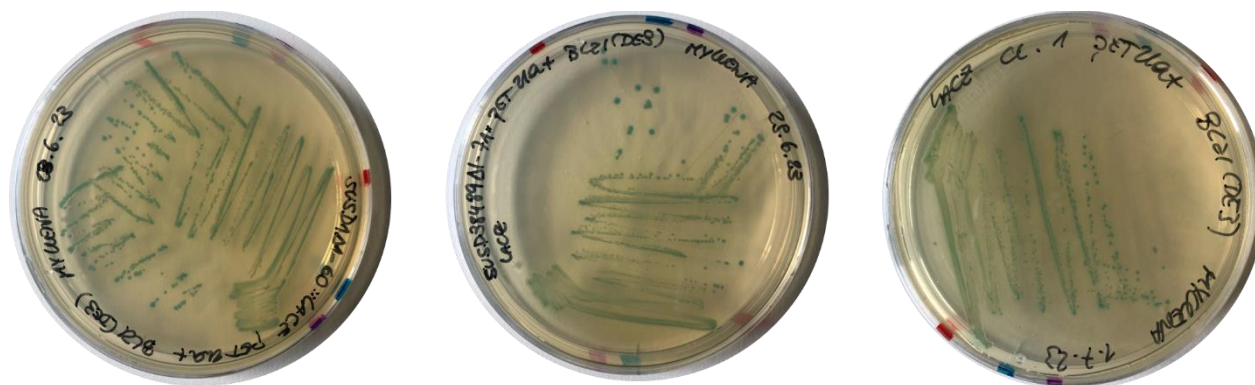


Figure S3: Translational fusion of *susD1Δ1-22* and *susD38489Δ1-25* with *lacZ*. To check for the correct expression of *lacZ* by its capability of degrading X-GAL, agar plates containing LB, 100 mg/mL of ampicillin, 1 mM of isopropyl-β-D-thiogalactopyranoside (IPTG) and 20 mg/mL of X-GAL were prepared. The proteins were cloned and transformed in the expression vector *E. coli* BL21(DE3), and incubated overnight at 37 °C. X-GAL is the natural substrate of *lacZ* and, when utilized, produces a visible blue color on the bacterial colonies.

SusD70111 F3

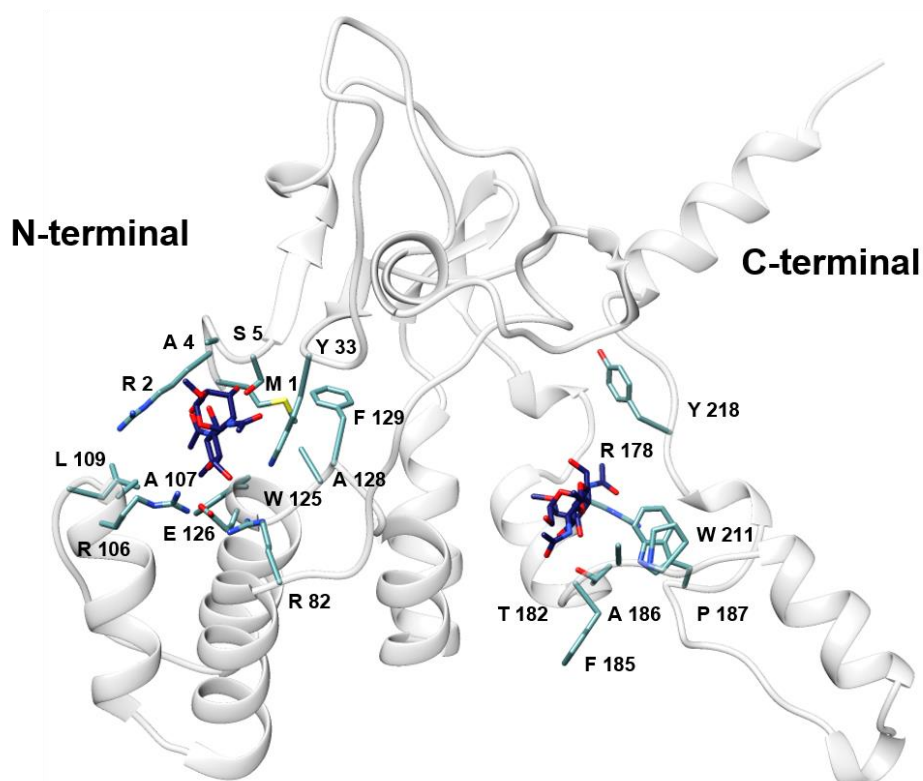


Figure S4: Structure of SusD70111_{F3} docking with chitin. Two putative binding sites were identified. The amino acids were exposed and identified by one letter code. The same sites were also predicted for CMC binding.

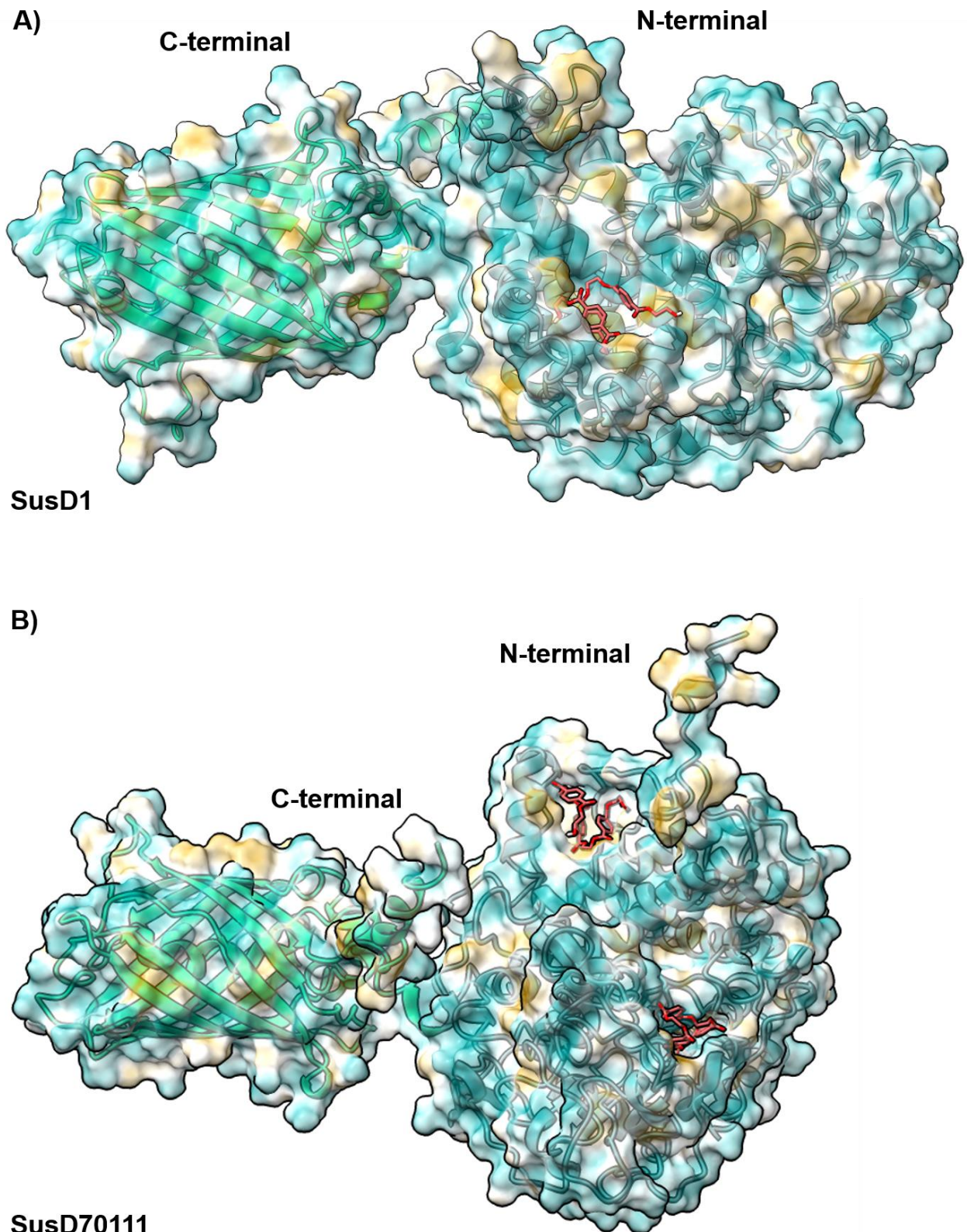


Figure S5: Docking studies of SusD1 Δ 1-22 or SusD70111 Δ 1-20 fused with sfGFP. A) SusD1 Δ 1-22::sfGFP::His₆-tag docking with PET trimer. One putative binding site was detected, being the same as the WT protein. **B)** SusD70111 Δ 1-20::sfGFP::His₆-tag docking with PET trimer. Two putative binding sites were detected, the same ones as the WT proteins. In both scenarios, the fusion with sfGFP appeared to not interfere with protein adsorption.

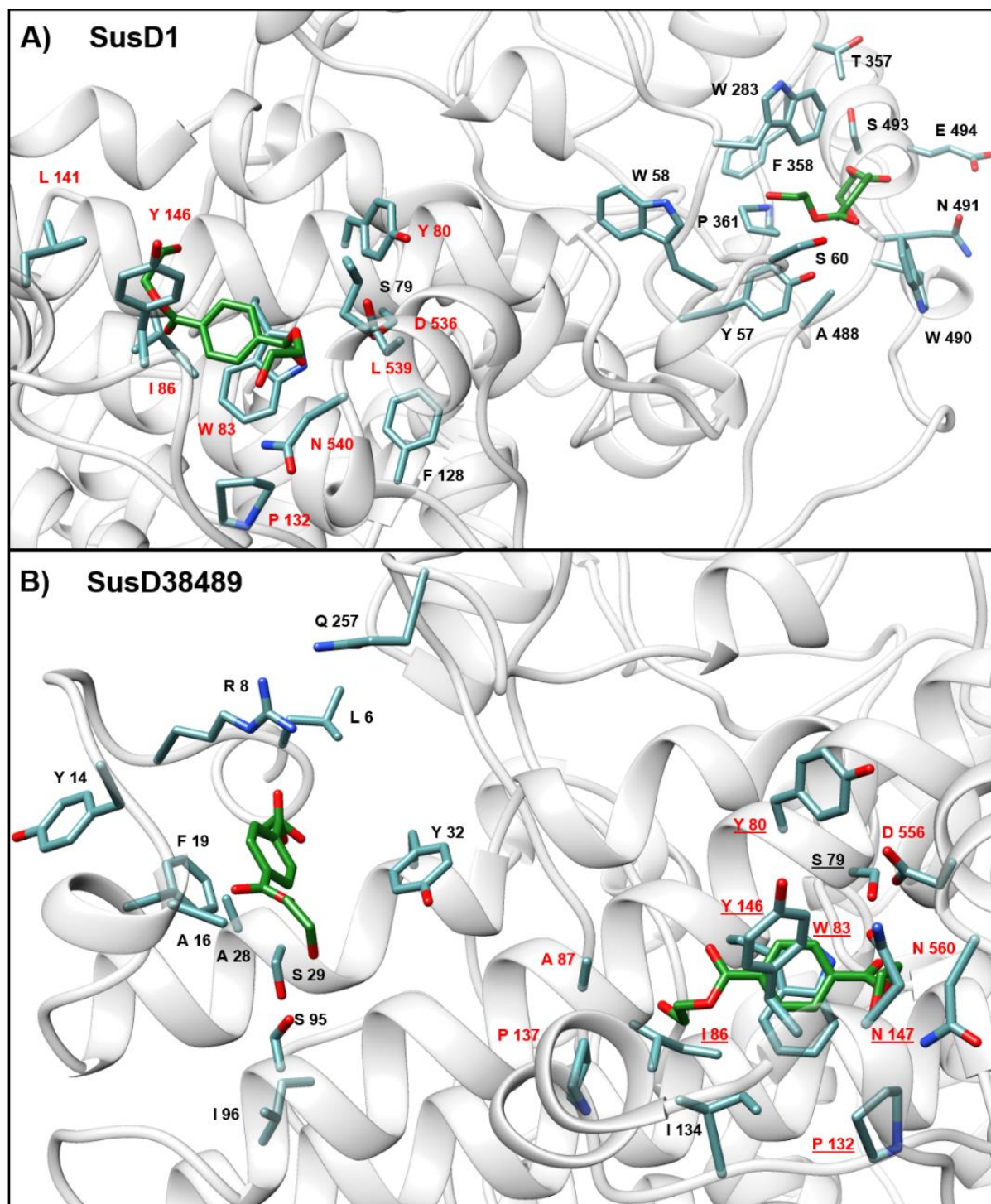


Figure S6: Docking of SusD1 (A) and SusD38489 (B) with bis(2-Hydroxyethyl) terephthalate (BHET). In both cases, two putative binding sites were detected. The amino acids are presented with one-letter code. Red indicates when the residue was also found in the predicted binding site of PET trimer, while underline points to the occurrence of the same residue in both SusD1 and SusD38489.

5.4 DNA and amino acid sequences

5.4.1 DNA

susD1

CATATGAACATCAAGAACTTGAAGTATGTCGCCGCCGCCATGTTGTTGGGCGTTTCTATGACCAGCTGCGATGATTTTCTTGATAAACC
TGTTGAAGATAACTATAACACCGAAAATTATTATACCGATGATAACTCTTGCATCGCCGGCGTTAATTATTTGTATAATAGCCCTTGGTAT
GATTTCCAACGCGGTTTTATTAAGATTGGTGAAGTTATGTCTGGTAATATGTATTGGGGTCTTCTCCTTATATGAATTTTAGCGTTAACG
GCACCGATCAGGATTTGGTTAATATGAGCTATAGCTTGTGGGCTGAAATTGGTCATGCCAATACCGTTTATAATTCTATTAAGGGCAGC
AGCGCCTCTGAAAGCGTTAAAAATCAGTGTATGGGCGAATGTTTGGCCTGGAAAGCCATGGCTTATTTCTTTTTGGTTGTTAGCTTTGG
TGACGTTCCGATTGTTTCATGATAATAGCGTTAATTTGGCTGCTGGCGATTATAATACCTTGCATAAAAATTCAAAAGGCCGATGTTTATGA
ATATATCATGATGACCTTGGAAAAGGCTATGGAATTGTTGCCGAAAACCAATCTACCACCGGTCGTATTGATTATTATTGCGCTGAAG
GTTTGTATGCCAAAGTTGCCTTGACCGCCGCCGCGTTAGCGGTCAGTTGGATAATAGCTTGTTCGAGAAAGCTAGTACCGCCTCTTT
GGATGTTATTAATAATTCTGGTCGTAAGTTGATGGCTAATTATGCCGATATTTTTCGTGGTAGCAATAATATTAGCGATGAATCTTTGTTG
GCTTGGCGTTGGACCGTTGGCTCTCATTGGACCTGCCAAAATACCTTGCAGAGCGATTTGATGCCGGAAGTTTTGATGAATTTGGTG
ACTGCTGGGGTGGCTGGGGTGGTCCGAGCGCTGATTTGCAAGATGCCCTTGGTTATGATGTTACCGAAAATCCGAAAATCGCTTGA
TGTTGATGCCCGCCGCAAAGCTACCATGATGGGCCCGGGCGATGTTTATGATTATTTTTGGCGGATAAAGATTTGGGCAATGGCAA
AAAGGCTTTGATATTTTGAAGTTTTATTTGATAAGGATTATAACAGCGCCGCTACCAATACCTTTCAGGGCCCGTGTGGTGTCAAAT
GTTAAACATGCCTATGGTGACAATGCCGATCATGAAGCCGAATGCGGTGGTATGAGCGCTGCTCGTATGTCTTATGCCGTTGCTACCC
ATATTTTGCCTTTGGCCGATGTTTATTTGGTTCATGCCGAAGCCGAAGTTTTGCAAGGTAACCACCAGCGCCACCGCCTTGGCCGC
TTTTAATGCTGTTTCGTTCTCGCTCTGTTCCGAGCGCTGTTGATAAAACCCAGTTGTCTTTTGTATGATGTTTGGAAAGAACGTCGTTTGA
ATTGGCTGGTGAAGGTGACCGCTGGTATGATTTTGTTCGTGCTAGCTATTATGATGTTAATGCTTGCATTGCTGAATTGACCAGCCAAC
GTCGCAATGCTATTTGGAATTGTAGCGAAGTTTATAAAACCTATTTGCAATCTGATGGCGCCACCTGGGATGCTACCAATATTCAATATG
ATGAAAGCACCCCTATTCCTAATGTTACCGCTAATTCTTTAACTTGCCGATCCTACCGAAGATGTTGCTTTGAATCCGAATTTGGGCA
GCAATGCTGAAGCCATTCATGTTGATGTTTCGTACCGAATATGCTTATGTCCGAC

susD38489

ATGAAAACAAATATTTATTCGAAGTTCCTGGGTCTTGCAGCCGTTGCCGTAACCGCTATGGGTATGGCTTCGTGTGAAGACTTCCTGGA
TCGTCGAGCGAGGATAACTACAACGCGGACAACCTTCTATAACCAACGATGCCGCTGTTGAGGCCAGCGTAGGCTACCTCTACAACCTCT
CCTTGGTATGACTTCCAGCGTGGCTTCATCAAAGTTGGTGAAGTTTTCTCTGGCAACATGTACTGGGGTTCATCTCCCTACCTCAACTT
CTCTGTAACCGGTACCGACGTTGACCTTGTCAACATGTCGTAATCTTTGTGGTTCGAAATTGCACATACCTGTGTTGTTTACCAGTCAA
TCGAAGGCTCAACCGCCTCTCAGTCGGTAAAAGACCAGTGCATGGGTGAGTGTGTTGACCCTCAAGGCTTTGGCTTACTTCTATCTCGT
ACGTTCAATTCGGTGTATGACCTATCATCCACGACCCATCTGCAGCAATCGCTGCTGGCGACTACAACAGCGTACAGAAGGTTGAGAAA
GCTGATGTATATGAGTATATCGTCATGACCCTTGAGAAGGCTCTGGAGCTTCTTCCAAAGCGCACTCTCAACACCGGACATATCGACTA
CTACTGTGCTGAGGCACTCCTTTCTAAGGTATATCTTACTCGTGCAGGTGTGAGTGGTTCTCTTAAACAACAGCGACCTCGAAATGGCTG
CTAAGCTGGCTAAGGATGTCATCGACAATTCGGGCCGTCACCTGGAGCCTGTTTACTCTGACATTTTCCGTGGTTACACACAACACCGGT
GAAGAGAGCTTGATCGCTTGGCGATGGACCGTAGGTGCACAGTGGACCTGCCAGAACACTCTCCAGTCGGATTTGATCATGGAGAAC
TTCGGTGACCAGGGTGACCTCTGGGGCGGCTGGGGTGGTCTTCTACCGACCTGATGCGTGCTTTCCGGCGTTATCGACCTGAAGCGT

V. Supplementary Material

GATCCAGAAAATGCCGGCAACGACAAGAATAATCCAGACTTCGCCGTGATCACCTCATTCTCTCTCCTGAGGCTCGTGCCAATGCCG
ACCGCGACAGCCGTCGTCAGGCTACCATGATGCTTCCTGGTGACGTTTACAGCTACTTCTGGCGCAACAAGGGTGGTTTTCGACCTTCT
GAAGTTCTACTACGACAAGAATACTACAACCTCTGCTGCTACTGAGGAGTTCCAGGGCCCATGTGGTTGTCAGAACGTTAAGCACCTCTAC
GGCAACGACGCCGACCACATTGCTGAAGTTGGCTTCTCTCCTGCTCGTATGGCTTACGCATTCCATACCCACGTTCTCCGCCTGGCAG
ATGTTTATCTCATCTTCGCTGAGGCTAAGACCCTCTTGGGCCAGGGTAGCGATGCTGCTGCTCTTCTGCTGCTTTCAACGCTGTACGTCA
GCGTGCTATCGCAGGCGAGCCAGCAGCTACCTCACTTACCTTCGACATGATCTGGAAGGAGCGTCTGCTGGAATTTGCAGGCGAGGG
TGACCGTTGGTATGACTTCGTACGTCGTTCTTACTACGATGCTGATGCTTGTCTCGCTGAGATTAAGTCACAGTTCCGTAACAACCTCT
GGGGCTGCAGTGAATGTACAAGAATACTTTCGAGAGCGGTGCTTGGTGGGAACCAACCCAGACCGATGACTCGGTTACAACAACG
ACATCCCTGTGCCAAGCAACATTACCAAGAGTGATTCACTTTGCCATTCCCAACCGAGGATGTGGCTCAGAATCCAAACGTAGGCTC
GGATGCTCAGGCTATCCATGTGACGCTACGTAATACCTATTCATATTA

susD70111

ATGAAAAGATATTGAATTTTGCAGCAGTCGCTGTTCTTGCACCTTTCTTTCGCATCTTGCAGAAAATTCCTTGATACAACCAACTATTGG
TCTAAGACCGCTGAGGACTTCCCTGCAAAATGAAGCAGATGCAGCTCAGATCCTTACCGGTGTATACAACAACCTCAACGCTTCAATCG
GTAACAGCGTGACCTCAACCACTTCTGTGGTCTTTGGCAGCTTCTGACGATTGTCTCGGTGGTGGTGGTAACAACGACCAGGCAAT
GCAGGCAGAGGACCTCATGCTTACTTTCCGGTGTAGATATGTACAACCTACTTACTGCGACAGATATACAGGTATCGCTCGTGCCAACA
ACGCAATTGCATCGTTCCCTAATTGTGGTCTTGCAGAGGACGTCCTCGGTGAGTATATGGGTGAGGCTTACTTCCCTCGCGCGTACTA
CTACTATGAGCTCGCTTCAATGTTCCGGCAACATCCCTTGCCTATCACTACAGCGGCTAATGCAACTGAGCCACAGATCAGCGGTGAG
GCACCTTTGGGGACAGATCCTCGAGGACTGCCAGACTGCAATCAACTACTTCCCTAACAAGAAGGCATCTGGTGACGGTCACGTTGACA
AGTATTGTGCTGAGGCACTCCTCGGTGCTGTTTACCTCTTCCGTTTCCCTTGGTATCGAGACTTTCACTCTTCTAGCGGTAAA
ACCCTCGGTAGAGCAGATGCTGCAAAGGTTATTGAAGACTGTGTGAAGACTTCAAGGTTACAGCCTCGTTTCTGATTACCACAACCTTTG
GGCTTATACCAACAGAATATCTGTAGATGACGAGCTCTCTCCTTGGAAAGGTAATGGTTATGAGTATGTTTCTGATGATTCAGGTGCA
ACCCTGAGGCTATGTTTATGATCAAGTTCAACACTCAGCCTTCCATGGAGCACTACTATCGGTTACTCTAACCAGACCGCTCTTCTCATG
GGTATCCGTGGCCAGGCTGGTACATCAACTGGTACTGTTTCCATTCCGGTGTGGTTGGGATATGTGCCCTGTGAGCCACAGCTTGT
TAAAGGATTGGGAGACTGCTGAACCAGACGATATCCGTGCTGAGGCTTCAATCATCCCTGTGACTAAGTTCAACAAGACTTATTCATTC
GGTGGTGACTCCAACATCCAGGAGACCGGTTACTATCAGACCAAGACCATGCCGGTTATCGGTGTAAGGCAGAAGGCTCTAACGAG
TTCTATGCTACTTACTCTAACGCTATGTATCCTGGTCTTACCTGGTACAGAGGGTAACACAGATAACTTCCAGCTCAACTCTATCGATGAT
ATGGTATTGATCCGCTTCGCAGAGGTTCTCCTCATGGATGCAGAGCTCAACAACAACCAGGACAGCTTCGATCAGGTACGTCATCGCG
CAGGTCTTCCCTCAAAGGCTATCTCTACCAAGGCTATCCAGGACGAGCGTTCGTTGGGAGCTTGGTTTTCGAGGGACTCCGTTTTCAACGA
TCTCCGTGTTTTCCGGTGTGAGTATGCAAAGACTGCTCTTGACAAACAGGACGGTGTGTCTTGTCTACAACATGGGCGAGGCAACAGGT
AACACTGCTTCCAAGTTCAATGGTGGTTATGGCGCTCGCTACGCTGCAACTCTCGGTTTTCGCACCGCTTCTGAGCTCAGATCGCTC
TTTCTGCAGCAGCCGGTGAGGAGTACAAGTATACTCAGAACGCTGGTTGGGATACTAATGATGCCGCTTATGCAGGTTGGAATA

susD70111_{F3}

ACAGCGCATATGCGTGAGGCTTCAATCATCCCTGTGACTAAGTTCAACAAGACTTATTCATTCGGTGGTGACTCCAACATCCAGGAGAC
CGGTTACTATCAGACCAAGACCATGCCGGTTATCGGTGTAAGGCAGAAGGCTCTAACGAGTTCTATGCTACTTACTCTAACGCTATGT
ATCCTGGTCTTACCTGGTCAGAGGGTAACACAGATAACTTCCAGCTCAACTCTATCGATGATATGGTATTGATCCGCTTCGCAGAGGTT
CTCCTCATGGATGCAGAGCTCAACAACAACCAGGACAGCTTCGATCAGGTACGTCATCGCGCAGGTCTTCCCTCAAAGGCTATCTCTA
CCAAGGCTATCCAGGACGAGCGTTCGTTGGGAGCTTGTTCGAGGGACTCCGTTTCAACGATCTCCGTGTTTTCCGGTGTGAGTATGC
AAAGACTGCTCTTGACAAACAGGACGGTGTGTCTTGTCTACAACATGGGCGAGGCAACAGGTAACACTGCTTCCAAGTTCAATGGTGGT

TATGGCGCTCGCTACGCTGCAACTCTCGGTTTTGCACCGCTTCCTGCAGCTCAGATCGCTCTTTCTGCAGCAGCCGGTGAGGAGTAC
AAGTATACTCAGAACGCTGGTTGGGATACTAATGATGCCGCTTATGCAGGTTGGAACGTCGACCGCTGT

5.4.2 Amino acid

SusD1 MNIKNLKYVAAAMLLGVSMTSCDDFLDKPVEDNYNTENYYTDDNSCIAGVNYLYNSPWYDFQRGFIKIGEVMMSGNMYWGSSPYMNFVSVNG
TDQDLVNMSYSLWAEIGHANTVYNSIKGSSASESVKNQCMGECLAWKAMAYFFLVRSFGDVPIVHDNSVNLAAAGDYNTLHKIQKADVYIEIM
MTLEKAMELLPKTKSTTGRIDYYCAEGLYAKVALTAAGVSGQLDNSLLQKASTASLDVINNSGRKLMANYADIFRGSNNISDESLFAWRWTV
GSHWTCQNTLQSDLMPGDFDEFGDCWGGWGGPSADLQDAFGYDVTENPKNRLDVDARRKATMMGPGDVYDYFWRDKDLGNGKKGFDI
LKFYFDKDYNSAATNTFQGPCGVQNVKHAYGDNADHEAECGGMSAARMSYAVATHILRLADVYLVHAEAEVLQGKTTSATALAAFNAVRSR
SVPSAVDKTQLSFDDVWKERRLELAGEGDRWYDFVRRSYDVNACIAELTSQRRNAIWNCEVYKTYFESDGATWDATNIQYDESTPIPNV
TANSFNLPYPTEDVALNPNLGSNAEAIHVDRTEYAY

SusD38489 MKTNIYSKFLGLAAVAVTAMGMASCEDFLDRPSEDNYNADNFYTNDAAVEASVGYLYNSPWYDFQRGFIK/GEVFSGNMYWGSSPYLNFS
VNGTDVLDVNMSYSLWSEIAHTCVVYQSIEGSTASQSVKDQCMGECLTLKALAYFYLVRSFGDVPIIHDPSAIIAAGDYNVQKVEKADVYIEY
IVMTLEKALELLPKRTLNTGHIDYYCAEALLSKVYLTRAGVSGSLNNSDLEMAAKLAKDVIDNSGRHLEPVYSDIFRGSHTGEEGLIWRWTV
GAQWTCQNTLQSDLIMENFGDQDLWGGWGGPSTDLMRAFGVIDLKRDPENAGNDKNNPDFAVITSFLSPEARANADRDSRRQATMMLP
GDVYSYFWRNKGGFDLLKFYYDKNYNSAATEEFQGPCGCQNVKHLYGNDADHIAE VGFSPARMAYAFHTHVLRRLADVYLIFAEAKTLLGQG
SDAAALAAFNAVRQRAIAGEPAATSLTFDMIWKERRLEFAGEGDRWYDFVRRSYDADACLAIEIKSQFRNNLWGC/SVMYKNYFESGAWWE
PTQTDVLGYNNDIPVPSNITKSVFTLPFPTEDVAQNPNVGSDAQAIHVDRNTYSY

SusD70111 MKKILNFAAVAVLALS FASCEKFLDTTNYWSKTAEDFPANEADAAQILTGVYNNLNASIGNSVHLNHFLWSLAASDDCLGGGGNNDQAMQAE
DLMLTFGVDMYNSFYCDRYTGIARANNAIASFPNCGLAEDVLGQYMGEAYFLRAYYYYELASMFNIPCPITTAANATEPQISGEALWGQILE
DCQTAINYFPNKKASGDGHVDKYCAEALLGRVYLFASGFLGIETFTLPSGKTLGRADAAKVIEDCVKTSGLVSDYHNLWAYTNRISVDDEL
SPWKNGYIEYVSDDSGVNPEAMFMKFNTQPSWSTTIGYSNQTALFMGIRGQAGTSTGDCFPFGVGMCPVSPQLVKDWETAEPDDIR
REASIIPTKFNKTYSGGDSNIQETGYQTKTMPVIGRKAEGSNEFYATYSNAMYPGLTWSEGNTDNFQLNSIDDMVLIRFAEVLLMDAELN
NNQDSFDQVRHRAGLPSKAISTKAIQDERRWELAFEGRLRFNDLRRFGVEYAKTALDKQDGVSCYNMGEATGNTASKFNGGYGARYAATLG
FAPLPAAQIALSAAAGEEYKYTQNAGWDTNDAAYAGWN

SusD70111_{F3} TAHMREASIIPTKFNKTYSGGDSNIQETGYQTKTMPVIGRKAEGSNEFYAYSNAMYPGLTWSEGNTDNFQLNSIDDMVLIRFAEVLLMDA
ELNNNQDSFDQVRHRAGLPSKAISTKAIQDERRWELAFEGRLRFNDLRRFGVEYAKTALDKQDGVSCYNMGEATGNTASKFNGGYGARYAA
TLGFAPLPAAQIALSAAAGEEYKYTQNAGWDTNDAAYAGWNVDR

VI. Acknowledgement

To Professor Streit, for the mentorship and the opportunity to join his group and conduct this research.

To Jenny and Pablo, for all the scientific knowledge and advice shared.

To my Lab friends, for all the good and bad times that we spent together.

To my friends in Brazil. Thank you for always being present, despite the distance.

Last, but not least:

To my fiancée Jasper. I am glad that I met you early during this journey. Thank you for these unforgettable 4 years, for your personality, patience and care with me. Also, thank you for being my German tutor. A bright future is ahead of us. Love you, “jorgeous”.

To my parents, I love you to the moon and back. I am very grateful for all the love shared with me on our Sunday video calls. Your support was very important, especially when your only daughter is so far away. Both of you are my whole models of strength and resilience. I love how you take care of our pets, including your “grandson” (my cat) Bilbo. PS: don’t worry, when it is the right time, I will give you proper grandkids.

This is a samba verse, for my parents to understand:

*“(...) Erga essa cabeça, mete o pé e vai na fé
Manda essa tristeza embora
Basta acreditar que um novo dia vai raiar
Sua hora vai chegar. (...)”*

Grupo Revelação – Tá escrito

VII. References

VII. References

- Acuna-Amador, L., Primot, A., Cadieu, E., Roulet, A., & Barloy-Hubler, F. (2018). Genomic repeats, misassembly and reannotation: a case study with long-read resequencing of *Porphyromonas gingivalis* reference strains. *BMC Genomics*, 19(1), 54. <https://doi.org/10.1186/s12864-017-4429-4>
- Anderson, K. L., & Salyers, A. A. (1989). Biochemical evidence that starch breakdown by *Bacteroides thetaiotaomicron* involves outer membrane starch-binding sites and periplasmic starch-degrading enzymes. *J Bacteriol*, 171(6), 3192-3198. <https://doi.org/10.1128/jb.171.6.3192-3198.1989>
- Anni, H., Nikolaeva, O., & Israel, Y. (2001). Selection of phage-display library peptides recognizing ethanol targets on proteins. *Alcohol*, 25(3), 201-209. [https://doi.org/10.1016/s0741-8329\(01\)00164-1](https://doi.org/10.1016/s0741-8329(01)00164-1)
- Arai, R. (2021). Design of helical linkers for fusion proteins and protein-based nanostructures. *Methods Enzymol*, 647, 209-230. <https://doi.org/10.1016/bs.mie.2020.10.003>
- Armougom, F., Moretti, S., Poirot, O., Audic, S., Dumas, P., Schaeli, B., Keduas, V., & Notredame, C. (2006). Expresso: automatic incorporation of structural information in multiple sequence alignments using 3D-Coffee. *Nucleic Acids Res*, 34(Web Server issue), W604-608. <https://doi.org/10.1093/nar/gkl092>
- Bakolitsa, C., Xu, Q., Rife, C. L., Abdubek, P., Astakhova, T., Axelrod, H. L., Carlton, D., Chen, C., Chiu, H. J., Clayton, T., Das, D., Deller, M. C., Duan, L., Ellrott, K., Farr, C. L., Feuerhelm, J., Grant, J. C., Grzechnik, A., Han, G. W.,...Wilson, I. A. (2010). Structure of BT_3984, a member of the SusD/RagB family of nutrient-binding molecules. *Acta Crystallogr Sect F Struct Biol Cryst Commun*, 66(Pt 10), 1274-1280. <https://doi.org/10.1107/S1744309110032999>
- Berman, H. M., Westbrook, J., Feng, Z., Gilliland, G., Bhat, T. N., Weissig, H., Shindyalov, I. N., & Bourne, P. E. (2000). The Protein Data Bank. *Nucleic Acids Res*, 28(1), 235-242. <https://doi.org/10.1093/nar/28.1.235>
- Biundo, A., Reich, J., Ribitsch, D., & Guebitz, G. M. (2018). Synergistic effect of mutagenesis and truncation to improve a polyesterase from *Clostridium botulinum* for polyester hydrolysis. *Sci Rep*, 8(1), 3745. <https://doi.org/10.1038/s41598-018-21825-9>
- Biundo, A., Ribitsch, D., & Guebitz, G. M. (2018). Surface engineering of polyester-degrading enzymes to improve efficiency and tune specificity. *Appl Microbiol Biotechnol*, 102(8), 3551-3559. <https://doi.org/10.1007/s00253-018-8850-7>
- Biundo, A., Ribitsch, D., Steinkellner, G., Gruber, K., & Guebitz, G. M. (2017). Polyester hydrolysis is enhanced by a truncated esterase: Less is more. *Biotechnol J*, 12(8). <https://doi.org/10.1002/biot.201600450>
- Bjursell, M. K., Martens, E. C., & Gordon, J. I. (2006). Functional genomic and metabolic studies of the adaptations of a prominent adult human gut symbiont, *Bacteroides thetaiotaomicron*, to the suckling period. *J Biol Chem*, 281(47), 36269-36279. <https://doi.org/10.1074/jbc.M606509200>
- Blasing, M., & Amelung, W. (2018). Plastics in soil: Analytical methods and possible sources. *Sci Total Environ*, 612, 422-435. <https://doi.org/10.1016/j.scitotenv.2017.08.086>
- Bolam, D. N., & Koropatkin, N. M. (2012). Glycan recognition by the Bacteroidetes Sus-like systems. *Curr Opin Struct Biol*, 22(5), 563-569. <https://doi.org/10.1016/j.sbi.2012.06.006>
- Bolam, D. N., & van den Berg, B. (2018). TonB-dependent transport by the gut microbiota: novel aspects of an old problem. *Curr Opin Struct Biol*, 51, 35-43. <https://doi.org/10.1016/j.sbi.2018.03.001>
- Brandon, J. A., Jones, W., & Ohman, M. D. (2019). Multidecadal increase in plastic particles in coastal ocean sediments. *Sci Adv*, 5(9), eaax0587. <https://doi.org/10.1126/sciadv.aax0587>

VII. References

- Budd, K., Gunn, J. C., Finch, T., Klymus, K., Sitati, N., & Eggert, L. S. (2020). Effects of diet, habitat, and phylogeny on the fecal microbiome of wild African savanna (*Loxodonta africana*) and forest elephants (*L. cyclotis*). *Ecol Evol*, *10*(12), 5637-5650. <https://doi.org/10.1002/ece3.6305>
- Burley, S. K., Bhikadiya, C., Bi, C., Bittrich, S., Chen, L., Crichlow, G. V., Christie, C. H., Dalenberg, K., Di Costanzo, L., Duarte, J. M., Dutta, S., Feng, Z., Ganesan, S., Goodsell, D. S., Ghosh, S., Green, R. K., Guranovic, V., Guzenko, D., Hudson, B. P.,...Zhuravleva, M. (2021). RCSB Protein Data Bank: powerful new tools for exploring 3D structures of biological macromolecules for basic and applied research and education in fundamental biology, biomedicine, biotechnology, bioengineering and energy sciences. *Nucleic Acids Res*, *49*(D1), D437-D451. <https://doi.org/10.1093/nar/gkaa1038>
- Cameron, E. A., Kwiatkowski, K. J., Lee, B. H., Hamaker, B. R., Koropatkin, N. M., & Martens, E. C. (2014). Multifunctional nutrient-binding proteins adapt human symbiotic bacteria for glycan competition in the gut by separately promoting enhanced sensing and catalysis. *mBio*, *5*(5), e01441-01414. <https://doi.org/10.1128/mBio.01441-14>
- Campaniello, D., Corbo, M. R., Sinigaglia, M., Speranza, B., Racioppo, A., Altieri, C., & Bevilacqua, A. (2022). How Diet and Physical Activity Modulate Gut Microbiota: Evidence, and Perspectives. *Nutrients*, *14*(12). <https://doi.org/10.3390/nu14122456>
- Chaudet, M. M., & Rose, D. R. (2016). Suggested alternative starch utilization system from the human gut bacterium *Bacteroides thetaiotaomicron*. *Biochem Cell Biol*, *94*(3), 241-246. <https://doi.org/10.1139/bcb-2016-0002>
- Chen, K. H., Y.; Dong, X.; Sun, Y. (2021). Molecular Insights into the Enhanced Performance of EKylated PETase Toward PET Degradation. *ACS Catal*, *11*(12), 7358–7370. <https://doi.org/https://doi.org/10.1021/acscatal.1c01062>
- Cho, K. H., & Salyers, A. A. (2001). Biochemical analysis of interactions between outer membrane proteins that contribute to starch utilization by *Bacteroides thetaiotaomicron*. *J Bacteriol*, *183*(24), 7224-7230. <https://doi.org/10.1128/JB.183.24.7224-7230.2001>
- Chow, J., Perez-Garcia, P., Dierkes, R., & Streit, W. R. (2022). Microbial enzymes will offer limited solutions to the global plastic pollution crisis. *Microb Biotechnol*. <https://doi.org/10.1111/1751-7915.14135>
- Correia, V. G., Trovao, F., Pinheiro, B. A., Bras, J. L. A., Silva, L. M., Nunes, C., Coimbra, M. A., Liu, Y., Feizi, T., Fontes, C., Mulloy, B., Chai, W., Carvalho, A. L., & Palma, A. S. (2021). Mapping Molecular Recognition of beta1,3-1,4-Glucans by a Surface Glycan-Binding Protein from the Human Gut Symbiont *Bacteroides ovatus*. *Microbiol Spectr*, *9*(3), e0182621. <https://doi.org/10.1128/Spectrum.01826-21>
- Crognale, S., Braguglia, C. M., Gallipoli, A., Gianico, A., Rossetti, S., & Montecchio, D. (2021). Direct Conversion of Food Waste Extract into Caproate: Metagenomics Assessment of Chain Elongation Process. *Microorganisms*, *9*(2). <https://doi.org/10.3390/microorganisms9020327>
- Cui, Y., Chen, Y., Sun, J., Zhu, T., Pang, H., Li, C., Geng, W. C., & Wu, B. (2024). Computational redesign of a hydrolase for nearly complete PET depolymerization at industrially relevant high-solids loading. *Nat Commun*, *15*(1), 1417. <https://doi.org/10.1038/s41467-024-45662-9>
- Cui, Y. C., Y.; Liu, X.; Dong, S.; Tian, Y.; Qiao, Y.; Mitra, R.; Han, J.; Li, C.; Han, X.; Liu, W.; Chen, Q.; Wei, W.; Wang, X.; Du, W.; Tang, S.; Xiang, H.; Liu, H.; Liang, Y.; Houk, K.N.; Wu, B. (2021). Computational Redesign of a PETase for Plastic Biodegradation under Ambient Condition by the GRAPE Strategy. *ACS Catal*, *11*(3), 1340-1350. <https://doi.org/https://doi.org/10.1021/acscatal.0c05126>
- Dai, L., Qu, Y., Huang, J. W., Hu, Y., Hu, H., Li, S., Chen, C. C., & Guo, R. T. (2021). Enhancing PET hydrolytic enzyme activity by fusion of the cellulose-binding domain of

VII. References

- cellobiohydrolase I from *Trichoderma reesei*. *J Biotechnol*, 334, 47-50. <https://doi.org/10.1016/j.jbiotec.2021.05.006>
- Dai, X., Zhu, Y., Luo, Y., Song, L., Liu, D., Liu, L., Chen, F., Wang, M., Li, J., Zeng, X., Dong, Z., Hu, S., Li, L., Xu, J., Huang, L., & Dong, X. (2012). Metagenomic insights into the fibrolytic microbiome in yak rumen. *PLoS One*, 7(7), e40430. <https://doi.org/10.1371/journal.pone.0040430>
- Danso, D., Schmeisser, C., Chow, J., Zimmermann, W., Wei, R., Leggewie, C., Li, X., Hazen, T., & Streit, W. R. (2018). New Insights into the Function and Global Distribution of Polyethylene Terephthalate (PET)-Degrading Bacteria and Enzymes in Marine and Terrestrial Metagenomes. *Appl Environ Microbiol*, 84(8). <https://doi.org/10.1128/AEM.02773-17>
- Dejean, G., Tamura, K., Cabrera, A., Jain, N., Pudlo, N. A., Pereira, G., Viborg, A. H., Van Petegem, F., Martens, E. C., & Brumer, H. (2020). Synergy between Cell Surface Glycosidases and Glycan-Binding Proteins Dictates the Utilization of Specific Beta(1,3)-Glucans by Human Gut Bacteroides. *mBio*, 11(2). <https://doi.org/10.1128/mBio.00095-20>
- Di Tommaso, P., Moretti, S., Xenarios, I., Orobitg, M., Montanyola, A., Chang, J. M., Taly, J. F., & Notredame, C. (2011). T-Coffee: a web server for the multiple sequence alignment of protein and RNA sequences using structural information and homology extension. *Nucleic Acids Res*, 39(Web Server issue), W13-17. <https://doi.org/10.1093/nar/gkr245>
- Diedrich, K. G., J.; Schöning-Stierand, K.; Rarey, M. (2021). GeoMine: interactive pattern mining of protein-ligand interfaces in the Protein Data Bank. *Bioinformatics*, 37(3), 424-425.
- Dodd, D., Mackie, R. I., & Cann, I. K. (2011). Xylan degradation, a metabolic property shared by rumen and human colonic Bacteroidetes. *Mol Microbiol*, 79(2), 292-304. <https://doi.org/10.1111/j.1365-2958.2010.07473.x>
- Don, R. H., Cox, P. T., Wainwright, B. J., Baker, K., & Mattick, J. S. (1991). 'Touchdown' PCR to circumvent spurious priming during gene amplification. *Nucleic Acids Res*, 19(14), 4008. <https://doi.org/10.1093/nar/19.14.4008>
- Ejima, H., Matsuno, H., & Serizawa, T. (2010). Biological identification of peptides that specifically bind to poly(phenylene vinylene) surfaces: recognition of the branched or linear structure of the conjugated polymer. *Langmuir*, 26(22), 17278-17285. <https://doi.org/10.1021/la102018f>
- Espino-Rammer, L., Ribitsch, D., Przulucka, A., Marold, A., Greimel, K. J., Herrero Acero, E., Guebitz, G. M., Kubicek, C. P., & Druzhinina, I. S. (2013). Two novel class II hydrophobins from *Trichoderma* spp. stimulate enzymatic hydrolysis of poly(ethylene terephthalate) when expressed as fusion proteins. *Appl Environ Microbiol*, 79(14), 4230-4238. <https://doi.org/10.1128/AEM.01132-13>
- Falkenstein, P., Grasing, D., Bielytskyi, P., Zimmermann, W., Matysik, J., Wei, R., & Song, C. (2020). UV Pretreatment Impairs the Enzymatic Degradation of Polyethylene Terephthalate. *Front Microbiol*, 11, 689. <https://doi.org/10.3389/fmicb.2020.00689>
- Foley, M. H., Cockburn, D. W., & Koropatkin, N. M. (2016). The Sus operon: a model system for starch uptake by the human gut Bacteroidetes. *Cell Mol Life Sci*, 73(14), 2603-2617. <https://doi.org/10.1007/s00018-016-2242-x>
- Foley, M. H., Martens, E. C., & Koropatkin, N. M. (2018). SusE facilitates starch uptake independent of starch binding in *B. theta*. *Mol Microbiol*, 108(5), 551-566. <https://doi.org/10.1111/mmi.13949>
- Forsberg, Z., Nelson, C. E., Dalhus, B., Mekasha, S., Loose, J. S., Crouch, L. I., Rohr, A. K., Gardner, J. G., Eijsink, V. G., & Vaaje-Kolstad, G. (2016). Structural and Functional Analysis of a Lytic Polysaccharide Monoxygenase Important for Efficient Utilization of Chitin in *Cellvibrio japonicus*. *J Biol Chem*, 291(14), 7300-7312. <https://doi.org/10.1074/jbc.M115.700161>

VII. References

- Gabler, F., Nam, S. Z., Till, S., Mirdita, M., Steinegger, M., Soding, J., Lupas, A. N., & Alva, V. (2020). Protein Sequence Analysis Using the MPI Bioinformatics Toolkit. *Curr Protoc Bioinformatics*, 72(1), e108. <https://doi.org/10.1002/cpbi.108>
- Gasteiger E., H. C., Gattiker A., Duvaud S., Wilkins M.R., Appel R.D., Bairoch A.;. (2005). Protein Identification and Analysis Tools on the Expasy Server. *John M. Walker (ed): The Proteomics Protocols Handbook*, Humana Press, 571-607. <https://doi.org/https://doi.org/10.1385/1-59259-890-0:571>
- Geyer, R., Jambeck, J. R., & Law, K. L. (2017). Production, use, and fate of all plastics ever made. *Sci Adv*, 3(7), e1700782. <https://doi.org/10.1126/sciadv.1700782>
- Gharechahi, J., Sarikhan, S., Han, J. L., Ding, X. Z., & Salekdeh, G. H. (2022). Functional and phylogenetic analyses of camel rumen microbiota associated with different lignocellulosic substrates. *NPJ Biofilms Microbiomes*, 8(1), 46. <https://doi.org/10.1038/s41522-022-00309-9>
- Glenwright, A. J., Pothula, K. R., Bhamidimarri, S. P., Chorev, D. S., Basle, A., Firbank, S. J., Zheng, H., Robinson, C. V., Winterhalter, M., Kleinekathofer, U., Bolam, D. N., & van den Berg, B. (2017). Structural basis for nutrient acquisition by dominant members of the human gut microbiota. *Nature*, 541(7637), 407-411. <https://doi.org/10.1038/nature20828>
- Goddard, T. D., Huang, C. C., Meng, E. C., Pettersen, E. F., Couch, G. S., Morris, J. H., & Ferrin, T. E. (2018). UCSF ChimeraX: Meeting modern challenges in visualization and analysis. *Protein Sci*, 27(1), 14-25. <https://doi.org/10.1002/pro.3235>
- Gotoh, K. Y., A.; Kobayashi, Y. . (2011). Wettability characteristics of poly(ethylene terephthalate) films treated by atmospheric pressure plasma and ultraviolet excimer light. *Polymer Journal*, 43, 545-551. <https://doi.org/https://doi.org/10.1038/pj.2011.20>
- Goulas, T., Garcia-Ferrer, I., Hutcherson, J. A., Potempa, B. A., Potempa, J., Scott, D. A., & Gomis-Ruth, F. X. (2016). Structure of RagB, a major immunodominant outer-membrane surface receptor antigen of *Porphyromonas gingivalis*. *Mol Oral Microbiol*, 31(6), 472-485. <https://doi.org/10.1111/omi.12140>
- Graham, R. E., E.; Brizendine, R.K.; Salvachúa, D.; Michener, W.E.; Li, Y.; Tan, Z.; Beckham, G.T.; McGeehan, J.E.; Pickford, A.R. (2022). The role of binding modules in enzymatic poly(ethylene terephthalate) hydrolysis at high-solids loadings. *Chem Catalysis*, 2(10), 2644-2657. <https://doi.org/https://doi.org/10.1016/j.checat.2022.07.018>
- Gray, D. A., White, J. B. R., Oluwole, A. O., Rath, P., Glenwright, A. J., Mazur, A., Zahn, M., Basle, A., Morland, C., Evans, S. L., Cartmell, A., Robinson, C. V., Hiller, S., Ranson, N. A., Bolam, D. N., & van den Berg, B. (2021). Insights into SusCD-mediated glycan import by a prominent gut symbiont. *Nat Commun*, 12(1), 44. <https://doi.org/10.1038/s41467-020-20285-y>
- Gricajeva, A. N., A.K.; Gudiukaite, R. (2021). Insights into polyester plastic biodegradation by carboxyl ester hydrolases. *Journal of Chemical Technology and Biotechnology*, 97(2), 359-380. <https://doi.org/https://doi.org/10.1002/jctb.6745>
- Guo, W., Duan, J., Shi, Z., Yu, X., & Shao, Z. (2023). Biodegradation of PET by the membrane-anchored PET esterase from the marine bacterium *Rhodococcus pyridinivorans* P23. *Commun Biol*, 6(1), 1090. <https://doi.org/10.1038/s42003-023-05470-1>
- Hall, L. M., Fawell, S. C., Shi, X., Faray-Kele, M. C., Aduse-Opoku, J., Whiley, R. A., & Curtis, M. A. (2005). Sequence diversity and antigenic variation at the rag locus of *Porphyromonas gingivalis*. *Infect Immun*, 73(7), 4253-4262. <https://doi.org/10.1128/IAI.73.7.4253-4262.2005>
- Hanahan, D. (1983). Studies on transformation of *Escherichia coli* with plasmids. *J Mol Biol*, 166(4), 557-580. [https://doi.org/10.1016/s0022-2836\(83\)80284-8](https://doi.org/10.1016/s0022-2836(83)80284-8)

VII. References

- Hanley, S. A., Aduse-Opoku, J., & Curtis, M. A. (1999). A 55-kilodalton immunodominant antigen of *Porphyromonas gingivalis* W50 has arisen via horizontal gene transfer. *Infect Immun*, 67(3), 1157-1171. <https://doi.org/10.1128/IAI.67.3.1157-1171.1999>
- Hashimoto, H. (2006). Recent structural studies of carbohydrate-binding modules. *Cell Mol Life Sci*, 63(24), 2954-2967. <https://doi.org/10.1007/s00018-006-6195-3>
- Holm, L. (2022). Dali server: structural unification of protein families. *Nucleic Acids Res*, 50(W1), W210-215. <https://doi.org/10.1093/nar/gkac387>
- Hu, X., Li, S., Mu, R., Guo, J., Zhao, C., Cao, Y., Zhang, N., & Fu, Y. (2022). The Rumen Microbiota Contributes to the Development of Mastitis in Dairy Cows. *Microbiol Spectr*, 10(1), e0251221. <https://doi.org/10.1128/spectrum.02512-21>
- Ilmberger, N., Gullert, S., Dannenberg, J., Rabausch, U., Torres, J., Wemheuer, B., Alawi, M., Poehlein, A., Chow, J., Turaev, D., Rattei, T., Schmeisser, C., Salomon, J., Olsen, P. B., Daniel, R., Grundhoff, A., Borchert, M. S., & Streit, W. R. (2014). A comparative metagenome survey of the fecal microbiota of a breast- and a plant-fed Asian elephant reveals an unexpectedly high diversity of glycoside hydrolase family enzymes. *PLoS One*, 9(9), e106707. <https://doi.org/10.1371/journal.pone.0106707>
- Itoh, T., Hibi, T., Suzuki, F., Sugimoto, I., Fujiwara, A., Inaka, K., Tanaka, H., Ohta, K., Fujii, Y., Taketo, A., & Kimoto, H. (2016). Crystal Structure of Chitinase ChiW from *Paenibacillus* sp. str. FPU-7 Reveals a Novel Type of Bacterial Cell-Surface-Expressed Multi-Modular Enzyme Machinery. *PLoS One*, 11(12), e0167310. <https://doi.org/10.1371/journal.pone.0167310>
- Itoh, Y., Watanabe, J., Fukada, H., Mizuno, R., Kezuka, Y., Nonaka, T., & Watanabe, T. (2006). Importance of Trp59 and Trp60 in chitin-binding, hydrolytic, and antifungal activities of *Streptomyces griseus* chitinase C. *Appl Microbiol Biotechnol*, 72(6), 1176-1184. <https://doi.org/10.1007/s00253-006-0405-7>
- Jambeck, J. R., Geyer, R., Wilcox, C., Siegler, T. R., Perryman, M., Andrady, A., Narayan, R., & Law, K. L. (2015). Marine pollution. Plastic waste inputs from land into the ocean. *Science*, 347(6223), 768-771. <https://doi.org/10.1126/science.1260352>
- Ji, Y., Lu, Y., Puetz, H., & Schwaneberg, U. (2021). Anchor peptides promote degradation of mixed plastics for recycling. *Methods Enzymol*, 648, 271-292. <https://doi.org/10.1016/bs.mie.2020.12.027>
- Jog, J. (1995). Crystallization of Polyethyleneterephthalate. *J Macromol Sci Part C*, 35(3), 531-553. <https://doi.org/https://doi.org/10.1080/15321799508014598>
- Jumper, J., Evans, R., Pritzel, A., Green, T., Figurnov, M., Ronneberger, O., Tunyasuvunakool, K., Bates, R., Zidek, A., Potapenko, A., Bridgland, A., Meyer, C., Kohl, S. A. A., Ballard, A. J., Cowie, A., Romera-Paredes, B., Nikolov, S., Jain, R., Adler, J.,...Hassabis, D. (2021). Highly accurate protein structure prediction with AlphaFold. *Nature*, 596(7873), 583-589. <https://doi.org/10.1038/s41586-021-03819-2>
- Kandel, S., Sripiboon, S., Jenjaroenpun, P., Ussery, D. W., Nookaew, I., Robeson, M. S., 2nd, & Wongsurawat, T. (2020). 16S rRNA Gene Amplicon Profiling of Baby and Adult Captive Elephants in Thailand. *Microbiol Resour Announc*, 9(24). <https://doi.org/10.1128/MRA.00248-20>
- Karpenahalli, M. R., Lupas, A. N., & Soding, J. (2007). TPRpred: a tool for prediction of TPR-, PPR- and SEL1-like repeats from protein sequences. *BMC Bioinformatics*, 8, 2. <https://doi.org/10.1186/1471-2105-8-2>
- Kim, K., Oh, J., Han, D., Kim, E. E., Lee, B., & Kim, Y. (2006). Crystal structure of PilF: functional implication in the type 4 pilus biogenesis in *Pseudomonas aeruginosa*. *Biochem Biophys Res Commun*, 340(4), 1028-1038. <https://doi.org/10.1016/j.bbrc.2005.12.108>
- Kitamura, E., & Kamei, Y. (2003). Molecular cloning, sequencing and expression of the gene encoding a novel chitinase A from a marine bacterium, *Pseudomonas* sp PE2, and its

- domain structure. *Appl Microbiol Biotechnol*, 61(2), 140-149. <https://doi.org/10.1007/s00253-002-1154-x>
- Kitamura, E., & Kamei, Y. (2006). Molecular cloning of the gene encoding beta-1,3(4)-glucanase A from a marine bacterium, *Pseudomonas* sp. PE2, an essential enzyme for the degradation of *Pythium porphyrae* cell walls. *Appl Microbiol Biotechnol*, 71(5), 630-637. <https://doi.org/10.1007/s00253-005-0200-x>
- Koropatkin, N., Martens, E. C., Gordon, J. I., & Smith, T. J. (2009). Structure of a SusD homologue, BT1043, involved in mucin O-glycan utilization in a prominent human gut symbiont. *Biochemistry*, 48(7), 1532-1542. <https://doi.org/10.1021/bi801942a>
- Koropatkin, N. M., Martens, E. C., Gordon, J. I., & Smith, T. J. (2008). Starch catabolism by a prominent human gut symbiont is directed by the recognition of amylose helices. *Structure*, 16(7), 1105-1115. <https://doi.org/10.1016/j.str.2008.03.017>
- Koropatkin, N. M., & Smith, T. J. (2010). SusG: a unique cell-membrane-associated alpha-amylase from a prominent human gut symbiont targets complex starch molecules. *Structure*, 18(2), 200-215. <https://doi.org/10.1016/j.str.2009.12.010>
- Kuba, Y., Takashima, T., Uechi, K., & Taira, T. (2018). Purification, cDNA cloning, and characterization of plant chitinase with a novel domain combination from lycophyte *Selaginella doederleinii*. *Biosci Biotechnol Biochem*, 82(10), 1742-1752. <https://doi.org/10.1080/09168451.2018.1491285>
- Kumari, A., Chaudhary, D. R., & Jha, B. (2019). Destabilization of polyethylene and polyvinylchloride structure by marine bacterial strain. *Environ Sci Pollut Res Int*, 26(2), 1507-1516. <https://doi.org/10.1007/s11356-018-3465-1>
- Larsbrink, J., Zhu, Y., Kharade, S. S., Kwiatkowski, K. J., Eijsink, V. G., Koropatkin, N. M., McBride, M. J., & Pope, P. B. (2016). A polysaccharide utilization locus from *Flavobacterium johnsoniae* enables conversion of recalcitrant chitin. *Biotechnol Biofuels*, 9, 260. <https://doi.org/10.1186/s13068-016-0674-z>
- Leslie, H. A., van Velzen, M. J. M., Brandsma, S. H., Vethaak, A. D., Garcia-Vallejo, J. J., & Lamoree, M. H. (2022). Discovery and quantification of plastic particle pollution in human blood. *Environ Int*, 163, 107199. <https://doi.org/10.1016/j.envint.2022.107199>
- Letunic, I., & Bork, P. (2024). Interactive Tree of Life (iTOL) v6: recent updates to the phylogenetic tree display and annotation tool. *Nucleic Acids Res*. <https://doi.org/10.1093/nar/gkae268>
- Li, A., Sheng, Y., Cui, H., Wang, M., Wu, L., Song, Y., Yang, R., Li, X., & Huang, H. (2023). Discovery and mechanism-guided engineering of BHET hydrolases for improved PET recycling and upcycling. *Nat Commun*, 14(1), 4169. <https://doi.org/10.1038/s41467-023-39929-w>
- Li, G., Jiang, Y., Li, Q., An, D., Bao, M., Lang, L., Han, L., Huang, X., & Jiang, C. (2022). Comparative and functional analyses of fecal microbiome in Asian elephants. *Antonie Van Leeuwenhoek*, 115(9), 1187-1202. <https://doi.org/10.1007/s10482-022-01757-1>
- Li, H., Lu, Z., Hao, M. S., Kvammen, A., Inman, A. R., Srivastava, V., Bulone, V., & McKee, L. S. (2023). Family 92 carbohydrate-binding modules specific for beta-1,6-glucans increase the thermostability of a bacterial chitinase. *Biochimie*, 212, 153-160. <https://doi.org/10.1016/j.biochi.2023.04.019>
- Lin, J., Yan, D., Fu, J., Chen, Y., & Ou, H. (2020). Ultraviolet-C and vacuum ultraviolet inducing surface degradation of microplastics. *Water Res*, 186, 116360. <https://doi.org/10.1016/j.watres.2020.116360>
- Liu, F., Wang, T., Yang, W., Zhang, Y., Gong, Y., Fan, X., Wang, G., Lu, Z., & Wang, J. (2023). Current advances in the structural biology and molecular engineering of PETase. *Front Bioeng Biotechnol*, 11, 1263996. <https://doi.org/10.3389/fbioe.2023.1263996>
- Liu, Y., Wang, P., Tian, J., Seidi, F., Guo, J., Zhu, W., Xiao, H., & Song, J. (2022). Carbohydrate-Binding Modules of Potential Resources: Occurrence in Nature, Function, and Application

VII. References

- in Fiber Recognition and Treatment. *Polymers (Basel)*, 14(9). <https://doi.org/10.3390/polym14091806>
- Lu, H., Diaz, D. J., Czarnecki, N. J., Zhu, C., Kim, W., Shroff, R., Acosta, D. J., Alexander, B. R., Cole, H. O., Zhang, Y., Lynd, N. A., Ellington, A. D., & Alper, H. S. (2022). Machine learning-aided engineering of hydrolases for PET depolymerization. *Nature*, 604(7907), 662-667. <https://doi.org/10.1038/s41586-022-04599-z>
- Lu, S., Wang, J., Chitsaz, F., Derbyshire, M. K., Geer, R. C., Gonzales, N. R., Gwadz, M., Hurwitz, D. I., Marchler, G. H., Song, J. S., Thanki, N., Yamashita, R. A., Yang, M., Zhang, D., Zheng, C., Lanczycki, C. J., & Marchler-Bauer, A. (2020). CDD/SPARCLE: the conserved domain database in 2020. *Nucleic Acids Res*, 48(D1), D265-D268. <https://doi.org/10.1093/nar/gkz991>
- Lu, Z., Kvammen, A., Li, H., Hao, M., Inman, A. R., Bulone, V., & McKee, L. S. (2023). A polysaccharide utilization locus from *Chitinophaga pinensis* simultaneously targets chitin and beta-glucans found in fungal cell walls. *mSphere*, 8(4), e0024423. <https://doi.org/10.1128/msphere.00244-23>
- Mackenzie, A. K., Pope, P. B., Pedersen, H. L., Gupta, R., Morrison, M., Willats, W. G., & Eijsink, V. G. (2012). Two SusD-like proteins encoded within a polysaccharide utilization locus of an uncultured ruminant Bacteroidetes phylotype bind strongly to cellulose. *Appl Environ Microbiol*, 78(16), 5935-5937. <https://doi.org/10.1128/AEM.01164-12>
- Madej, M., White, J. B. R., Nowakowska, Z., Rawson, S., Scavenius, C., Enghild, J. J., Bereta, G. P., Pothula, K., Kleinekathoefer, U., Basle, A., Ranson, N. A., Potempa, J., & van den Berg, B. (2020). Structural and functional insights into oligopeptide acquisition by the RagAB transporter from *Porphyromonas gingivalis*. *Nat Microbiol*, 5(8), 1016-1025. <https://doi.org/10.1038/s41564-020-0716-y>
- Magne, F., Gotteland, M., Gauthier, L., Zazueta, A., Pesa, S., Navarrete, P., & Balamurugan, R. (2020). The Firmicutes/Bacteroidetes Ratio: A Relevant Marker of Gut Dysbiosis in Obese Patients? *Nutrients*, 12(5). <https://doi.org/10.3390/nu12051474>
- Makino, S., Reynolds, J. A., & Tanford, C. (1973). The binding of deoxycholate and Triton X-100 to proteins. *J Biol Chem*, 248(14), 4926-4932. <https://www.ncbi.nlm.nih.gov/pubmed/4736885>
- Maniatis, T. F., E.F. and Sambrook, J. (1982). *Molecular cloning. A laboratory manual*.
- Marchler-Bauer, A., Bo, Y., Han, L., He, J., Lanczycki, C. J., Lu, S., Chitsaz, F., Derbyshire, M. K., Geer, R. C., Gonzales, N. R., Gwadz, M., Hurwitz, D. I., Lu, F., Marchler, G. H., Song, J. S., Thanki, N., Wang, Z., Yamashita, R. A., Zhang, D.,...Bryant, S. H. (2017). CDD/SPARCLE: functional classification of proteins via subfamily domain architectures. *Nucleic Acids Res*, 45(D1), D200-D203. <https://doi.org/10.1093/nar/gkw1129>
- Marchler-Bauer, A., & Bryant, S. H. (2004). CD-Search: protein domain annotations on the fly. *Nucleic Acids Res*, 32(Web Server issue), W327-331. <https://doi.org/10.1093/nar/gkh454>
- Marchler-Bauer, A., Derbyshire, M. K., Gonzales, N. R., Lu, S., Chitsaz, F., Geer, L. Y., Geer, R. C., He, J., Gwadz, M., Hurwitz, D. I., Lanczycki, C. J., Lu, F., Marchler, G. H., Song, J. S., Thanki, N., Wang, Z., Yamashita, R. A., Zhang, D., Zheng, C., & Bryant, S. H. (2015). CDD: NCBI's conserved domain database. *Nucleic Acids Res*, 43(Database issue), D222-226. <https://doi.org/10.1093/nar/gku1221>
- Marchler-Bauer, A., Lu, S., Anderson, J. B., Chitsaz, F., Derbyshire, M. K., DeWeese-Scott, C., Fong, J. H., Geer, L. Y., Geer, R. C., Gonzales, N. R., Gwadz, M., Hurwitz, D. I., Jackson, J. D., Ke, Z., Lanczycki, C. J., Lu, F., Marchler, G. H., Mullokandov, M., Omelchenko, M. V.,...Bryant, S. H. (2011). CDD: a Conserved Domain Database for the functional annotation of proteins. *Nucleic Acids Res*, 39(Database issue), D225-229. <https://doi.org/10.1093/nar/gkq1189>

VII. References

- Martens, E. C., Koropatkin, N. M., Smith, T. J., & Gordon, J. I. (2009). Complex glycan catabolism by the human gut microbiota: the Bacteroidetes Sus-like paradigm. *J Biol Chem*, *284*(37), 24673-24677. <https://doi.org/10.1074/jbc.R109.022848>
- Mine, S., Nakamura, T., Sato, T., Ikegami, T., & Uegaki, K. (2014). Solution structure of the chitin-binding domain 1 (ChBD1) of a hyperthermophilic chitinase from *Pyrococcus furiosus*. *J Biochem*, *155*(2), 115-122. <https://doi.org/10.1093/jb/mvt104>
- Moser, F., Irwin, D., Chen, S., & Wilson, D. B. (2008). Regulation and characterization of *Thermobifida fusca* carbohydrate-binding module proteins E7 and E8. *Biotechnol Bioeng*, *100*(6), 1066-1077. <https://doi.org/10.1002/bit.21856>
- Mystkowska, A. A., Robb, C., Vidal-Melgosa, S., Vanni, C., Fernandez-Guerra, A., Hohne, M., & Hehemann, J. H. (2018). Molecular recognition of the beta-glucans laminarin and pustulan by a SusD-like glycan-binding protein of a marine Bacteroidetes. *FEBS J*, *285*(23), 4465-4481. <https://doi.org/10.1111/febs.14674>
- Nagano, K., Murakami, Y., Nishikawa, K., Sakakibara, J., Shimozato, K., & Yoshimura, F. (2007). Characterization of RagA and RagB in *Porphyromonas gingivalis*: study using gene-deletion mutants. *J Med Microbiol*, *56*(Pt 11), 1536-1548. <https://doi.org/10.1099/jmm.0.47289-0>
- Nelson, K. E., Fleischmann, R. D., DeBoy, R. T., Paulsen, I. T., Fouts, D. E., Eisen, J. A., Daugherty, S. C., Dodson, R. J., Durkin, A. S., Gwinn, M., Haft, D. H., Kolonay, J. F., Nelson, W. C., Mason, T., Tallon, L., Gray, J., Granger, D., Tettelin, H., Dong, H.,...Fraser, C. M. (2003). Complete genome sequence of the oral pathogenic Bacterium *porphyromonas gingivalis* strain W83. *J Bacteriol*, *185*(18), 5591-5601. <https://doi.org/10.1128/JB.185.18.5591-5601.2003>
- Notredame, C., Higgins, D. G., & Heringa, J. (2000). T-Coffee: A novel method for fast and accurate multiple sequence alignment. *J Mol Biol*, *302*(1), 205-217. <https://doi.org/10.1006/jmbi.2000.4042>
- O'Sullivan, O., Suhre, K., Abergel, C., Higgins, D. G., & Notredame, C. (2004). 3DCoffee: combining protein sequences and structures within multiple sequence alignments. *J Mol Biol*, *340*(2), 385-395. <https://doi.org/10.1016/j.jmb.2004.04.058>
- Perz, V., Zumstein, M. T., Sander, M., Zitzenbacher, S., Ribitsch, D., & Guebitz, G. M. (2015). Biomimetic Approach to Enhance Enzymatic Hydrolysis of the Synthetic Polyester Poly(1,4-butylene adipate): Fusing Binding Modules to Esterases. *Biomacromolecules*, *16*(12), 3889-3896. <https://doi.org/10.1021/acs.biomac.5b01219>
- Pettersen, E. F., Goddard, T. D., Huang, C. C., Couch, G. S., Greenblatt, D. M., Meng, E. C., & Ferrin, T. E. (2004). UCSF Chimera--a visualization system for exploratory research and analysis. *J Comput Chem*, *25*(13), 1605-1612. <https://doi.org/10.1002/jcc.20084>
- Pettersen, E. F., Goddard, T. D., Huang, C. C., Meng, E. C., Couch, G. S., Croll, T. I., Morris, J. H., & Ferrin, T. E. (2021). UCSF ChimeraX: Structure visualization for researchers, educators, and developers. *Protein Sci*, *30*(1), 70-82. <https://doi.org/10.1002/pro.3943>
- Pham, T. H., Webb, J. S., & Rehm, B. H. (2004). The role of polyhydroxyalkanoate biosynthesis by *Pseudomonas aeruginosa* in rhamnolipid and alginate production as well as stress tolerance and biofilm formation. *Microbiology (Reading)*, *150*(Pt 10), 3405-3413. <https://doi.org/10.1099/mic.0.27357-0>
- Phansopa, C., Roy, S., Rafferty, J. B., Douglas, C. W., Pandhal, J., Wright, P. C., Kelly, D. J., & Stafford, G. P. (2014). Structural and functional characterization of NanU, a novel high-affinity sialic acid-inducible binding protein of oral and gut-dwelling Bacteroidetes species. *Biochem J*, *458*(3), 499-511. <https://doi.org/10.1042/BJ20131415>
- Poirot, O., Suhre, K., Abergel, C., O'Toole, E., & Notredame, C. (2004). 3DCoffee@igs: a web server for combining sequences and structures into a multiple sequence alignment. *Nucleic Acids Res*, *32*(Web Server issue), W37-40. <https://doi.org/10.1093/nar/gkh382>

VII. References

- Puspitasari, N., Tsai, S. L., & Lee, C. K. (2021a). Class I hydrophobins pretreatment stimulates PETase for monomers recycling of waste PETs. *Int J Biol Macromol*, 176, 157-164. <https://doi.org/10.1016/j.ijbiomac.2021.02.026>
- Puspitasari, N., Tsai, S. L., & Lee, C. K. (2021b). Fungal Hydrophobin RolA Enhanced PETase Hydrolysis of Polyethylene Terephthalate. *Appl Biochem Biotechnol*, 193(5), 1284-1295. <https://doi.org/10.1007/s12010-020-03358-y>
- Qiang, X., Sun, K., Xing, L., Xu, Y., Wang, H., Zhou, Z., Zhang, J., Zhang, F., Caliskan, B., Wang, M., & Qiu, Z. (2017). Discovery of a polystyrene binding peptide isolated from phage display library and its application in peptide immobilization. *Sci Rep*, 7(1), 2673. <https://doi.org/10.1038/s41598-017-02891-x>
- Qin, J., Li, R., Raes, J., Arumugam, M., Burgdorf, K. S., Manichanh, C., Nielsen, T., Pons, N., Levenez, F., Yamada, T., Mende, D. R., Li, J., Xu, J., Li, S., Li, D., Cao, J., Wang, B., Liang, H., Zheng, H.,... Wang, J. (2010). A human gut microbial gene catalogue established by metagenomic sequencing. *Nature*, 464(7285), 59-65. <https://doi.org/10.1038/nature08821>
- Qu, D., Sun, F., Feng, S., Yu, L., Tian, F., Zhang, H., Chen, W., & Zhai, Q. (2022). Protective effects of *Bacteroides fragilis* against lipopolysaccharide-induced systemic inflammation and their potential functional genes. *Food Funct*, 13(2), 1015-1025. <https://doi.org/10.1039/d1fo03073f>
- Qu, Z., Chen, K., Zhang, L., & Sun, Y. (2023). Computation-Based Design of Salt Bridges in PETase for Enhanced Thermostability and Performance for PET Degradation. *Chembiochem*, 24(21), e202300373. <https://doi.org/10.1002/cbic.202300373>
- Ragusa, A., Svelato, A., Santacroce, C., Catalano, P., Notarstefano, V., Carnevali, O., Papa, F., Rongioletti, M. C. A., Baiocco, F., Draghi, S., D'Amore, E., Rinaldo, D., Matta, M., & Giorgini, E. (2021). Plasticenta: First evidence of microplastics in human placenta. *Environ Int*, 146, 106274. <https://doi.org/10.1016/j.envint.2020.106274>
- Reeves, A. R., Wang, G. R., & Salyers, A. A. (1997). Characterization of four outer membrane proteins that play a role in utilization of starch by *Bacteroides thetaiotaomicron*. *J Bacteriol*, 179(3), 643-649. <https://doi.org/10.1128/jb.179.3.643-649.1997>
- Rennison, A. P., Westh, P., & Moller, M. S. (2023). Protein-plastic interactions: The driving forces behind the high affinity of a carbohydrate-binding module for polyethylene terephthalate. *Sci Total Environ*, 161948. <https://doi.org/10.1016/j.scitotenv.2023.161948>
- Ribitsch, D., Herrero Acero, E., Przylucka, A., Zitzenbacher, S., Marold, A., Gameraith, C., Tscheliessnig, R., Jungbauer, A., Rennhofer, H., Lichtenegger, H., Amenitsch, H., Bonazza, K., Kubicek, C. P., Druzhinina, I. S., & Guebitz, G. M. (2015). Enhanced cutinase-catalyzed hydrolysis of polyethylene terephthalate by covalent fusion to hydrophobins. *Appl Environ Microbiol*, 81(11), 3586-3592. <https://doi.org/10.1128/AEM.04111-14>
- Ribitsch, D., Yebra, A. O., Zitzenbacher, S., Wu, J., Nowitsch, S., Steinkellner, G., Greimel, K., Doliska, A., Oberdorfer, G., Gruber, C. C., Gruber, K., Schwab, H., Stana-Kleinschek, K., Acero, E. H., & Guebitz, G. M. (2013). Fusion of binding domains to *Thermobifida cellulolytica* cutinase to tune sorption characteristics and enhancing PET hydrolysis. *Biomacromolecules*, 14(6), 1769-1776. <https://doi.org/10.1021/bm400140u>
- Roda, S. F.-L., L.; Cañadas, R.; Santiago, G.; Ferrer, M.; Guallar, V. (2021). Computationally Driven Rational Design of Substrate Promiscuity on Serine Ester Hydrolases. *ACS Catal*(11), 3590-3601. <https://doi.org/https://doi.org/10.1021/acscatal.0c05015>
- Ronkvist, Å. M. X., W.; Lu, W.; Gross, R.A. (2009). Cutinase-Catalyzed Hydrolysis of Poly(ethylene terephthalate). *Macromolecules*, 42, 5128-5138.
- Rosewarne, C. P., Pope, P. B., Cheung, J. L., & Morrison, M. (2014). Analysis of the bovine rumen microbiome reveals a diversity of Sus-like polysaccharide utilization loci from the bacterial

- phylum Bacteroidetes. *J Ind Microbiol Biotechnol*, 41(3), 601-606. <https://doi.org/10.1007/s10295-013-1395-y>
- Roy, P. K., Hakkarainen, M., Varma, I. K., & Albertsson, A. C. (2011). Degradable polyethylene: fantasy or reality. *Environ Sci Technol*, 45(10), 4217-4227. <https://doi.org/10.1021/es104042f>
- Rudel, R. A., Attfield, K. R., Schifano, J. N., & Brody, J. G. (2007). Chemicals causing mammary gland tumors in animals signal new directions for epidemiology, chemicals testing, and risk assessment for breast cancer prevention. *Cancer*, 109(12 Suppl), 2635-2666. <https://doi.org/10.1002/cncr.22653>
- Sahihi, M., Fayon, P., Nauton, L., Goujon, F., Devemy, J., Dequidt, A., Hauret, P., & Malfreyt, P. (2024). Probing Enzymatic PET Degradation: Molecular Dynamics Analysis of Cutinase Adsorption and Stability. *J Chem Inf Model*. <https://doi.org/10.1021/acs.jcim.4c00079>
- Salmean, A. A., Guillouzo, A., Duffieux, D., Jam, M., Matard-Mann, M., Larocque, R., Pedersen, H. L., Michel, G., Czjzek, M., Willats, W. G. T., & Herve, C. (2018). Double blind microarray-based polysaccharide profiling enables parallel identification of uncharacterized polysaccharides and carbohydrate-binding proteins with unknown specificities. *Sci Rep*, 8(1), 2500. <https://doi.org/10.1038/s41598-018-20605-9>
- Sanjaya, R. E., Putri, K. D. A., Kurniati, A., Rohman, A., & Puspaningsih, N. N. T. (2021). In silico characterization of the GH5-cellulase family from uncultured microorganisms: physicochemical and structural studies. *J Genet Eng Biotechnol*, 19(1), 143. <https://doi.org/10.1186/s43141-021-00236-w>
- Serizawa, T., Sawada, T., & Kitayama, T. (2007). Peptide motifs that recognize differences in polymer-film surfaces. *Angew Chem Int Ed Engl*, 46(5), 723-726. <https://doi.org/10.1002/anie.200603212>
- Serizawa, T., Sawada, T., Matsuno, H., Matsubara, T., & Sato, T. (2005). A peptide motif recognizing a polymer stereoregularity. *J Am Chem Soc*, 127(40), 13780-13781. <https://doi.org/10.1021/ja054402o>
- Serizawa, T. M., H.; Sawada, T. (2011). Specific interfaces between synthetic polymers and biologically identified peptides. *Journal of Materials Chemistry*, 21(28), 10252-10260.
- Shapovalov, M. V., & Dunbrack, R. L., Jr. (2011). A smoothed backbone-dependent rotamer library for proteins derived from adaptive kernel density estimates and regressions. *Structure*, 19(6), 844-858. <https://doi.org/10.1016/j.str.2011.03.019>
- Sharma, K., Dhillon, A., & Goyal, A. (2018). Insights into Structure and Reaction Mechanism of α -Mannanases. *Curr Protein Pept Sci*, 19(1), 34-47. <https://doi.org/10.2174/1389203717666161013115724>
- Shipman, J. A., Berleman, J. E., & Salyers, A. A. (2000). Characterization of four outer membrane proteins involved in binding starch to the cell surface of *Bacteroides thetaiotaomicron*. *J Bacteriol*, 182(19), 5365-5372. <https://doi.org/10.1128/JB.182.19.5365-5372.2000>
- Silveira, M., Albano, R., Asensi, M., & Assef, A. P. (2014). The draft genome sequence of multidrug-resistant *Pseudomonas aeruginosa* strain CCBH4851, a nosocomial isolate belonging to clone SP (ST277) that is prevalent in Brazil. *Mem Inst Oswaldo Cruz*, 109(8), 1086-1087. <https://doi.org/10.1590/0074-0276140336>
- Sonnenburg, J. L., Xu, J., Leip, D. D., Chen, C. H., Westover, B. P., Weatherford, J., Buhler, J. D., & Gordon, J. I. (2005). Glycan foraging in vivo by an intestine-adapted bacterial symbiont. *Science*, 307(5717), 1955-1959. <https://doi.org/10.1126/science.1109051>
- Studier, F. W. (2005). Protein production by auto-induction in high density shaking cultures. *Protein Expr Purif*, 41(1), 207-234. <https://doi.org/10.1016/j.pep.2005.01.016>
- Studier, F. W., & Moffatt, B. A. (1986). Use of bacteriophage T7 RNA polymerase to direct selective high-level expression of cloned genes. *J Mol Biol*, 189(1), 113-130. [https://doi.org/10.1016/0022-2836\(86\)90385-2](https://doi.org/10.1016/0022-2836(86)90385-2)

VII. References

- Sulaiman, S., Yamato, S., Kanaya, E., Kim, J. J., Koga, Y., Takano, K., & Kanaya, S. (2012). Isolation of a novel cutinase homolog with polyethylene terephthalate-degrading activity from leaf-branch compost by using a metagenomic approach. *Appl Environ Microbiol*, 78(5), 1556-1562. <https://doi.org/10.1128/AEM.06725-11>
- Swaminathan, S. C., Y. (2012). Recognition of poly(dimethylsiloxane) with phage displayed peptides. *RSC Advances*, 2(33), 12724-12727.
- Taira, T., Gushiken, C., Sugata, K., Ohnuma, T., & Fukamizo, T. (2018). Unique GH18 chitinase from *Euglena gracilis*: full-length cDNA cloning and characterization of its catalytic domain. *Biosci Biotechnol Biochem*, 82(7), 1090-1100. <https://doi.org/10.1080/09168451.2018.1459463>
- Tamura, K., Dejean, G., Van Petegem, F., & Brumer, H. (2021). Distinct protein architectures mediate species-specific beta-glucan binding and metabolism in the human gut microbiota. *J Biol Chem*, 296, 100415. <https://doi.org/10.1016/j.jbc.2021.100415>
- Tamura, K., Foley, M. H., Gardill, B. R., Dejean, G., Schnizlein, M., Bahr, C. M. E., Louise Creagh, A., van Petegem, F., Koropatkin, N. M., & Brumer, H. (2019). Surface glycan-binding proteins are essential for cereal beta-glucan utilization by the human gut symbiont *Bacteroides ovatus*. *Cell Mol Life Sci*, 76(21), 4319-4340. <https://doi.org/10.1007/s00018-019-03115-3>
- Tauzin, A. S., Kwiatkowski, K. J., Orlovsky, N. I., Smith, C. J., Creagh, A. L., Haynes, C. A., Wawrzak, Z., Brumer, H., & Koropatkin, N. M. (2016). Molecular Dissection of Xyloglucan Recognition in a Prominent Human Gut Symbiont. *mBio*, 7(2), e02134-02115. <https://doi.org/10.1128/mBio.02134-15>
- Temple, M. J., Cuskin, F., Basle, A., Hickey, N., Speciale, G., Williams, S. J., Gilbert, H. J., & Lowe, E. C. (2017). A Bacteroidetes locus dedicated to fungal 1,6-beta-glucan degradation: Unique substrate conformation drives specificity of the key endo-1,6-beta-glucanase. *J Biol Chem*, 292(25), 10639-10650. <https://doi.org/10.1074/jbc.M117.787606>
- Teufel, F., Almagro Armenteros, J. J., Johansen, A. R., Gislason, M. H., Pihl, S. I., Tsirigos, K. D., Winther, O., Brunak, S., von Heijne, G., & Nielsen, H. (2022). SignalP 6.0 predicts all five types of signal peptides using protein language models. *Nat Biotechnol*, 40(7), 1023-1025. <https://doi.org/10.1038/s41587-021-01156-3>
- Thomsen, T. B., Almdal, K., & Meyer, A. S. (2023). Significance of poly(ethylene terephthalate) (PET) substrate crystallinity on enzymatic degradation. *N Biotechnol*, 78, 162-172. <https://doi.org/10.1016/j.nbt.2023.11.001>
- Thomsen, T. B., Hunt, C. J., & Meyer, A. S. (2022). Influence of substrate crystallinity and glass transition temperature on enzymatic degradation of polyethylene terephthalate (PET). *N Biotechnol*, 69, 28-35. <https://doi.org/10.1016/j.nbt.2022.02.006>
- Trott, O., & Olson, A. J. (2010). AutoDock Vina: improving the speed and accuracy of docking with a new scoring function, efficient optimization, and multithreading. *J Comput Chem*, 31(2), 455-461. <https://doi.org/10.1002/jcc.21334>
- Tsai, C. W., Ruaan, R. C., & Liu, C. I. (2012). Adsorption of antimicrobial indolicidin-derived peptides on hydrophobic surfaces. *Langmuir*, 28(28), 10446-10452. <https://doi.org/10.1021/la301401v>
- Uni, F., Lee, S., Yatsunami, R., Fukui, T., & Nakamura, S. (2009). Role of exposed aromatic residues in substrate-binding of CBM family 5 chitin-binding domain of alkaline chitinase. *Nucleic Acids Symp Ser (Oxf)*(53), 311-312. <https://doi.org/10.1093/nass/nrp156>
- Uni, F., Lee, S., Yatsunami, R., Fukui, T., & Nakamura, S. (2012). Mutational analysis of a CBM family 5 chitin-binding domain of an alkaline chitinase from *Bacillus* sp. J813. *Biosci Biotechnol Biochem*, 76(3), 530-535. <https://doi.org/10.1271/bbb.110835>
- Walker, J. A., Takasuka, T. E., Deng, K., Bianchetti, C. M., Udell, H. S., Prom, B. M., Kim, H., Adams, P. D., Northen, T. R., & Fox, B. G. (2015). Multifunctional cellulase catalysis

VII. References

- targeted by fusion to different carbohydrate-binding modules. *Biotechnol Biofuels*, 8, 220. <https://doi.org/10.1186/s13068-015-0402-0>
- Wang, C., Zhang, R., Liu, B. T., Liu, C. L., & Du, Z. J. (2019). *Paracnuella aquatica* gen. nov., sp. nov., a member of the family Chitinophagaceae isolated from a hot spring. *Int J Syst Evol Microbiol*, 69(8), 2360-2366. <https://doi.org/10.1099/ijsem.0.003476>
- Watanabe, T., Maruyama, F., Nozawa, T., Aoki, A., Okano, S., Shibata, Y., Oshima, K., Kurokawa, K., Hattori, M., Nakagawa, I., & Abiko, Y. (2011). Complete genome sequence of the bacterium *Porphyromonas gingivalis* TDC60, which causes periodontal disease. *J Bacteriol*, 193(16), 4259-4260. <https://doi.org/10.1128/JB.05269-11>
- Weber, J., Petrovic, D., Strodel, B., Smits, S. H. J., Kolkenbrock, S., Leggewie, C., & Jaeger, K. E. (2019). Interaction of carbohydrate-binding modules with poly(ethylene terephthalate). *Appl Microbiol Biotechnol*, 103(12), 4801-4812. <https://doi.org/10.1007/s00253-019-09760-9>
- Wellen, R. C., E.; Rabello, MS. (2011). Nonisothermal cold crystallization of poly(ethylene terephthalate). *J Mater Res*, 26, 1107-1115.
- Whiteford, J. R., & Spanu, P. D. (2002). Hydrophobins and the interactions between fungi and plants. *Mol Plant Pathol*, 3(5), 391-400. <https://doi.org/10.1046/j.1364-3703.2002.00129.x>
- Wu, J. J., Zhu, S., Tang, Y. F., Gu, F., Liu, J. X., & Sun, H. Z. (2022). Microbiota-host crosstalk in the newborn and adult rumen at single-cell resolution. *BMC Biol*, 20(1), 280. <https://doi.org/10.1186/s12915-022-01490-1>
- Xue, M. Y., Sun, H. Z., Wu, X. H., Liu, J. X., & Guan, L. L. (2020). Multi-omics reveals that the rumen microbiome and its metabolome together with the host metabolome contribute to individualized dairy cow performance. *Microbiome*, 8(1), 64. <https://doi.org/10.1186/s40168-020-00819-8>
- Xue, R., Chen, Y., Rong, H., Wei, R., Cui, Z., Zhou, J., Dong, W., & Jiang, M. (2021). Fusion of Chitin-Binding Domain From Chitinolyticbacter meiyuanensis SYBC-H1 to the Leaf-Branch Compost Cutinase for Enhanced PET Hydrolysis. *Front Bioeng Biotechnol*, 9, 762854. <https://doi.org/10.3389/fbioe.2021.762854>
- Yoshida, S., Hiraga, K., Takehana, T., Taniguchi, I., Yamaji, H., Maeda, Y., Toyohara, K., Miyamoto, K., Kimura, Y., & Oda, K. (2016). A bacterium that degrades and assimilates poly(ethylene terephthalate). *Science*, 351(6278), 1196-1199. <https://doi.org/10.1126/science.aad6359>
- Yu, K., Liu, C., Kim, B. G., & Lee, D. Y. (2015). Synthetic fusion protein design and applications. *Biotechnol Adv*, 33(1), 155-164. <https://doi.org/10.1016/j.biotechadv.2014.11.005>
- Zeineldin, M., Barakat, R., Elolimy, A., Salem, A. Z. M., Elghandour, M. M. Y., & Monroy, J. C. (2018). Synergetic action between the rumen microbiota and bovine health. *Microb Pathog*, 124, 106-115. <https://doi.org/10.1016/j.micpath.2018.08.038>
- Zhang, C., Chen, J., Wu, Q., Xu, B., & Huang, Z. (2023). The Gut Microbiota of Young Asian Elephants with Different Milk-Containing Diets. *Animals (Basel)*, 13(5). <https://doi.org/10.3390/ani13050916>
- Zhang, H., Perez-Garcia, P., Dierkes, R. F., Applegate, V., Schumacher, J., Chibani, C. M., Sternagel, S., Preuss, L., Weigert, S., Schmeisser, C., Danso, D., Pleiss, J., Almeida, A., Hocker, B., Hallam, S. J., Schmitz, R. A., Smits, S. H. J., Chow, J., & Streit, W. R. (2021). The Bacteroidetes *Aequorivita* sp. and *Kaistella jeonii* Produce Promiscuous Esterases With PET-Hydrolyzing Activity. *Front Microbiol*, 12, 803896. <https://doi.org/10.3389/fmicb.2021.803896>
- Zhang, Y., Chen, S., Xu, M., Cavaco-Paulo, A., Wu, J., & Chen, J. (2010). Characterization of *Thermobifida fusca* cutinase-carbohydrate-binding module fusion proteins and their potential application in bioscouring. *Appl Environ Microbiol*, 76(20), 6870-6876. <https://doi.org/10.1128/AEM.00896-10>

VII. References

- Zhang, Y., Wang, L., Chen, J., & Wu, J. (2013). Enhanced activity toward PET by site-directed mutagenesis of *Thermobifida fusca* cutinase-CBM fusion protein. *Carbohydr Polym*, *97*(1), 124-129. <https://doi.org/10.1016/j.carbpol.2013.04.042>
- Zhu, Y., Kwiatkowski, K. J., Yang, T., Kharade, S. S., Bahr, C. M., Koropatkin, N. M., Liu, W., & McBride, M. J. (2015). Outer membrane proteins related to SusC and SusD are not required for *Cytophaga hutchinsonii* cellulose utilization. *Appl Microbiol Biotechnol*, *99*(15), 6339-6350. <https://doi.org/10.1007/s00253-015-6555-8>
- Zimmermann, L., Stephens, A., Nam, S. Z., Rau, D., Kubler, J., Lozajic, M., Gabler, F., Soding, J., Lupas, A. N., & Alva, V. (2018). A Completely Reimplemented MPI Bioinformatics Toolkit with a New HHpred Server at its Core. *J Mol Biol*, *430*(15), 2237-2243. <https://doi.org/10.1016/j.jmb.2017.12.007>